FUNDAMENTAL STUDIES OF SUBSONIC AND TRANSONIC FLOW SEPARATION. PART I. FIRST PHASE SUMMARY REPORT

J. M. Wu

Tennessee University Space Institute

Prepared for:

Arnold Engineering Development Center

September 1975

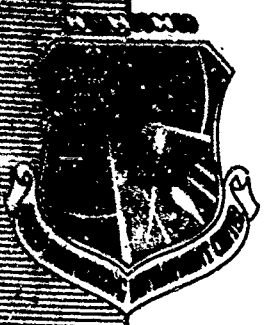

FUNDAMENTAL STUDIES OF SUBSONIC AND TRANSONIC FLOW SEPARATION

PART I – FIRST PHASE SUMMARY REPORT

THE UNIVERSITY OF TENNESSEE SPACE INSTITUTE
TULLAHOMA, TENNESSEE 37388

September 1975

Final Report for Period June 1972 – December 1973

Prepared for

ARNOLD ENGINEERING DEVELOPMENT CENTER (DY)
AIR FORCE SYSTEMS COMMAND
ARNOLD AIR FORCE STATION, TENNESSEE 37389

NOTICES

When U. S. Government drawings specifications, or other data are used for any purpose other than a definitely related Government procurement operation, the Government thereby incurs no responsibility nor any obligation whatsoever, and the fact that the Government may have formulated, furnished, or in any way supplied the said drawings, specifications, or other data, is not to be regarded by implication or otherwise, or in any manner licensing the holder or any other person or corporation, or conveying any rights or permission to manufacture, use, or sell any patented invention that may in any way be related thereto.

Qualified users may obtain copies of this report from the Defense Documentation Center.

References to named commercial products in this report are not to be considered in any sense as an endorsement of the product by the United States Air Force or the Government.

This final report was submitted by The University of Tennessee Space Institute, Tullahoma, TN 37388, under contract F40600-72-C-0011, with the Arnold Engineering Development Center, Arnold Air Force Station, TN 37389. Captain Carlos Tirres was the AEDC technical monitor.

This report has been reviewed by the Information Office (OI) and is releasable to the National Technical Information Service (NTIS). At NTIS, it will be available to the general public, including foreign nations.

APPROVAL STATEMENT

This technical report has been reviewed and is approved for publication.

FOR THE COMMANDER

Carlos Tirres
CARLOS TIRRES
Captain, USAF
Research & Development
Division
Directorate of Technology

Robert O Dietz
ROBERT O. DIETZ
Director of Technology

REPORT DOCUMENTATION PAGE		READ INSTRUCTIONS BEFORE COMPLETING FORM
1 REPORT NUMBER AEDC-TR-75-95	2 GOVT ACCESSION NO.	3 RECIPIENT'S CATALOG NUMBER
4 TITLE (and Subtitle) FUNDAMENTAL STUDIES OF SUBSONIC AND TRANSONIC FLOW SEPARATION, PART I--FIRST PHASE SUMMARY REPORT		5 TYPE OF REPORT & PERIOD COVERED Final Report - June 1972 - December 1973 6 PERFORMING ORG. REPORT NUMBER
7 AUTHOR(s) J. M. Wu, et al.		8 CONTRACT OR GRANT NUMBER(s) F40600-72-C-0011
9 PERFORMING ORGANIZATION NAME AND ADDRESS The University of Tennessee Space Institute Tullahoma, Tennessee 37388		10 PROGRAM ELEMENT, PROJECT, TASK AREA & WORK UNIT NUMBERS Program Element 65807F
11 CONTROLLING OFFICE NAME AND ADDRESS Arnold Engineering Development Center(DYFS) Air Force Systems Command Arnold Air Force Station, Tennessee 37389		12. REPORT DATE September 1975 13 NUMBER OF PAGES 129
14 MONITORING AGENCY NAME & ADDRESS(if different from Controlling Office)		15 SECURITY CLASS. (of this report) UNCLASSIFIED 15a DECLASSIFICATION DOWNGRADING SCHEDULE N/A
16 DISTRIBUTION STATEMENT (of this Report) Approved for public release; distribution unlimited.		
17 DISTRIBUTION STATEMENT (of the abstract entered in Block 20, if different from Report)		
18 SUPPLEMENTARY NOTES Available in DDC		
19 KEY WORDS (Continue on reverse side if necessary and identify by block number) transonic flow subsonic flow turbulent flow Reynolds number effects cavity flow flow separation upstream disturbance transonic wind tunnels		
20 ABSTRACT (Continue on reverse side if necessary and identify by block number) The work reported herein represents the first phase of a fundamental study of subsonic and transonic flow separation. The UTSI transonic flow wind tunnel which was specially modified for this study is described. Results for the calibration of the facility are also included. The experimental effort includes studies of the flow over forward and rearward facing steps and shallow cavities. Such configurations are taken to be representative--in a fundamen-		

DD FORM JAN 73 1473 EDITION OF 1 NOV 65 IS OBSOLETE

20. ABSTRACT (Continued)

tal sense regarding the mechanism of flow separation--of the situation existing in the flow over an airfoil. Moreover, through this study we hope to gain insight into the effects of an upstream disturbance on the downstream flow separation. Particular interest centers around the influence of Reynolds number on the entire flow mechanism during separation. In this study, attention was restricted to the subsonic range of Mach numbers and included values of 0.56, 0.77 and 0.91. The Reynolds number based on model length varied between 30×10^6 to 130×10^6. Theoretical work aimed at developing techniques for predicting transonic flows with separation are also reported. The major effort was concerned with the computation of the potential flow field over cavity like shapes and comparison with experimental data. Some preliminary studies of the viscous flow were also conducted. The results are discussed in relation to developing an initial understanding of the flow separation process. Recommendations for future work are also made.

PREFACE

The work reported herein was conducted at the University of Tennessee Space Institute, Tullahoma, Tennessee, and was supported by the Arnold Engineering Development Center under Contract Number AF F40600-72-C-0011 during the period June 1972 to December 1973. The technical monitor for this contract period was Capt. Carlos Tirres.

The reproducibles used in the reproduction of this report were supplied by the authors: J. M. Wu, T. H. Moulden, G. M. Elfstrom, K. C. Reddy, C. H. Chen, R. Nygaard, L. Shen, H. H. Venghaus, and K. Anjaneyulu.

TABLE OF CONTENTS

ILLUSTRATIONS

APPENDIXES

TABLES

ILLUSTRATIONS

1.0 INTRODUCTION

It has been known for some time that under certain conditions, particularly when separation is evident, transonic flow can be extremely sensitive to changes in Reynolds number or to disturbances in the boundary-layer. As a consequence of this, ground-test results may deviate significantly from conditions in actual flight. There is a profound need, therefore, for a research program aimed at obtaining a basic understanding of such phenomena. At the same time there would be better background for the interpretation of current ground-test results. The investigation reported herein is the first phase of a systematic study of this vital problem.

In order to accomplish the above objectives, experimental and theoretical studies have been initiated. The experimental study is aimed at providing detailed measurements of the viscous layer under various flow conditions. It can be anticipated that the probing of a very thin viscous layer developing over the surface of a conventionally mounted model will not yield satisfactory results due to the limitation of the model size in an existing transonic wind tunnel. Furthermore, it is difficult to match the real flight Reynolds number in the tunnel. Such difficulties may be overcome if the wind tunnel wall itself is modified properly so as to act as the testing model. These problems are addressed more fully in the following. A clear cut leading edge is especially desirable in any boundary-layer study. The existing UTSI blowdown transonic flow wind tunnel has been modified for basic research into viscous flow phenomena.

The tunnel has the capability of generating flows with a wide range of Reynolds number. The upper bound to the Reynolds number obtainable is in the same order as that of flight conditions, while the lower bound roughly corresponds to that of most existing conventional transonic wind tunnels. Thus, it is possible by careful research to shed light on the so-called "scaling" effect.

It is a well accepted technique to employ a forward facing step model for generating an adverse pressure gradient

in flow separation studies. In the present work, the influence of an upstream disturbance, created by a rearward facing step, is also studied. The flow over a rearward facing step will generate a local separation which corresponds to a significant flow disturbance. The parameters connected with flow separation in an adverse pressure gradient are studied in detail both with and without the upstream disturbance.

For this phase of the experimental study, emphasis was placed on subsonic free stream flows. The flow field was probed in detail by a traversing pitot probe. The study is also assisted by closely placed surface static pressure measurements and by surface oil flow studies. The experimental study is also coupled with a theoretical computation of the streamlines adjacent to the model surface. The theoretical computational schemes have been extended by attempting to consider an airfoil with a wake and the more difficult task of a flow with separation.

The measurements of various flow conditions and configurations show some significant results for the effects of Mach number, Reynolds number and upstream disturbance. The boundary layer profiles have also been analyzed in the light of the wall and wake laws. Knowledge of the variation of the wake component under various flow conditions is the key to understanding the role of the Reynolds number and of the upstream disturbance. Such information, supplemented by further explanation, may also assist in the understanding of the relationship between ground simulation and real flight conditions.

2.0 DISCUSSION OF TRANSONIC FLOW SEPARATION

The remarks in this section will be concerned with the general background and motivation of the subject under study. Our understanding of transonic flow separation, as it exists in its present limited state, is outlined with particular reference to airfoil flows. Areas where knowledge is limited or even non-existent are discussed. This leads naturally into an exposition of the principles and aims of the work reported herein.

2.1 TRANSONIC FLOW SENSITIVITY

As is well known (Ref. 1), the one-dimensional isentropic flow of a fluid (we may think of this as flow within a streamtube) is governed by the relation:

$$\frac{dM}{dA} = \frac{-M/A}{1 - M^2} \tag{2.1}$$

or equivantly:

$$\frac{dp}{dA} = \frac{\rho u^2/A}{1 - M^2} \tag{2.2}$$

between the cross-section area A and the Mach number M. It follows that near M = 1, a very large change in Mach number, as well as in the pressure, results from a small change in area. This observation leads to the idea that a transonic flow will be extremely sensitive to small changes in body contour. It should be cautioned here that any real flow will be three-dimensional and viscous, so that the result embodied in Equations (2.1) and (2.2) would need some modification. The basic concept is still valid. Indeed Morawetz (Ref. 2) has shown that if the transonic flow past a given contour is continuous, then the flow past a slightly distorted contour will exhibit a discontinuity, or shock wave. This result, of course, reflects a mathematical idealization of a physical situation,and more recent computational and experimental studies have established the existence of shock free supercritical flows.

Another consequence of Equation (2.1) is that the lateral extent of a disturbance is large. Thus, in a slightly supersonic stream, the characteristics--inclined at $\sin^{-1}$ (1/M) to the streamline--are almost perpendicular to the local flow.

An immediate implication of the non-existence of a neighboring solution is that the small distortion to the streamlines of the flow due to the development of the boundary layer could significantly change the nature of the

flow. In particular, it could be expected that a contour whose potential flow is shock-free may, when tested in a real airstream, exhibit a shock wave. Two major criticisms have been leveled against such an inference. One of them is that the results of Morawetz were derived from the inviscid flow equations with the additional assumption that the flow is steady. It can be expected that the real flow, exhibiting viscosity, will be somewhat less influenced by small contour changes. Some experimental evidence can be presented on this point. Figure (1) shows the experimental data from Ref. (3) as compared with the exact theory for quasi-elliptic airfoils. The flow in this example is transonic but shock free. It is seen that the agreement between theory and experiment is of the same order as that shown in Fig. (2) for an entirely subsonic flow. Both airfoils were tested at nominally the same Reynolds number and boundary layer conditions.

The data shown in Fig. (1) are for a flow that is unseparated and shock free; though transonic. Under such conditions, the transonic flow is no more influenced by viscous effects than is a subsonic flow. Thus, the onset of transonic conditions by itself does not necessarily imply a large sensitivity of the flow to small changes in either upstream or boundary conditions.

It is also well known (Refs. 4 and 5) that a transonic flow is non-steady, in contradiction to the Morawetz hypothesis. Thus, even when the basic characteristics of a flow (say, shock position) appear steady, the local flow velocity field is not. An essentially small amplitude, wave-like motion is superimposed upon the flow; but it is not the intent of the present work to discuss this phenomenon. Only in situations where flow separation takes place does the flow exhibit marked sensitivity to small changes in conditions. The separation may be either shock induced, or a rear separation, or a combination of the two. The most familar example of the type of sensitivity encountered is that present on the C-141 wing (Ref. 6). Briefly, in this type of situation, a change in the free stream Reynolds number causes changes in the development of the boundary layer; which in turn greatly affects the geometry of the separation. Recent tests performed in the AEDC 4 ft. Transonic Wind Tunnel on the C-141 airfoil section, mounted between end plates, clearly illustrates the problem. The pattern of

flow separation and shock wave movement over the airfoil with increasing free stream Mach number at fixed incidence are shown in Fig. 3. References (6 and 7) discuss the flow in greater detail. These large changes in flow geometry--due to the non-linear nature of the transonic flow and of the interaction with the viscous flow--are not the initial concern of the present work. First of all, attention must be restricted to obtaining an understanding of the basic phenomena associated with separation in a transonic flow. To this end, a series of basic experimental studies are undertaken.

Once the separation process is better understood, this knowledge can be used to predict the behavior of the entire flow. The planned procedure is to generate an understanding of the physical properties of flow separation through careful basic experiments and then to utilize such experimental information to guide theoretical developments.

2.2 SOME REMARKS ON THE BOUNDARY LAYER INFLUENCE

For a given airfoil in a transonic flow, the interaction between the shock and the flow near the surface is dependent upon the Reynolds number. Not only is the flow, locally under the shock, influenced by changes in Reynolds number but also the subsequent boundary layer development over the remainder of the airfoil can be significantly altered. Again, if the flow is caused to separate near the trailing-edge, then the entire flow field may change drastically--even ahead of the shock. Thus, as shown in Fig. (3), it is possible for the shock position to move forward as the free stream Mach number increases. In broad terms, this results in a reduction in lift; which is equivalent to a decrease of incidence or free stream Mach number.

At low values of Reynolds number, the boundary layer may well be laminar at the point where the shock wave impinges. As is well known, such an interaction is completely different from that associated with a turbulent boundary layer (Refs. 8 and 9). Increases of Reynolds number from this condition will produce flows wherein transition takes place in the immediate vicinity of the shock interaction. The Reynolds number (based on body length) at which this situation occurs depends very much on the surface pressure distribution over the body. Thus, if the pressure decreases

slowly over a large part of the chord (and maybe as far as the shock location), then a much larger chord Reynolds number would be demanded before transition moves sufficiently ahead of the shock interaction for this to be characteristic of a turbulent flow.

In an effort to reduce the disparity between a wind tunnel test conducted at low Reynolds number and results anticipated in high Reynolds number flight, it is customary to force transition at some point near the front of the body. Such a procedure introduces difficulties. In the first place, there is no reason to suppose that the properties of the boundary layer, when artifically tripped, will resemble those of a boundary layer undergoing natural transition. If the boundary layer does not encounter any undue disturbance for a considerable distance (in terms of boundary layer thickness), then its subsequent behavior will be little different from the natural flow. It is readily observed, however, that by adjusting the location of the tripping device, the flow field can be changed within wide limits. Figure (4) shows the effect of transition position on the location of the shock wave for the C-141 wing (Ref. 6). The same effect is indicated in the variation of trailing-edge pressure; which is a useful indicator of flow separation (Ref. 10). The suggestion of Blackwell (Ref. 11) that the transition strip be located at that position which reproduces the experimental value of trailing-edge pressure, may not be feasible. In the first place, during exploratory testing, the high Reynolds number data will not be available. Secondly, as pointed out above, a tripped boundary layer does not give anything more than a superficial representation of a higher Reynolds number flow.

By moving the transition ahead of the shock interaction, the trip has somewhat the same consequences as an increase in the Reynolds number. The effect on the integral thicknesses of the boundary layer will not, however, be in the desired sense. The precise way in which the shock boundary layer interaction and the subsequent downstream flow are influenced by the upstream boundary layer properties is not fully understood; nor is there much understanding of the way in which the development of the flow downstream of the shock is related to the entire flow field. The last point

has some significance in an airfoil flow. The way in which the boundary layer develops downstream of the shock wave determines, to a large extent, the lift and drag on the airfoil. During the interaction process, the boundary layer may well be forced into a separated state--this is almost certain if the Mach number upstream of the shock is greater than 1.2 (see Ref. 12). Once this separation has taken place, two possibilities exist: either the flow remains separated with attendant large drag increase and lift decrease or reattachment occurs. If the latter condition holds, there are again two possibilities. The flow will either continue unseparated to the trailing edge or will suffer a second separation due to the pressure rise over the rear of the airfoil. In the first case, the lift and drag will be almost unaffected by the shock interaction, but on further increase of free-stream Mach number (or incidence) the separated region under the shock will be enlarged and ultimately cover the entire length to the trailing edge. In the situation where the flow suffers a second separation, the entire airfoil flow becomes very sensitive to small changes in free stream conditions (Refs. 6 and 7). The implication is that there exists an urgent need to undertake a basic study of separation in a transonic flow: the object of the present work.

2.3 THE SELECTION OF A WIND TUNNEL MODEL

In the preceding discussion of flow separation on an airfoil, it was indicated that the boundary layer flow was strongly influenced by the pressure field under which it develops. The pressure field is modified by the presence of the boundary layer. This latter effect is of great significance in determining the overall airfoil flow, but is not an essential feature of the boundary layer development and possible separation.

In order to progress towards an understanding of the entire airfoil flow with separation, it is necessary to first develop knowledge concerning the separation process. This can best be done if the separation is studied alone--with as little influence from other factors as possible. This type of approach has already been used in fundamental studies of shock induced boundary layer separation in supersonic flow (Ref. 13).

The obvious first step is to remove the gradients (as far as possible) from the external pressure field. Hence, we are led to a study of the transonic flow over backward and forward facing steps, as a means of studying in great detail the separation and reattachment processes. In particular, there is substantial interest in the influence of Reynolds number on the separation mechanism. The objectives are very much different from those of Ref. (14), where only the drag, in transonic flow of various cut-out configurations, was studied.

Backward and forward facing step studies are vital for obtaining information concerning the basic nature of the separation and reattachment mechanism. However, as was pointed out above, the extreme sensitivity of an airfoil flow to small changes in boundary layer conditions is characterized by the presence of both a shock induced separation and a rear separation. In order to study this situation and the flow Reynolds number effect, it is necessary to investigate the re-separation of a boundary layer that is influenced by a previous separation and reattachment. In the context of the present experimental set-up, this suggests studying the flow inside a long cavity. In this way, the reattached shear layer from the flow over a back step is forced to suffer separation induced by the forward facing step. By changing the length of the cavity, the boundary layer growth--simulating the distance on the airfoil between the shock location and the trailing edge--can be varied within wide limits. The sensitivity of the boundary layer to re-separation, which must be a function of the flow conditions, can then be studied.

3.0 TEST PROCEDURES AND TECHNIQUES

Recently, most difficulties related to transonic flow testing have centered around the accurate representation of the flow pattern as it occurs in flight. In response to this need, two approaches can be taken in transonic flow testing. One is to simulate the required high Reynolds number flow directly in wind tunnels by increasing the total pressure according to the concept of a Ludwig tube or by reducing the temperature as in a cryogenic tunnel. The other method is to develop testing techniques that enable us to extrapolate the aerodynamic characteristics into regions far beyond those

existing in the current wind tunnels. The truly high Reynolds number tunnels of any significant size are not yet available. In the currently available transonic wind tunnels, only limited size models can be tested which reduce the Reynolds number. In order to simulate the high Reynolds number boundary layer flow, an artificial trip mechanism is necessary which may lead to erroneous results. An additional unknown factor is how to adjust the tunnel wall open area ratio to obtain results with minimum wall interference.

In order to avoid some of the difficulties mentioned above, the existing blowdown wind tunnel at UTSI has been modified with two major objectives. One is to utilize a specially designed wind tunnel wall as the testing model for achieving high Reynolds number flows. The other is to employ a sufficiently long model such that a detailed probing of the boundary layer can be accomplished. Especially the response of the high Reynolds number boundary layer flow to changes in the external pressure field can be studied in detail

3.1 UTSI TRANSONIC TUNNEL

In general, most wind tunnels have been designed to have a uniform flow in the center core of the test section. It is this portion of the flow that is utilized for the purpose of testing with the model hung in the middle of this uniform flow section. The measurements are made either on the model or in the nearby flow field. Such a design philosophy is based on the principle of versatile usage of the tunnel. As a consequence, the model may have a wide variety of shapes but be limited in size. The size limitation is extremely important in transonic flow experiments. Because of the nature of transonic flow (Ref. 17), the projected area of the model is usually below 1% of the tunnel cross-sectional area in order to realize small wall interference. In other words, it is excellent to use the conventional wind tunnel for an "inviscid flow" type study, i.e., for the overall flow pattern and its induced flow field around the model. However, it is extremely poor for the viscous flow investigation because of the significant scaling effect due to a very small model size compared to the prototype size. The simulation of the flow pattern thus may be erroneous if flow separation is present.

The UTSI circular cross sectional blowdown tunnel (Ref. 18) has been converted into a tunnel with rectangular cross section. Instead of utilizing the center core flow, the wall of the tunnel has been designed as a long flat-plate model. By utilizing both short and extremely long distances from the leading edge of the model and coupling this with the stilling chamber pressure variation, a wide range of Reynolds number flows can be established. Thus, the scaling effect associated with the viscous flow can be studied.

Emphasis during the modification has also been placed upon the required versatility in changing the model and the tunnel components to meet future possible testing requirements. The tunnel concept may be described as multi-component type construction (or, building block construction). The tunnel throat section, the test section, the floor, the wall, the boundary layer bleeding devices, etc. are all freely replaceable or interchangeable while not altering the overall flow conditions. This interchangeability gives the tunnel considerable versatility. The modified tunnel has some unique features, and is specifically designed for the transonic viscous flow investigations.

The sectional view of the tunnel is illustrated in Fig. 5. The nominal test section dimensions are 12 inches in width, 11 inches in height, and the length of the entire section is 144 inches. A boundary layer suction device is mounted in front of the leading edge, not only to suck away the developed boundary layer from the tunnel throat section, but also to establish a clean and well defined boundary-layer flow along the model. For subsonic testing, the leading edge is somewhat rounded but can be interchanged with a sharp edged configuration for supersonic flow testing.

The model (tunnel floor) is constructed of various sectional pieces as shown in Figs. 5 and 6. All these pieces can be moved or modified independently to allow tailoring for the special needs of any particular experiment. The model has enough space underneath for placing various sensing instruments. Each model component is attached to the two horizontally laid beams for support as shown in Fig. 5. Two side wall boundary layer suction devices are moveable along the flow direction. These two devices are used to ensure the two-dimensionality of the flow by sucking away the

excessive side wall boundary layers. On top of the test section there is a plenum chamber separated from the test from section by a porous panel. Panels of different porosity can be installed at different locations along the tunnel to minimize the wall interference. At the end of the test section, a moveable choke is installed in the diffuser section (Fig. 5) for adjusting the flow Mach number in the test section. The air flow is exhausted into the atmosphere through a vertical exhaust pipe as shown in Fig. 5. The detailed construction can be better visualized through a pictorial view of the test section as illustrated in Fig. 6.

The operational Reynolds number range of the UTSI wind tunnel is designed to be as follows:

$$5 \times 10^6 < Re/ft < 3 \times 10^7$$

$$4 \times 10^6 < Re_L < 2 \times 10^8$$

(Re_L based on length from the leading edge)

The corresponding free stream Mach number range is

$$0.60 < M < 1.50$$

The temperature change of the wind tunnel wall during the test period ie expected to be within 10°C. The wind tunnel wall is thus planned to be approximately adiabatic through the entire testing time.

Inside the diffuser, a center body is used as a choking device. The axial movement from zero inches to 16.4 inches is possible, which corresponds to a mimimum choking cross-sectional area of 62 square inches to a maximum opening of 123 square inches. This diffuser area adjustment is necessary to obtain the required subsonic Mach number in the test section.

The mass flow rate in the wind tunnel is a function of the Mach number, the maximum value being about 190 lb/sec. The nominal running time of the tunnel is in the range of 10 to 60 seconds. The operational envelope of the tunnel, the

wind tunnel flow quality and the UTSI air supply system are explained in Appendix A of this report.

3.2 TEST MODELS AND INSTRUMENTATION

Through special design, as discussed in the previous sections, the floor of the wind tunnel test section is used as the test model (Fig. 7a). It has a total length of 144 inches and is 12 inches wide from the leading edge to 74 inches downstream and then narrows to 10.5 inches for the remainder of the test section. There are three adjustable boundary layer suction devices, one of them is beneath the leading edge and the other two are located at the beginning of both sides of the narrowed floor. These suction devices are for the purpose of ensuring a natural boundary layer starting from the leading edge and also to help generate a two-dimensional flow along the model. The whole floor is composed of seven pieces of steel block which are 7, 10, 12, 18, 27, 39 and 40 inches long respectively. All the blocks, except the 7 inch piece which forms the leading edge, can be arranged in any sequence and moved up or down by as much as 3.75 inches as desired. The floor can be used as either a flat plate model, a forward facing step model or a rearward facing step model of different heights located at different stations. It can also be arranged as "cavity like" models of different lengths and depths at various locations.

During this phase of the experiment, a one inch high forward facing step model (Fig. 7b), located at 74 inches downstream from the leading edge, is tested to show the Reynolds number and Mach number effects on flow separation. Two "cavity like" models (Figs. 7c and d) which have a cavity 1 inch deep and 40 inches and 27.5 inches long respectively were tested. Both have a forward facing step located at 74 inches from the leading edge. These cavities are tested to study the effect of different upstream disturbances. The flat plate model is also tested under the same flow condition as a reference.

Surface pressure taps are distributed longitudinally, 2 inches to the right of the center line of the model surface. A total of 79 pressure taps are used to acquire data every 0.25 inches in a region 10 inches ahead of rht forward facing step, every 0.5 inches in the region 34 to 44 inches and every 1.0 inch from 44 to 64 from the leading edge.

In order to measure the total pressure variation across the boundary layer by a traversing pitot probe at any desired station on the model, two floor blocks are slotted along their center lines and filled with small blocks of different lengths as shown in Fig. 8. The traversing pitot probe is screw mounted such that it can slide freely along this slot.

A variable speed vertical traversing pitot probe is used to measure the total pressure variation across the boundary layer. The traversing mechanism is composed of a travel unislide assembly and a speed control (Figs. 9a and b), with an approximate motor speed range of $1 \sim 500$ rpm which converts to a linear probe velocity of $0.0007 \sim 0.45$ in./sec. and a maximum traversing distance of 3.5 inches is permitted. The pressure transducer is mounted close to the travel mechanism but below the floor and is connected to the pitot tube by a 0.0655 inch inside diameter flexible tube. The probe tip is circular in shape and is interchangeable between three different tip outside diameters of 0.04, 0.011 and 0.023 inch, respectively, which have been used for the measurements. The boundary layer velocity profiles measured by two different tips are found to be in good agreement (Fig. 10).

The minimum traversing time required, based on time-lag considerations, is estimated by Kinslow's formula (Ref. 19) which can be written as,

$$\tau = \frac{Km}{2P_t} \ell n \quad \frac{(P_t + P_m)\ (P_t - P_i)}{(P_t - P_m)\ (P_t + P_i)} \tag{3.1}$$

$$Km = \frac{16\pi\mu\ell_1}{3A_1^2(c + 1)} \{ V_1 + (c^2 + 3c + 3)V_2 + 3\ (c + 1)^2\ V_m \} \tag{3.2}$$

where,

P_m = Pressure at the measuring device

P_t = True pressure

P_i = Initial pressure in pitot

A_1, A_2 = Internal cross sectional area of first and second tube respectively

d_1, d_2 = Inside diameter of first and second tube respectively

V_1, V_2 and V_m = Internal volume of first tube, second tube and measuring device respectively.

$$C = \frac{\ell_2}{\ell_1}\left(\frac{A_1}{A_2}\right)^2$$

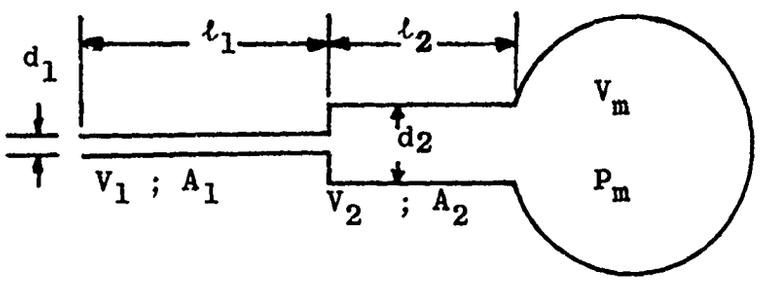

The lag times for four different cases, i.e., two different probe tips each referred to two different total pressures, have been calculated. The corresponding lag times are shown in Fig. 11. The maximum lag time for these cases is 1.16 seconds, which means that the traversing time for each run of the pitot tip across the boundary layer should exceed this value. In the present experiments, the average traversing time is about 9.2 seconds with a minimum tip opening of 0.0081 inches. For most of the tests, in this study, a 0.0165 inch inside diameter tube is employed and, therefore, the data is lag free. The calibration values for the lag-time are shown in Fig. 12.

4.0 DISCUSSION OF RESULTS

The main features of the experimental results obtained are summarized herein. These results lead us to important observations based upon the data analysis. A discussion of these observations will be presented in section 4.4.

4.1 TOTAL PRESSURE AND VELOCITY PROFILES

The shear layer velocity profiles obtained from the measured local total pressure distribution across the viscous layer and the corresponding surface static pressure, at different stations on different models are shown in Figs. 13 to 16. The variations of the velocity profiles along the different models are exhibited in Figs. 17-20. The static pressure gradient across the shear layer is assumed to be negligible for this investigation. This assumption is probably quite accurate in the flat plate and the rearward facing step cases, as indicated by the tunnel side wall static pressure measurements (Fig. 21). However, it may not be true in the forward facing step configuration (Ref. 23).

The main features of the flow, as observed from a study of these figures, are summarized as follows:

(1) Even with a 40 inch long cavity (Figs. 15 and 19), the disturbed velocity profile cannot fully recover to the upstream disturbance free case. This is shown from a comparison with the corresponding profile on the flat plate model (Figs. 13 and 17).

(2) The pressure distribution on the forward facing step model (Figs. 24a and b) shows that the upstream effect due to the step can reach further than 23 step heights upstream from the root of the step for a flow condition of $M_j = 0.6$ and $Re_L = 32.5 \times 10^6$. Since the static pressure variation further upstream has not been measured during this study, it is difficult to ascertain the exact distance of the upstream influence caused by the forward facing step.

(3) The velocity profiles ahead of the forward facing step at the same station for different Mach numbers and Reynolds numbers have also been compared. The result is shown in Figs. 23a and b. At station 61, the velocity profile at a

Mach number of 0.9 and Reynolds number of 72 x 10^6 appears to be fuller than that for a Mach number of 0.6 and a Reynolds number of 32 x 10^6. At station 69, the normalized velocity profile at higher Mach number and Reynolds number becomes even fuller. The comparison of various velocity profiles for different model configurations at the locations corresponding to the same reference station are given in Fig. 22e. The reference station is the station where the surface pressure begins to rise due to the forward facing step. The values measured at this station have been used as the equivalent free stream conditions with respect to the corresponding models. These reference stations are not at the same location for the different model configurations. In Figs. 22a, b, c, and d, the velocity profiles are shown compared at the same measuring stations. These comparisons show the upstream disturbance effect rather well.

(4) The shear layer development is plotted in Figs. 17 to 20 for the flat plate, the forward facing step, the 40 inch long cavity and the 27.5 inch cavity models, respectively. The deformation of the shear layer can be examined in these figures. The distortion of the velocity profiles at the different stations is significantly large (Figs. 19 and 20); however, for the different cavity models they are similar at the corresponding stations. The velocity profiles without an upstream disturbance (see Fig. 18), however, are very much different from those of the cavity models. The profiles for the forward facing step model are much closer to the flat plate case. The effect of model geometry on the displacement thickness is significant and will be discussed in subsection 4.4.3.

4.2 WALL STATIC PRESSURE DISTRIBUTIONS

The wall static pressure distributions for two different cavity length configurations and for the forward facing step are shown in Figs. 24 and 25 for various Mach numbers and Reynolds numbers. In these figures, the distance x, normalized by the step height (h), is measured along the model surface from the leading edge of the model. The wall static pressure is normalized by the total pressure (P_t) measured at the station 26.7 inches downstream from the leading edge.

For the cavity flow, the static pressure falls rapidly to the base pressure at the rearward facing step. The lowest pressure was recorded at a point approximately two step heights downstream of the step for $M_e = 0.6$ and $Re_L = 32.5 \times 10^6$. In all the test conditions reported herein, the reattachment zone, i.e., the region where the pressure increases from the base pressure to the plateau pressure value (see Fig. 24c and d), is about five step heights. It can also be seen from Fig. 24c, which shows results for a one inch deep, forty inches long cavity, that the pressure at the end of the reattaching process exhibits an overshoot before falling back to an approximately constant value. For the 27.5 inch long cavity, this overshoot is not so noticeable (Fig. 24d). The distance to the reattachment point was determined from surface oil flow studies. The results will be discussed in section 4.3.

In the region ahead of the forward facing step, the surface pressure distribution shows a rapid rise in pressure before the separation. The maximum value of the pressure is located at a distance of approximately one step height upstream of the step. For a given Mach number and Reynolds number, the peak pressure location ahead of the step is not influenced by an upstream disturbance such as the back step of the cavity (Fig. 25). For $M_e = 0.91$ and $Re_L = 72.5 \times 10^6$, the peak pressure location is also unchanged as seen in Fig. 26.

The difference in pressure between the maximum value ahead of the forward facing step and the minimum value downstream of the back step is dependent upon cavity length. Thus for the long cavity, this pressure difference is 1.45 psi while it is only 1.25 psi for the short cavity. In both cases, however, the value of the nearly constant pressure over the mid section of the cavity is approximately the mean value of the corresponding maximum and minimum pressures. In other words, the magnitude of the pressure drop over the back step is approximately equal to the pressure rise induced by a forward facing step of the same height. However, this pressure rise is lower than that induced by the forward facing step along (see Fig. 25).

4.3 STUDIES USING SURFACE OIL FLOW

The surface oil flow photograph for the flow near the forward facing step in the 27.5 inch cavity at $M_e = 0.58$ and $Re_L = 32.5 \times 10^6$ is shown in Fig. 28 Based on this figure and some other records of surface oil flow, several observations can be made as follows:

(1) It is seen that the three-dimensional effects at the corner of the step and the tunnel wall make the flow pattern quite complicated (Figs. 27 and 28). However, the spanwise influence of this effect is not sufficient to destroy the two-dimensional nature of the flow over the major part of the span.

(2) These secondary flows are confined within a region less than two step heights from the side walls.

(3) There is a vortex in the flow ahead of the step with its center about 1.8 inches upstream of the step and 0.25 inches from the side wall.

(4) The oil flow on top of the step indicates a reattachment line at about 2.4 inches downstream of the step. There is also an accumulation of oil right at the step corner. This would result from the reversed flow in the separation bubble on the top of the step forcing the oil to the foremost portion of the vortex.

(5) The separation line on the floor ahead of the step is clearly seen and is about 1.1 step heights ahead of the step when $M_e = 0.6$ and $Re_L = 32.5 \times 10^6$. This distance is little affected by the presence of an upstream disturbance. Results are not available at higher Mach numbers.

(6) The reattachment region behind the back step is roughly defined by the oil flow. Two points are clear: the reattachment flow is quite three-dimensional; and for the 27.5 inch cavity the distance to reattachment is slightly shorter than that for the 40 inch cavity. This is for a free stream Mach number of 0.6 and a Reynolds number of 32.5×10^6.

(7) Within the recirculating region behind the back step there is an oil line about one inch from the step which

indicates a separation of the reversed flow and the presence of an inner vortex.

4.4 ANALYSIS OF THE EXPERIMENTAL RESULTS

From the measurements presented above, it is possible to derive some observations of interest. In this discussion, all the data has been suitably normalized so that proper comparisons are possible.

4.4.1 The Effect of Mach Number and Reynolds Number

The Mach number, indicating as it does the extent of the compressibility of the gas, has a large influence on the flow pattern. As shown in Fig. 26, an increase in Mach number causes a larger pressure rise ahead of the forward facing step. The reference pressure, P_i, for this plot is the pressure just ahead of the point where the pressure begins to increase ahead of the step. For the forward facing step alone, this is the free stream pressure, P_∞. In the case of the cavity flow, P_i is the pressure approximately midway along the cavity. As indicated above, the pressure rise induced by the step alone is larger than that for the forward facing step component of the cavity (Fig. 25). This result is not too surprising when it is realized that for the step alone, the approaching boundary layer has larger energy than that corresponding to the cavity flow.

In the highly turbulent region of the boundary layer, the pressure force is mainly balanced by the fluid inertia force (Ref. 24). At the station far upstream from the forward facing step, say station 61 which is at a distance of 23 step heights ahead of the forward facing step, the normalized velocity profile for the higher inertia (i.e., higher Mach number and Reynolds number) flow is slightly fuller than that of the lower inertia flow (Fig. 23). As the flow nears the step, the adverse pressure gradient of the higher inertia flow increases faster than that of the lower inertia flow (Fig. 26). It is known that in the outer viscous layer two forces dominate, i.e. the inertia force related to the local velocity and the prevailing pressure force. As the higher energy flow approaches the step, it is better able to resist the increased adverse pressure gradient. This may be seen from Figs. 23 a and b,

which show the normalized higher energy downstream velocity (station 69) becoming fuller. The upstream site (station 61) shows a smaller effect. This discussion is based upon only two completed measurements of the high inertia flow. Further tests may be necessary to confirm this. The Mach number and Reynolds number effects will also be studied separately.

For Mach numbers not too close to unity, the upstream effect of a disturbance in the flow--such as a forward facing step--can be damped within the same order of length scale. This can be seen on the normalized surface pressure plot of Fig. 26. However, the flow at a Mach number of 0.91, which has a much higher pressure peak than that for the 0.60 flow, shows a larger upstream influence. It can be expected (Refs. 25 and 26) that closer to sonic conditions, this interaction distance will increase markedly.

4.4.2 The Effect of an Upstream Disturbance on Separation

The influence of the upstream disturbance can be studied by comparing the flow in the cavity with that over an isolated forward facing step. Then, the back step of the cavity produces a disturbance ahead of the forward facing step similar to that associated with a shock boundary layer interaction.

The oil flow studies indicate that there is very little difference between the separation points for the isolated forward facing step and for the flow in the cavity. There are, however, differences in the distance to reattachment for the flow over the back step of various length cavities. Thus, for the 40 inch cavity, the reattachment distance is 5.9 inches while for the 27.5 inch cavity, this reduces to 5.2 inches. These results are for the same free stream conditions of $M_e = 0.56$ and $Re_L = 32.5 \times 10^6$. Such differences in distance to reattachment are attributable to different boundary layer thicknesses associated with the flow approaching the top of the step.

As far as the surface pressures are concerned, the most pronounced effect of changes in the upstream influence is exhibited in the magnitude of the peak pressure just ahead of the step. The comparison between the surface pressure

distributions for the forward facing step and the two cavities are shown in Fig. 25 For the shorter of the two cavities, this reduction in peak pressure is approximately 30% of the value associated with the forward facing step alone.

These differences in peak pressure can be expected since the flow that has negotiated the back step will suffer an increase in energy deficit thickness. As the flow redevelops along the floor of the cavity, the energy thickness will tend to recover to the flat plate value. This is reflected in an increase of peak pressure with cavity length.

Parallel to this energy deficit will be variations in the skin friction coefficient (see Fig. 30). The skin friction is, of course, directly related to the boundary layer velocity profile (as is the energy thickness). It is of interest, therefore, to compare the velocity profiles in the cavity with those ahead of the forward facing step. These profiles are shown on Figs. 18 to 20. In addition, Fig. 22 compares velocity profiles for the same distance ahead of the step for all three configurations. The distortion of the profile that results from the back step is then evident.

The peak pressure is located at about one step height ahead of the step for all the Mach numbers tested. At the same time, the oil flow studies indicated that separation occurred at about 1.1 step heights ahead of the step. It appears, therefore, that the peak pressure point is located just downstream of the separation point.

4.4.3 The Boundary Layer Wake Component

Utilizing the well known decomposition of the boundary layer velocity profile in terms of the wall and wake components (Ref. 27), we state

$$\frac{u}{u_\tau} = \frac{1}{K} \ln \left(\frac{u_\tau y}{\upsilon_w} \right) + B + \frac{\bar{\pi}}{K} \omega\left(\frac{y}{\delta}\right) \qquad (4.1)$$

where $K = 0.41$ and $B = 5.0$ are empirical constants. u_τ denotes the friction velocity. $\omega(y/\delta)$ is the wake component of the velocity profile whose form is again determined empirically.

This equation for the velocity profile in the boundary layer is generated on the assumption that the fluid properties are constant. To make some allowance for compressibility effects, the van Driest generalized velocity u* (see Ref. 27) can be substituted for u in the above equation.

Now

$$u^* = \frac{u_e}{a} \operatorname{Sin}^{-1} \left(a \frac{u}{u_e} \right) \tag{4.2}$$

where

$$a^2 = \frac{r(\gamma-1) M_e^2}{2 + r(\gamma-1) M_e^2}$$

and $r = (0.72)^{\frac{1}{3}}$ is the recovery factor. u_e and M_e denote local conditions at the external edge of the boundary layer.

If it is assumed that the wake component can be expressed by a simple form (Ref. 28), then:

$$\omega(y/\delta) = 1 - \cos \left(\frac{\pi y}{\delta} \right) \tag{4.3}$$

Utilizing the expression for displacement (Ref. 26), there results:

$$2\bar{\pi} - \ell n \ (1 + \bar{\pi}) = \frac{K u_e}{u_\tau} - \ell n \ \frac{\delta^* u_e}{\nu_w} - Kc - \ell n \, K \tag{4.4}$$

which can be solved for the friction velocity. Then the skin friction coefficient follows from

$$C_f = 2 \left(\frac{u_\tau}{u_e} \right)^2 \tag{4.5}$$

The data is then analyzed as follows (see Fig 29). First, for the same Mach number and Reynolds number, the skin friction for different configurations can be seen on Fig. 30. Then on Fig. 29 is shown the influence of Mach number on the forward facing step configuration. Examination of these figures shows that at the same station for a given configuration, the wake component is reduced as the Mach number and Reynolds number increase. In the center of the cavity, the wake component is little changed with distance along the cavity; but for the forward facing step alone, there is a strong increase in wake component as the step is approached (Fig. 29). It is also seen that the effect of the upstream disturbance--at a given distance ahead of the step--is to thicken the boundary layer (Fig. 31) and to strengthen the wake component (Fig. 29b). Thus, the effect of the upstream disturbance is to cause a stronger mixing process in the wake region of the boundary layer along the cavity floor. At the same time, the skin friction is reduced (Fig. 30). The skin friction decreases rapidly towards the separation point.

The above analysis of the skin friction is based on the theory given in this subsection. The conclusions reached, therefore, must be considered in this light. There is clearly an advantage to be gained in having an independent measurement of the local skin friction.

5.0 THEORETICAL PRINCIPLES AND NUMERICAL COMPUTATIONS

Parallel to the experimental work that has been described in the preceding sections, considerable effort has been expended on the development of supplemental theoretical techniques. It is considered that a parallel effort in both theoretical and experimental areas would be most beneficial for the entire program.

The ultimate aim of the theoretical work is to be able, via a matching between viscous and potential flows, to predict a transonic airfoil flow with shock waves and separation. In this section, various components aimed at achieving this objectives are described and discussed.

5.1 BASIC PRINCIPLES

It is assumed that the flow under discussion can be described by the Navier-Stokes equations for a compressible fluid. At the present time there is no effort being made to solve these full equations for a transonic flow, but as a long term effort, however, such a study should be made. For the present, attention has been restricted to consideration of the classical decomposition of the flow into viscous and potential motions matched together at the edge of the boundary layer.

A formal application of the singular perturbation theory to the Navier-Stokes equations will yield, to first order, an outer problem identical with the classical potential flow and an inner problem which can be identified with Prandtl's boundary layer equations. These two sets of equations are well known and need not be restated here. In the application of this theoretical development to a practical problem, certain difficulties become apparent. There are several reasons for this. First, the form of the solution is assumed to be such that the flow quantities could be expressed as asymptotic sequences with some power of the Reynolds number acting as the gauge functions. The subsequent theoretical treatment is then based upon the asymptotic limit of large Reynolds number. Because of this formulation, the inner solution space becomes of width proportional to a power of Reynolds number.

In many situations, it is possible to calculate (at least to some approximation) the inner and outer flows separately. Some iteration between these first order solutions is then possible (Refs. 30, 31, and 32) to yield results somewhat in agreement with experimental data. Such an iteration is in no way equivalent to determining higher order terms in the asymptotic sequence.

Boundary layer theory, as such, loses validity when the viscous region ceases to be of the thickness specified by the theory ($1/\sqrt{Re}$ for laminar incompressible flow). This situation pertains during flow separation where the viscous region grows very rapidly in thickness. An additional difficulty is also present; the simplifications associated with the inner solution approximations are such that the elliptic nature of the Navier-Stokes equations has been replaced by

the parabolicity of the boundary layer equations. Thus, any upstream influence present in a separation region is denied by the governing equation. In general terms, it is then no longer possible to generate solutions to the boundary layer equations once the separation condition is approached. Various approximation techniques (Ref. 32, for example) have enabled a continuation of the computation through a separation region, but such calculations can only be regarded as being indicative of the real situation.

The fundamental experimental study initiated herein should do much to aid the understanding of a transonic separated flow and in the development of theoretical studies.

5.2 DETAILS OF THE POTENTIAL FLOW CALCULATIONS

As described above, the application of singular perturbation theory yields as the first order solution the classical Euler equations for an inviscid fluid. These equations are non-linear and are usually (except in some numerical studies) linearized in terms of a suitable parameter. The remarks of this section are restricted to studies of such simplified equations.

In order to facilitate the analysis of experimental results, numerical computations have been performed for studying different aspects of cavity-like flows and airfoil flows. For flows at Mach number of order 0.6, subsonic small disturbance theory has been used and for flows at Mach numbers closer to 1, transonic small disturbance theory has been used.

5.2.1 Subsonic Small Disturbance Equations:

For subsonic flow past a cavity in an infinite flat wall, the small disturbance equations can be written as

$$K\,\varphi_{xx} + \varphi_{\bar{y}\bar{y}} = 0 \qquad \bar{y} = \delta^{\frac{1}{3}}\, y \qquad (5.1)$$

$$K = (1 - M_\infty^2)/\delta^{\frac{2}{3}}$$

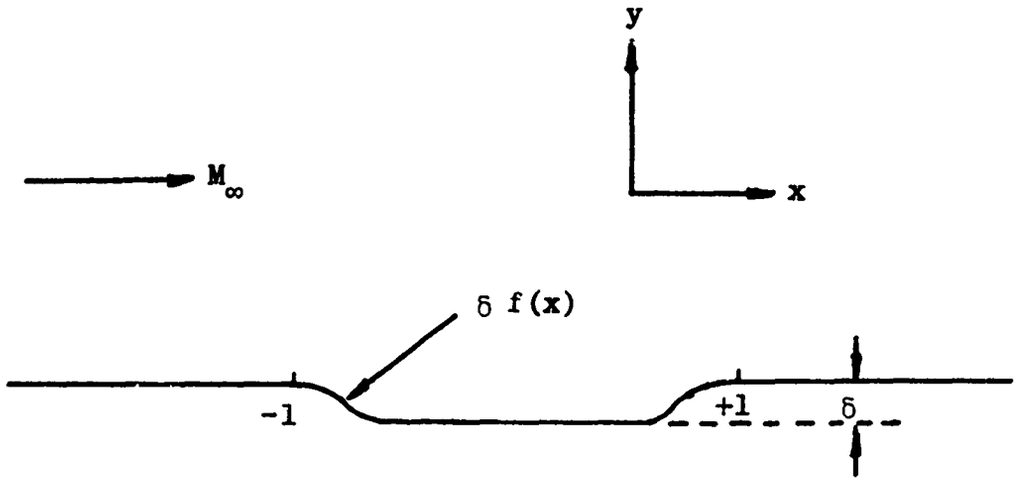

where φ is a stretched disturbance velocity potential defined by the following equations*

$$U = U_\infty \left(1 + \delta^{\frac{2}{3}} u + \ldots\ldots\right) \tag{5.2}$$

$$u = \frac{\partial \varphi}{\partial x}$$

where U is the velocity in x-direction and x and y are coordinates non-dimensionalised with respect to half cavity length.

The boundary conditions are:

At $\bar{y} = 0$,

$$\varphi_{\bar{y}}(x, 0) = \frac{df}{dx}(x), \qquad |x| < 1 \tag{5.3}$$

$$= 0 \quad , \qquad |x| > 1$$

*These equations are written in terms of the variables used in transonic small disturbance theory.

As $x^2 + \bar{y}^2 \to \infty$, $\varphi \to 0$.

By the use of Green's function technique we can obtain the solution of these equations as

$$\varphi(x, \bar{y}) = \frac{1}{2\pi\sqrt{K}} \int_{-1}^{1} f'(\xi) \ln \left[(x - \xi)^2 + K\bar{y}^2 \right] d\xi \quad (5.4)$$

The pressure coefficient $C_p(x)$ can be written as

$$C_p(x) = -2\,\delta^{\frac{2}{3}}\, \partial\varphi/\partial x\ (x, 0) \quad (5.5)$$

$$= \frac{2\delta}{\pi\sqrt{1 - M_\infty^2}} \int_{-1}^{1} \frac{f'(\xi)}{\xi - x}\, d\xi$$

Thus equation (5.5) gives the pressure coefficient along the cavity wall, in terms of the shape of the stream line separating the outer inviscid flow and the viscous flow closer to the wall, assuming that the pressure does not vary much in the y-direction through the viscous flow. Calculations have been performed for $C_p(x)$ with different assumptions for the separation streamline.

5.2.2 Inverse Computations

Assuming that $C_p(x)$ is known along the cavity wall, say, by experimental measurements, equation (5.5) can be solved as an integral equation and thus obtain $f(x)$, or, the shape of the invsicid streamline which can produce the given C_p. Equation (5.5) is rewritten as

$$\frac{1}{\pi} \oint_{-1}^{1} \frac{f'(\xi)}{\xi - x}\, d\xi = g(x) = \frac{C_p(x)\sqrt{1 - M_\infty^2}}{2\delta} \quad (5.6)$$

The left hand side term is a singular operator of $f'(\xi)$ known as Finite Hilbert operator which has a non-unique inverse operator. We can write the inverse solution as

$$f'(x) = -\frac{1}{\pi} \oint_{-1}^{1} \sqrt{\frac{1-y^2}{1-x^2}} \frac{g(y)}{y-x}\, dy + \frac{A}{\sqrt{1-x^2}} \qquad (5.7)$$

where A is an arbitrary constant. The right hand side of equation (5.7) has integrable singularities at both $x = -1$ and $x = 1$. We can integrate equation (4.7) and determine the integration constant and the arbitrary constant A by the condition that

$$f(x) = 0, \quad \text{at } x = \pm 1. \qquad (5.8)$$

$$f(x) = \int_{-1}^{x} f'(t)\, dt \qquad (5.9)$$

$$= -\frac{1}{\pi} \int_{-1}^{x} \oint_{-1}^{1} \sqrt{\frac{1-y^2}{1-t^2}} \frac{g(y)}{y-t}\, dy\, dt + A \int_{-1}^{x} \frac{dt}{\sqrt{1-t^2}}$$

The first integral in the above equation is zero at $x = 1$. Thus we obtain $A = 0$ and

$$f(x) = -\frac{1}{\pi} \int_{-1}^{x} \oint_{-1}^{1} \sqrt{\frac{1-y^2}{1-t^2}} \frac{g(y)}{y-t}\, dy\, dt \qquad (5.10)$$

This expression can be further simplified. After a lengthy manipulation of the integrals involved we can obtain

$$y(x) = \delta f(x) = -\frac{\sqrt{1-M_\infty^2}}{2\pi} \oint_{-1}^{1} \ln \left| \frac{r(\tilde{y}) + r(x)}{r(\tilde{y}) - r(x)} \right| C_p(\tilde{y})\, d\tilde{y} \qquad (5.11)$$

where $r(x) = \{(1-x)/(1+x)\}^{\frac{1}{2}}$

Thus, the inviscid stream line which produces a specific C_p distribution can be computed by the equation (5.11). For a specific case of experimental data for the pressure coefficient $C_p(x)$ along the cavity wall, the inviscid stream line shape

along the cavity wall which corresponds to the measured C (x) has been computed. Figure 32 gives these results. The downward turn of the inviscid streamline near the rearward facing step indicates the significant thinning of the viscous flow just before the corner. These calculations give a reasonably good approximation for the outer inviscid flow stream line under the assumption of dp/dy = 0 in the viscous layer. These computations can be extended for obtaining the entire inviscid flow field.

5.2.3 Transonic Small Disturbance Equations

The transonic small disturbance theory equations for flow past an infinite flat wall with a cavity can be written as

$$(K - \varphi_x)\,\varphi_{xx} + \varphi_{\bar{y}\bar{y}} = 0\,, \qquad \bar{y} = \delta^{\frac{1}{3}}\, y \tag{5.12}$$

$$K = (1 - M_\infty^2)/\delta^{\frac{2}{3}}$$

where φ and x and y are defined as before in Eq. (5.2)

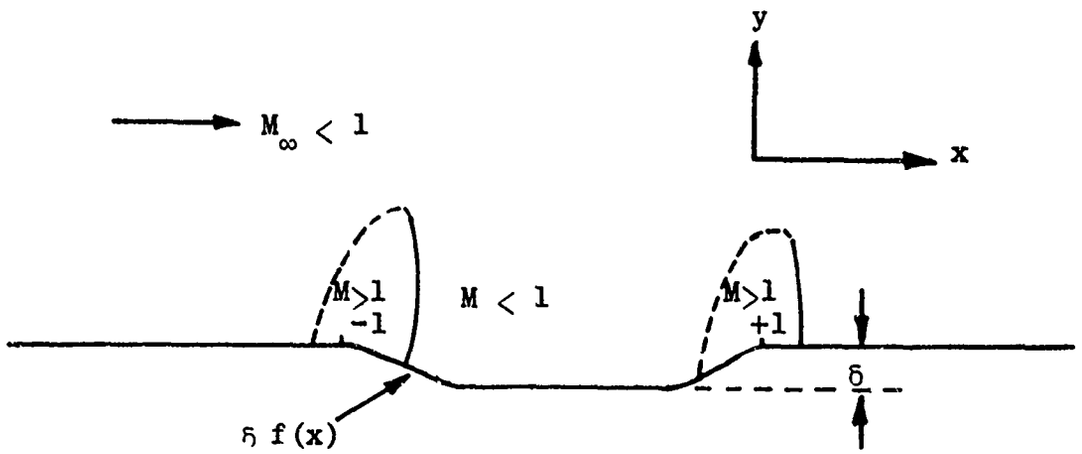

The boundary conditions are

At $\bar{y} = 0$,

$$\varphi_{\bar{y}}\,(x, 0) = f'(x), \qquad |x| < 1 \tag{5.13}$$

$$= 0\,, \qquad |x| > 1$$

As $x^2 + \bar{y}^2 \to \infty$, $\varphi \to 0$

Murman and Cole (Ref. 33) have solved transonic small disturbance equations for flows past a symmetric airfoil without lift by a difference method. They used a mixed finite difference scheme which used for x-derivatives elliptic difference operators in regions where the flow is subsonic and hyperbolic difference operators where the flow is supersonic and for y-derivatives elliptic difference operators everywhere. The non-linear difference equations are solved by a line relaxation technique. Krupp has generalized this method to include airfoil flows with lift. We have secured a modified version of the computer program of Krupp from NASA Ames and adapted it to our problem. The adaptation mainly involves the treatment of boundary conditions and corresponding changes in the way the iterative equations are solved.

The computational results for certain cavity shapes are shown in Figs. 33 to 35. These cavity configurations are hypothetical, but they do indicate the trend of inviscid transonic flow past a cavity. In the next phase of study, there will be experimental measurements for different types of cavities and it will be attempted to match the computations with measured data.

5.3 BOUNDARY LAYER CALCULATIONS

Despite their limitation to flows without separation, the boundary layer equations can be usefully employed in a number of calculations. In this section some results of such studies and also directions in which future work should proceed will be indicated.

For the turbulent flow, all boundary layer calculations to date have been undertaken with the aid of the integral method of Nash (Ref. 34). One point of a general nature should be made here concerning the comparison between theoretical and experimental results. The measured velocity profiles (see section 4) are not too well defined very close to the wall. This can lead to errors in the values for such integral quantities as momentum thickness. Any comparisons between theory and experiment must be made along with contemplation of this observation. The theory, of course, has other deficiencies.

5.3.1 Flow on the Floor of a Cavity

The flow on the floor of a cavity is sketched below.

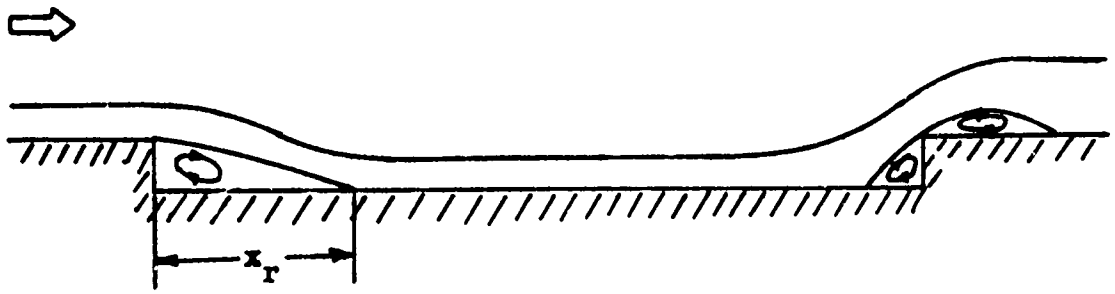

One central feature of a separated flow relates to the reattachment of a shear layer and its subsequent development as a boundary layer. From a theoretical point of view, the problem cannot be treated in the context of boundary layer theory since the flow is not characterized by a small length scale normal to the flow direction.

Two objectives can be delineated. First, the applicability of boundary layer theory to the flow immediately downstream of the reattachment point, x_r, can be discussed by performing calculations for the flow on the floor of the cavity. In such calculations, the experimentally determined starting conditions are used and also the experimental pressure distribution along the cavity floor. Second, the experimental data can be utilized to provide empirical information as an aid to theoretical developments.

At a free-stream Mach number of 0.56 and Reynolds number of 0.4×10^6 per inch, measured initial conditions just downstream of the experimentally determined reattachment point showed that $\theta = 0.193$ inches and the form factor $H = 2.82$. In the computer program, these were not acceptable initial conditions since when introduced into the empirical relation for the skin friction, they indicated a negative value for this quantity. It was found that if the initial values $\theta = 0.21$ inches, $H = 2.68$ were taken, then no such difficulties existed, the indicated skin friction then being just positive. However, the numerical technique in the computer program at hand was divergent for any chosen x-step away from the initial condition. That is, it was found impossible

to integrate the boundary layer equations away from the reattachment point with the current empirical relations for the associated turbulent flow quantities.

Some comments can be made concerning the reason for the experimental initial values being unacceptable in the theoretical work. The empirical information contained in the theory of Ref. 34 was all derived from boundary layer type flows. Here just at the stagnation condition, the flow is not of boundary layer type, even though the skin friction is non-negative. The reason lies more in the fact that in the outer flow, the normal component of velocity is still very large, greater than the 0 ($Re^{-\frac{1}{2}}$) demanded by the theory*. At the same time, there is, as mentioned above, uncertainty in the measured values of the integral properties.

It is unlikely that anything other than a solution for the full Navier-Stokes equations will be satisfactory in providing adequate solutions for flows of this type.

5.3.2 Development of the Boundary Layer Over the Flat Plate Ahead of the Cavity

The situation is as indicated diagramatically below.

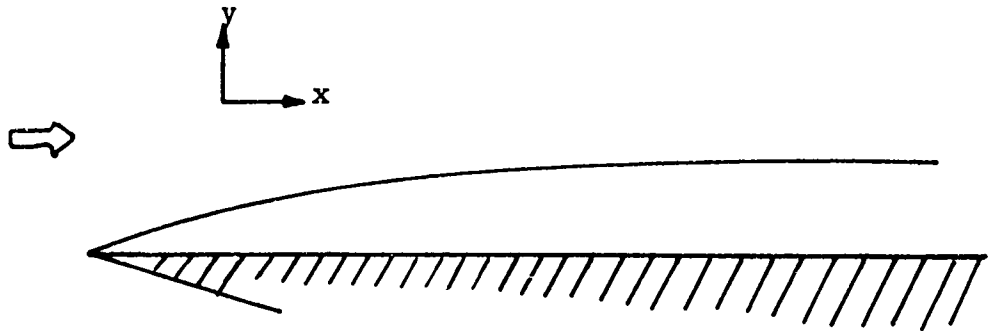

The same boundary layer theory as discussed above (Ref. 34) was used to check the measured boundary layer velocity profiles on the flat plate part of the model ahead of the step or cavity location. The comparison is shwon in Fig. 36.

*This is for laminar flow--the turbulent flow counterpart will be somewhat modified.

It is seen from this result that the measured boundary layer is somewhat thinner than that predicted by the theory. Several comments are in order concerning this finding. The calculation reported was based on flow starting at the leading edge of the plate and proceeding under a constant pressure. The real flow, on the other hand, will contain a slight pressure variation near the rounded leading edge. The two flows are not, therefore, strictly comparable.

5.3.3 Comments on Separation

It was remarked earlier that the boundary layer equations cease to be valid when the boundary layer is in a situation where the skin friction is almost zero. The equations lose their validity because the boundary layer region is no longer of thickness 0 ($Re^{1/n}$). On its own, this loss of validity would not cause the boundary layer equations to breakdown completely at separation. There is an additional reason for this.

Consider as an example, the boundary layer momentum equation for a steady incompressible fluid:

$$u \frac{\partial u}{\partial x} + v \frac{\partial u}{\partial y} + \frac{1}{\rho} \frac{\partial p}{\partial x} = \upsilon \frac{\partial^2 u}{\partial y^2} + \tau \qquad (5.14)$$

where τ is a suitable representation for the contribution from the turbulent fluctuations. Now, as a consequence of the asymptotic matching, the pressure gradient is a prescribed function of x obtained from the outer solution. On rewriting the momentum equation as an equation for the x-wise derivative of velocity:

$$\frac{\partial u}{\partial x} = \frac{1}{u}\left[\upsilon \frac{\partial^2 u}{\partial y} + \tau - \frac{1}{\rho} \frac{\partial p}{\partial x} - v \frac{\partial u}{\partial y} \right] \qquad (5.15)$$

it is seen that this derivative becomes undevined when u vanishes--as it will on some line in a separation region. In the full Navier Stokes equations however, (see Ref. 35)

the pressure field is determined as part of the solution and the above contingency does not arise.

It is often reported that the parabolic nature of the boundary layer equations, implying as it does that the solution at any given station is dependent only on conditions upstream, will preclude the possibility of profiles with negative velocities. That this is not so may be shown by consideration of the linearized parabolic equation:

$$\frac{\partial U}{\partial x} + F(x) = \lambda \frac{\partial^2 U}{\partial y^2} \tag{5.16}$$

Then, if $\lambda(y)$ is the initial profile at $x = 0$, it is readily found that the function $U(x, y)$ is given as:

$$U(x, y) = \Gamma(y) - \int_0^x F(\xi) \operatorname{erf}\left\{ \frac{y}{\sqrt{\lambda (x - \xi)}} \right\} d\xi \tag{5.17}$$

Some algebra then shows that

$$\left.\frac{\partial U}{\partial y}\right|_{y=0} = \left.\frac{d\Gamma}{dy}\right|_{y=0} - \int_0^x \frac{F(\xi)}{\sqrt{\pi\lambda\ (x - \xi)}}\ d\xi \tag{5.18}$$

and $\partial U/\partial y)_{y=0}$ can take either sign depending upon the nature of $F(x)$. Typical streamlines determined from this solution are presented in Fig. 37.

All this exercise does is to indicate that a parabolic type equation is capable of producing a solution space somewhat reminiscent of flow separation. It is not to be construed as a suggested technique for solving separation problems. As has been stated above, only the Navier-Stokes equations are acceptable for this.

6.0 CONCLUSIONS

The first phase of an experimental and theoretical program to study the upstream influence on the subsequent separation of a turbulent boundary layer has been conducted by employing long and shallow cavity models in subsonic and transonic flows. The experiments have been carried out with a natural turbulent boundary layer developing from the model leading edge. The extraordinarily long model results in a Reynolds number variation which covers the range from wind tunnel model scale to actual flight conditions. Therefore, this is the first step toward an understanding of the scaling effect as well as the phenomenon of flow separation, rehabilitation and its ability in negotiating an adverse pressure gradient.

The flow fields have been measured by densely placed wall static pressure taps and a traversing pitot probe. The static pressure variation in subsonic flow due to a forward facing step as well as due to the upstream disturbances produced by a rearward facing step have been studied carefully. It is shown that increasing the Mach number or Reynolds number will cause an increase of the separation and the peak pressures ahead of the forward facing step. However, the effect of Mach number and Reynolds number upon the separation distance ahead of a forward facing step is rather weak. The upstream influence of pressure rise can be very significant and extend twenty to thirty step heights ahead of the step. The normalized separation pressure variation with the normalized cavity length shows that a shorter cavity can generate a higher separation pressure. However, the influence of cavity length on the separation needs to be further studied.

Detailed velocity profiles are obtained by the pitot pressure measurements. These profiles indicate that the upstream disturbance extends very far downstream. They also indicate that the static pressure recovers faster than the velocity profiles. This implies that the relaxation distances for the pressure and the shear velocity profile are different. The velocity profiles have been analyzed by the wall and wake law and the departure from the wall component studied. The results indicate that the higher Mach number

or Reynolds number delays this departure. They show that the law of wall and wake can be employed for such an analysis.

A theoretical study employing a small disturbance transonic flow technique has been conducted. Also, an inverse method based on subsonic small disturbance theory has been developed to compute the inviscid flow stream lines for flow past shallow cavities corresponding to the experimentally measured surface pressure distributions. This, together with the transonic flow computer program adapted to inviscid flows past shallow cavities, provides a tool for correlating experimental pressure data at different Mach numbers. At transonic speeds, two supersonic pockets near the rearward and the forward facing steps have been identified. This needs to be extended to cover the flow over an airfoil with a separation and a wake. Through such a study, it is hoped that a better understanding of the transonic flow scaling problem can be obtained.

REFERENCES

1. Howarth, L. (Ed) Modern Developments in Fluid Dynamics--High Speed Flow, Oxford University Press, 1953.

2. Morawetz, C. S., "On the Non-Existence of Continuous Transonic Flows Past Aerofoils," Communications in Pure and Applied Mathematics, Vol. 9, p. 45, 1956.

3. Nieuwland, G. Y. and Spee, B. N., "Transonic Shock-Free Flow, Fact or Fiction?" AGARD C. P. 35, 1968.

4. Moulden, T. H., Cox, I. J. and Stringfellow, V. A., "A Preliminary Investigation of Shock Wave Development On Airfoils," APC CP 964, 1967.

5. Spee, B. H., "Wave Propagation in Transonic Flow Past Two-Dimensional Aerofoils," NLR TN T123, 1966.

6. Stanewsky, E. and Little, B. H., "Studies of Separation and Reattachment in Transonic Flow," AIAA Paper 70-541, 1970.

7. Studwell, V. E., "Investigation of Transonic Aerodynamic Phenomena for Wing Mounted External Stores," Ph.D. Thesis, Univ. of Tenn., 1973.

8. Liepmann, H. W., "The Interaction Between Boundary Layer and Shock Waves in Transonic Flow," J. Aero Sci., Vol. 13, p. 623, 1946.

9. Green, J. E., Interaction Between Shock Waves and Turbulent Boundary Layer. Progress in Aerospace Sciences, Vol. 11, Pergamon Press, 1971.

10. Pearcey, H. H., The Aerodynamic Design of Section Shapes for Swept Wings, Vol. 3-4, Advances in Aeronautical Sciences, Pergamon Press, 1961.

11. Blackwell, J. A., "Preliminary Study of the Effects of Reynolds Number and Boundary Layer Transition Location on Shock Induced Separation," NASA TN D5003, 1969.

12. Lumsdaine, E., "Study of Shock Wave and Turbulent Boundary Layer Interaction Using the Energy Integral Equation," 13th Midwestern Mechanics Conference, 1973.

13. Seddon, J., "The Flow Produced by Interaction of a Turbulent Boundary Layer With a Normal Shock Wave of Strength Sufficient to Cause Separation," ARC R&M 3502, 1960.

14. Howell, R. H. and Korst. H. H., "Drag Associated With Separated Flow O Two-Dimensional V-Shaped Notches Under Tra.. ic and Supersonic Conditions," NASA CR-1132, 1968.

15. Whitfield, J. D., Schueler, C. J. and Starr, R. F., "High Reynolds Number Transonic Wind Tunnels-- Blowdown or Ludwieg Tube," AGARD CP 83, 1971. Also AIAA Paper 73-212, 11th Aerospace Sciences Meeting, Washington, D. C., January, 1973.

16. Lo, C. F. and Carleton, W. E., "Transonic Scaling Effect on a Quasi Two-Dimensional C141 Airfoil Model," AEDC-TR-73-61, 1973.

17. Goethert, B. H., Transonic Wind Tunnel Testing, Pergamon Press, 1961.

18. Goethert, B. H., "Research and Engineering Studies and Analysis of Fan Engine Stall, Dynamic Interaction With Other Subsystems and System Performance," Air Force Aero Propulsion Laboratory AFAPL-TR-70-51, Wright-Patterson Air Force Base, Ohio, July, 1970.

19. Kinslow, Max, "Lag Time in Pressure Measuring Systems," Thesis, The University of Tennessee, 1959.

20. Gray, J. Don, "A Compendium of Flow Measurement Methods and Techniques," Short Course on "Flow Separation" at The University of Tennessee Space Institute, Tullahoma, Tennessee, Nov. 26-30, 1973.

21. Dudziniski, Thomas J. and Krause, Lloyd N., "Effect of Inlet Geometry on Flow Angle Characteristics of Miniature Total Pressure Tubes", NASA TN D-6406, July 1971.

22. Brederode, V. de and Bradshaw, P., "Three-Dimensional Flow in Nominally Two-Dimensional Separation Bubbles, in a Flow Behind a Rearward Facing Step," I. C. Aero Report 72-19, August, 1972.

23. Robertson, J. M. and Taulbee, D. B., "Turbulent Boundary Layer and Separation Flow Ahead of a Step," Developments in Mechanics, Vol. 5, Proc. of 11th Midwestern Mech. Conf.

24. Stratford, B. S., "The Prediction of Separation of the Turbulent Boundary Layer," J. Fluid Mech. 5, 1958.

25. Nash, J. F., Quincey, V. G and Callinan, J., "Experiments on Two-Dimensional Base Flow at Subsonic and Transonic Speeds," ARC R&M 3427, 1963.

26. Wilson, R., and Maurer, F., "An Experimental Investigation of Turbulent Separated Boundary Layers at Low Supersonic Mach Numbers," DLR FB 70-33, 1970.

27. Coles, Donald, "The Law of the Wake in the Turbulent Boundary Layer," JFM Vol. 1, p. 191, 1956.

28. Van Driest, E. R., "Turbulent Boundary Layer in Compressible Fluids", J Aeronautical Science, 18, pp. 145-160, 1951.

29. Coles, D. E. (et. al.) Eds., Computation of Turbulent Boundary Layers-1968, Proceedings, Stanford Conference, 1968.

30. Lock, R. C., Powell, B. J., Sells, C. C. L. and Wilby, P. G., "The Prediction of Aerofoil Pressure Distributions for Sub-Critical Viscous Flows," AGARD CP 35, 1968.

31. Moulden, T. H., Spring, D. J. Saisi, R. O., Aoyama, K. and Wu, J. M., "Bodies of Revolution at Transonic Speeds: The Estimation of Reynolds Number Effects," AGARD CP 83. 1972.

32. Klineberg, J. M. and Steger, J. L., "Calculation of Separated Flows at Subsonic and Transonic Speeds," Proceedings Third International Conference on Numerical Methods in Fluid Mechanics, 1972.

33. Murman, E. M. and Cole, J. D., "Calculation of Plane Steady Transonic Flows," AIAA Journal, Vol. 7, p. 114, 1971.

34. Nash, J. F., "A Practical Calculation Method for Compressible Turbulent Boundary Layers in Two-Dimensional and Axially Symmetric Flows," Lockheed Georgia Research Memo, ER 9428, 1967.

35. Moulden, T. H. and Wu, J. M., "On the Conditions at the Separation Point of a Laminar Boundary Layer," ZAMM, Vol. 52, p. 248, 1972.

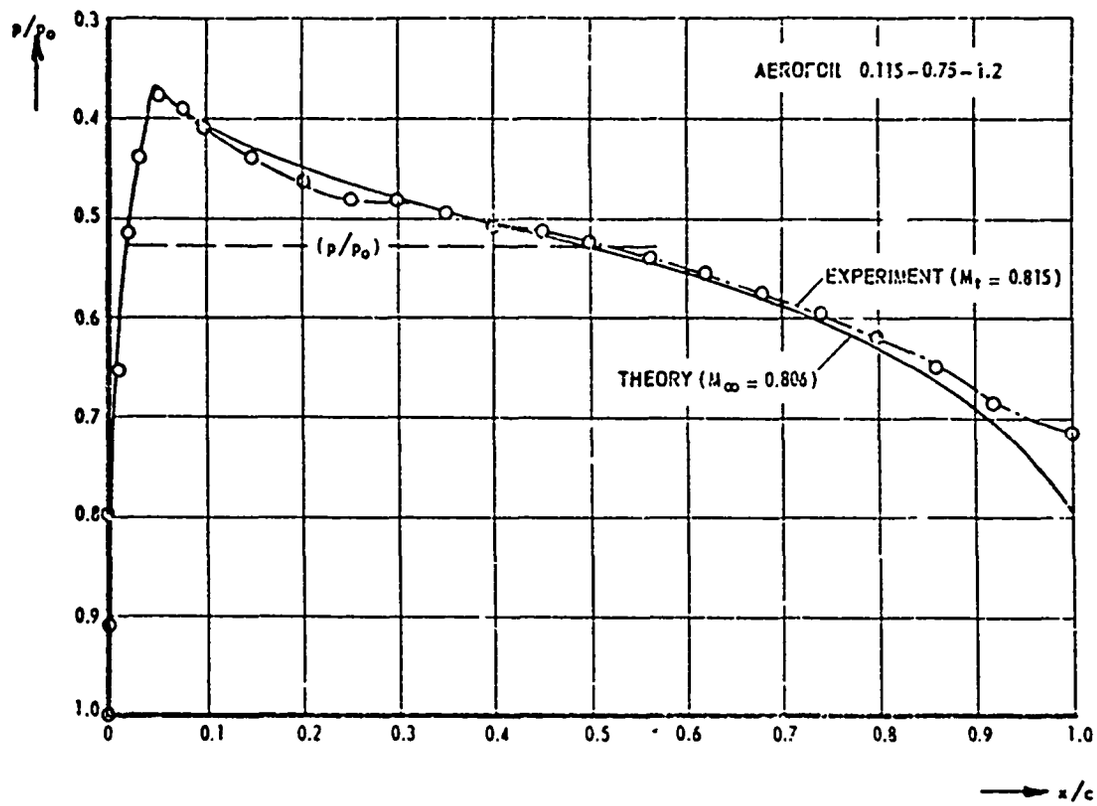

Figure 1. Comparison between theory and experiment for quasi-elliptic airfoil in transonic flow--data from Ref. (3).

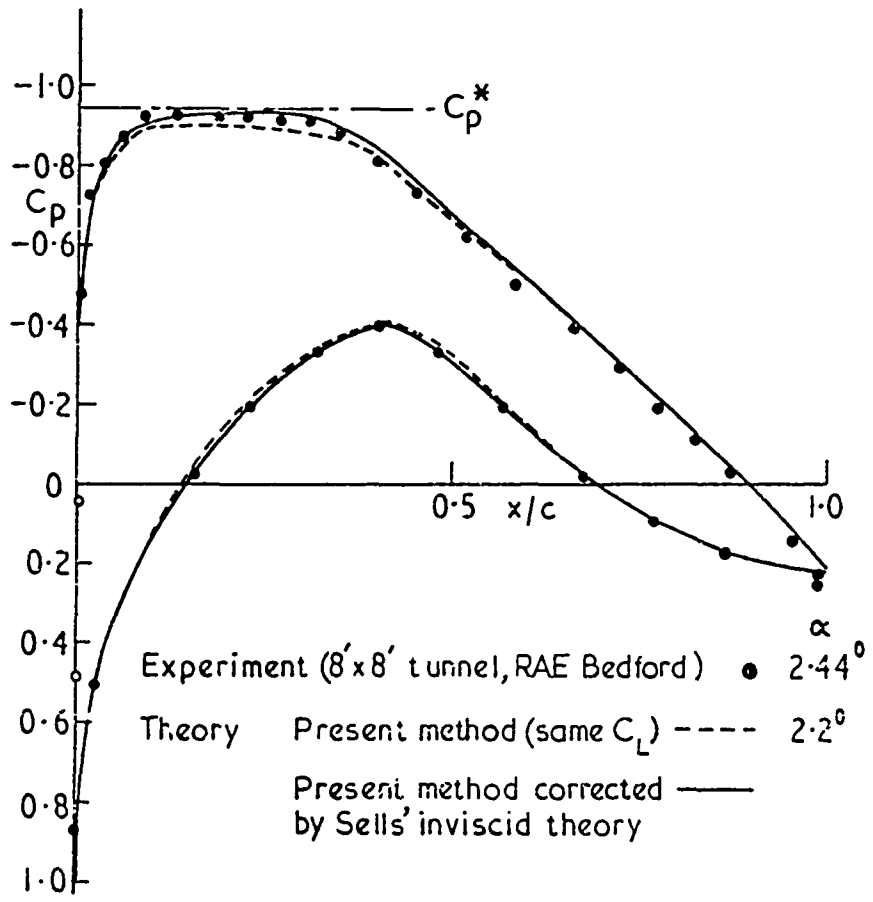

Figure 2. Comparison between theory and experiment for subsonic flow--data from Ref. (29).

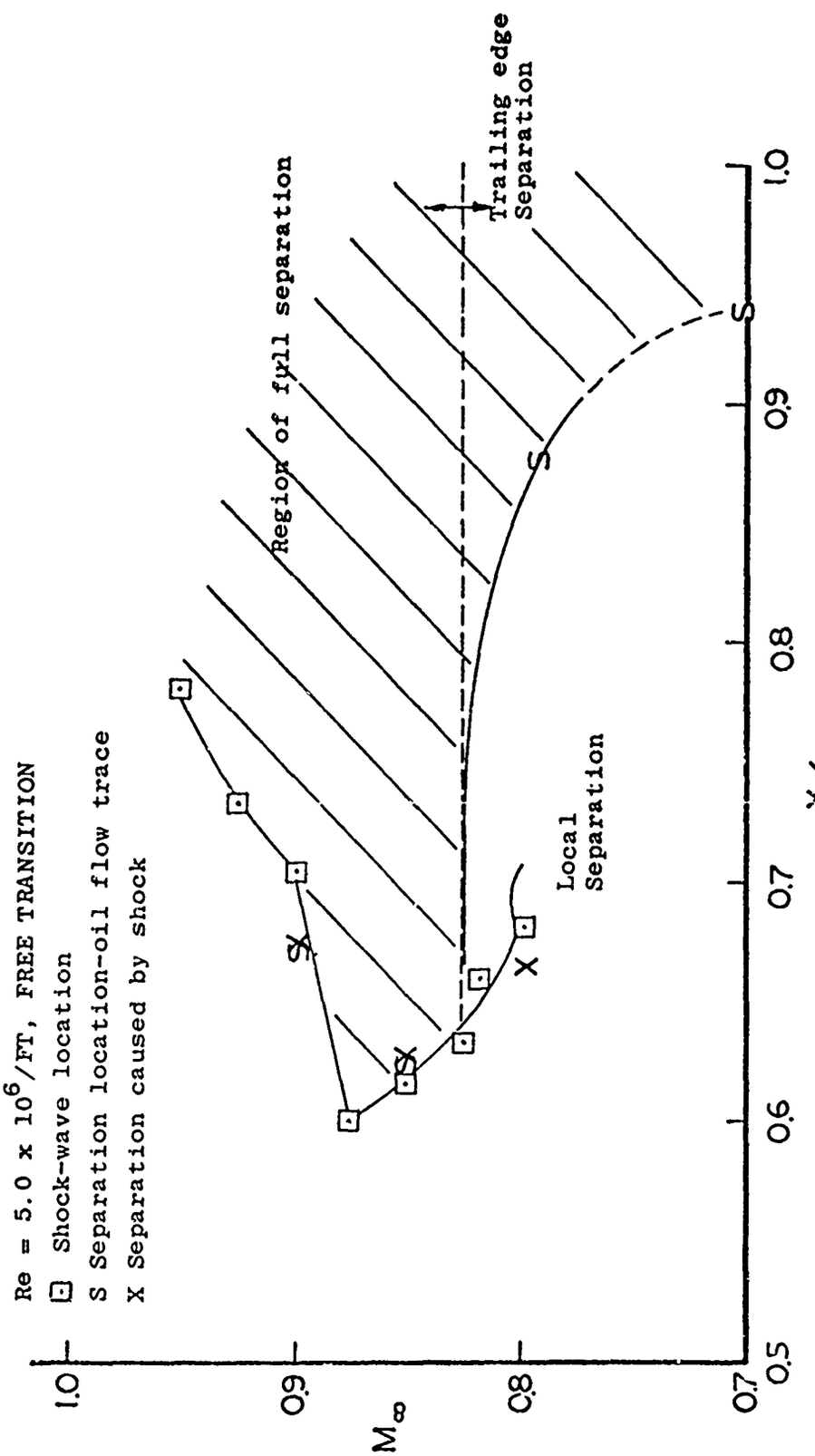

Figure 3. Variation of shock wave location with Mach number for C141 airfoil--from Ref. (7).

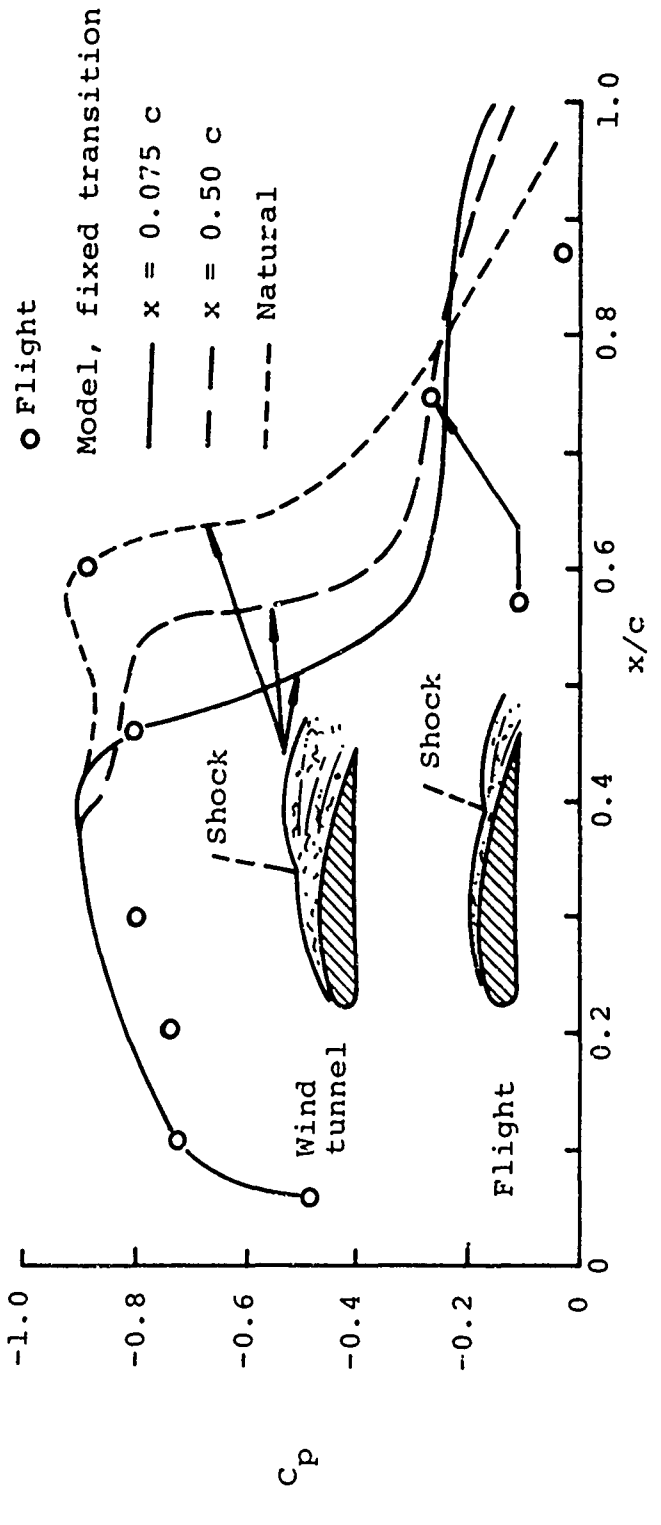

Figure 4. Surface pressure distribution showing strong influence of Reynolds number

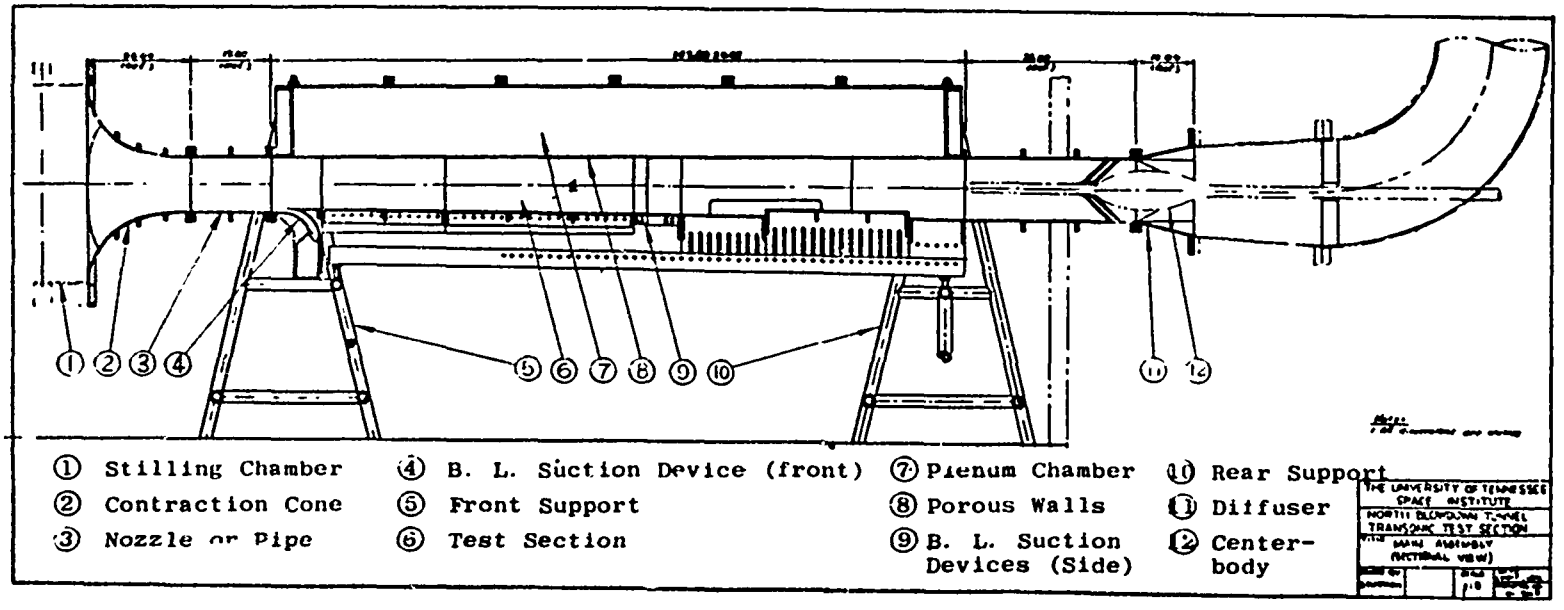

Figure 5. Sectional view of The University of Tennessee Space Institute wind tunnel.

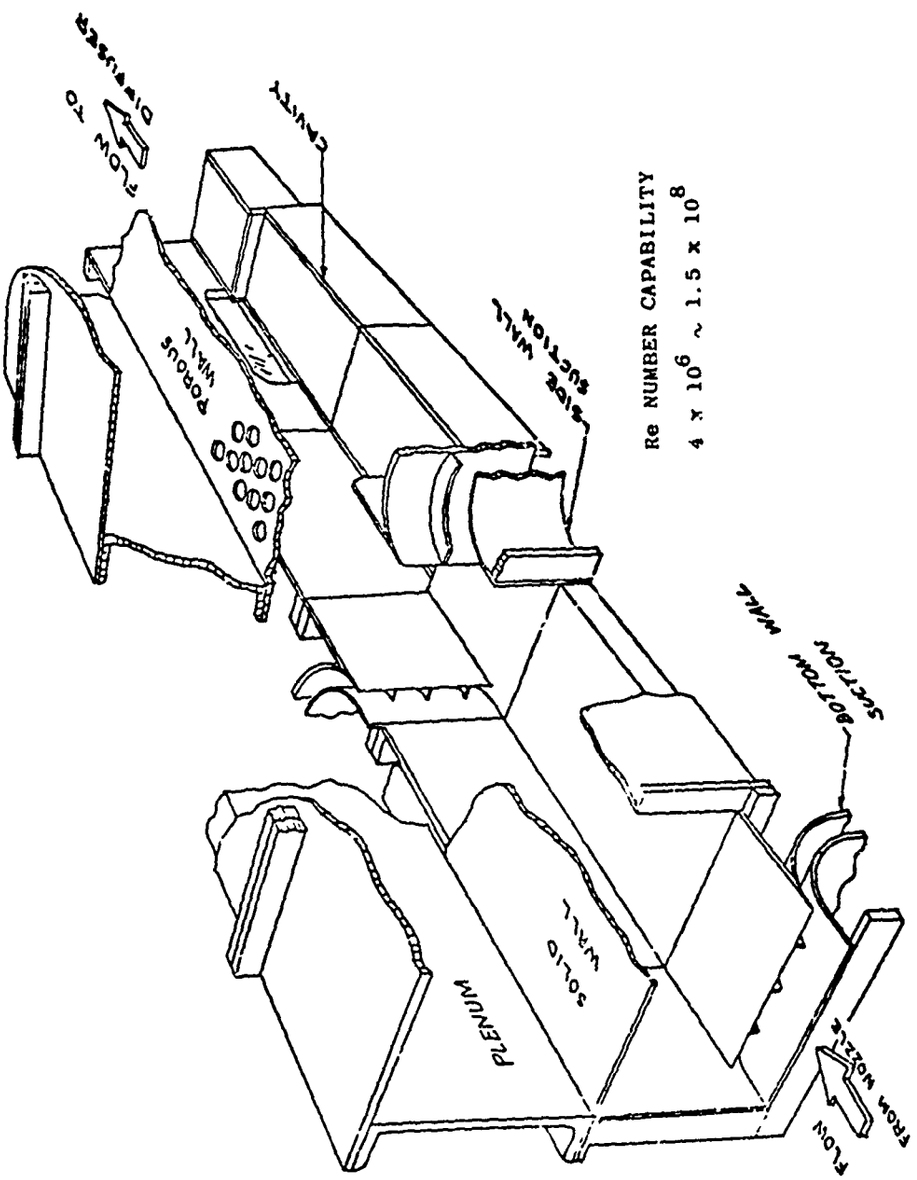

Figure 6. Pictorial view of test section.

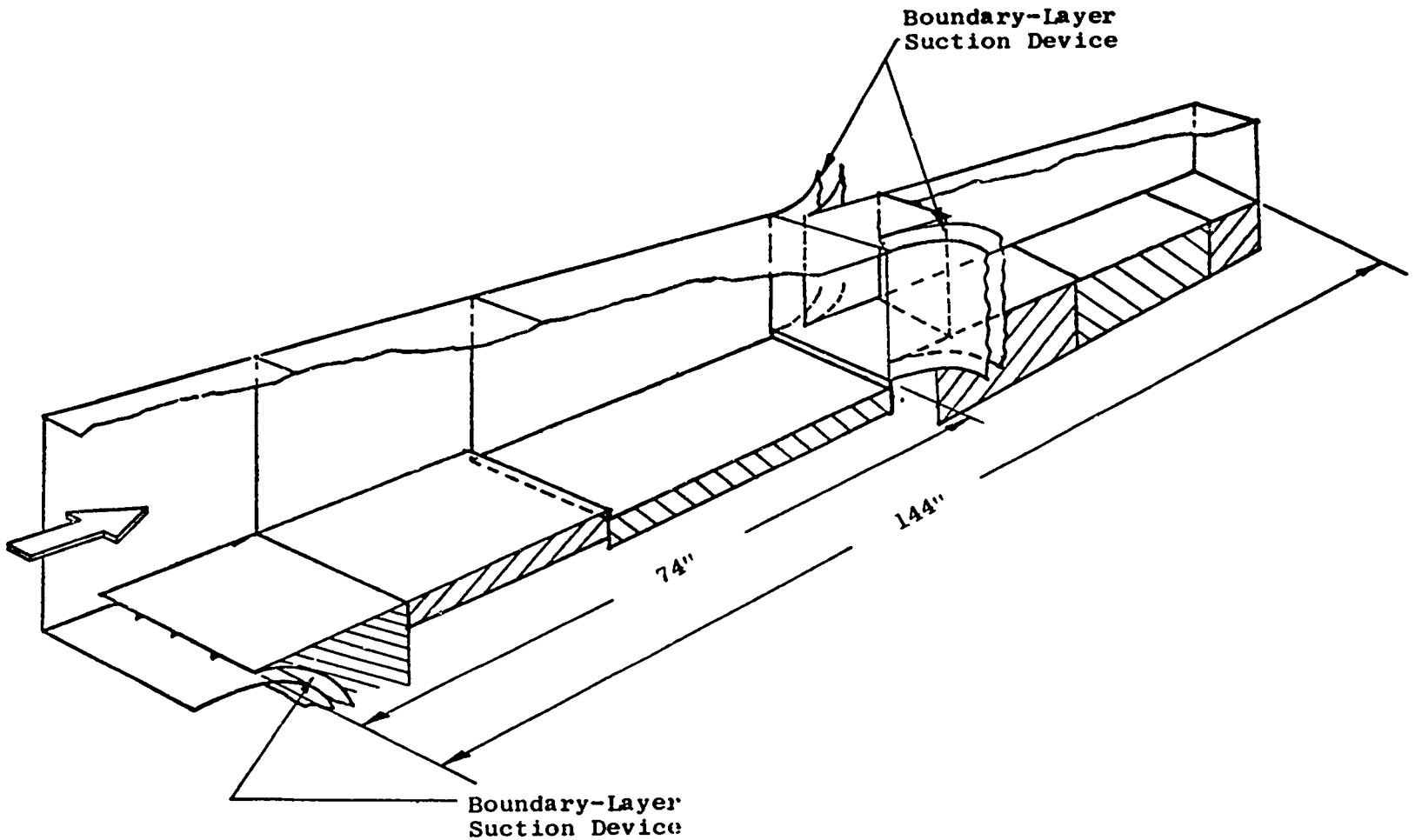

a. Pictorial View of Model Installation

Figure 7. Model configurations and dimensions

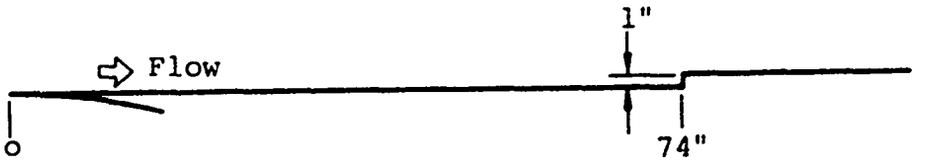

(b) Forward-facing step model

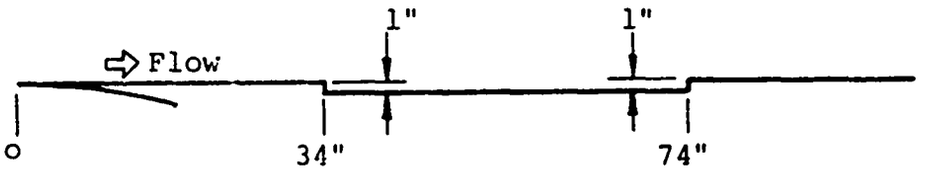

(c) 40-inch long shallow-cavity model

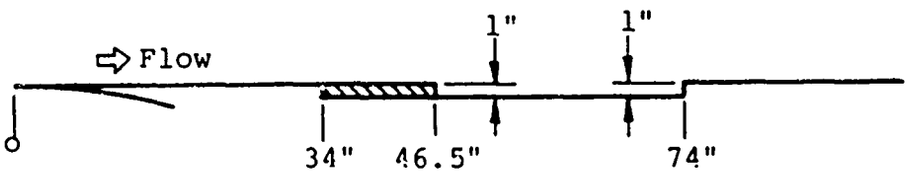

(d) 27.5-inch long shallow-cavity model

Figure 7. Concluded

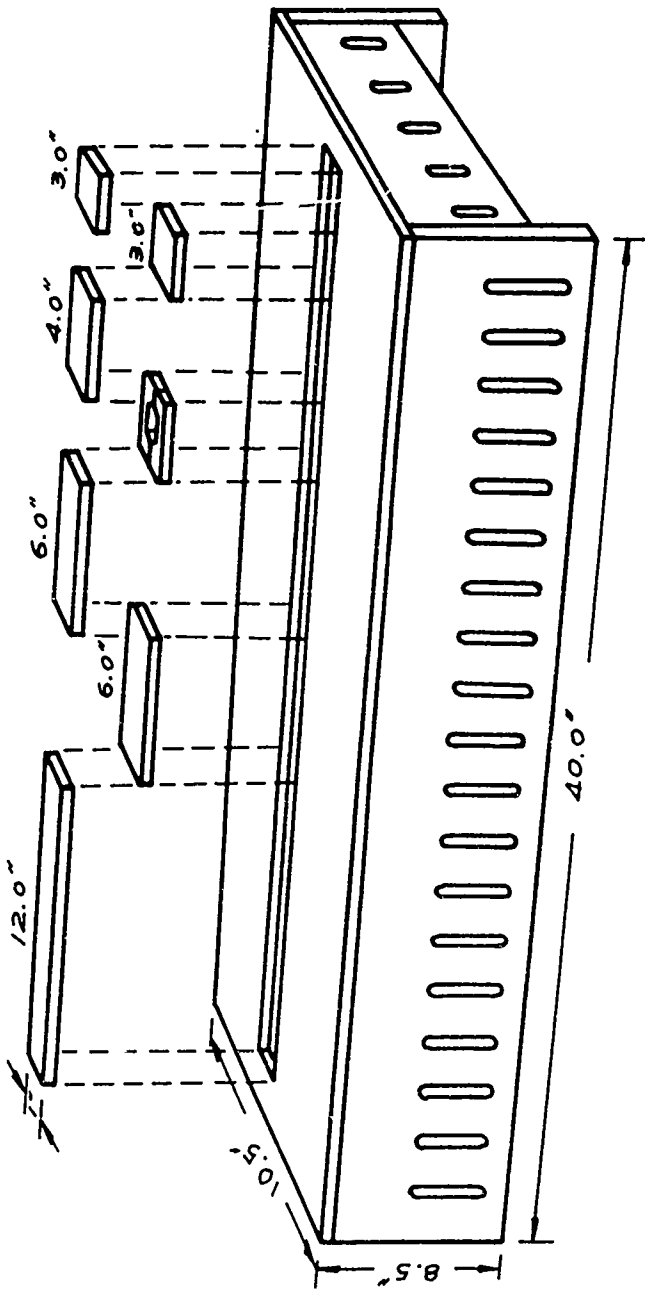

Figure 8. Typical slotted model block.

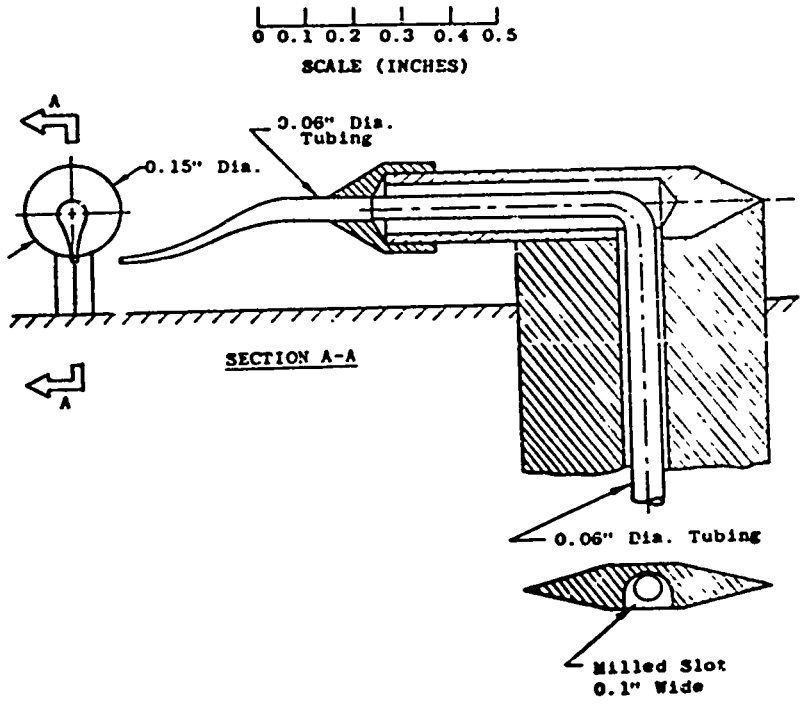

a. Cross-Sectional View

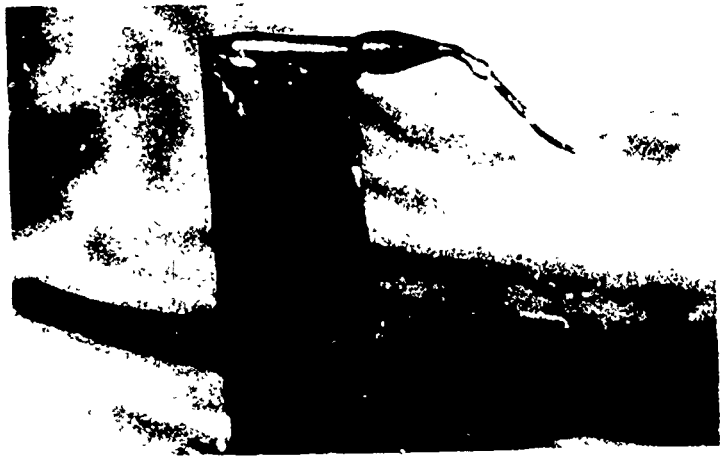

b. Pictorial View

Figure 9. Cross-sectional and pictorial view of traversing probe

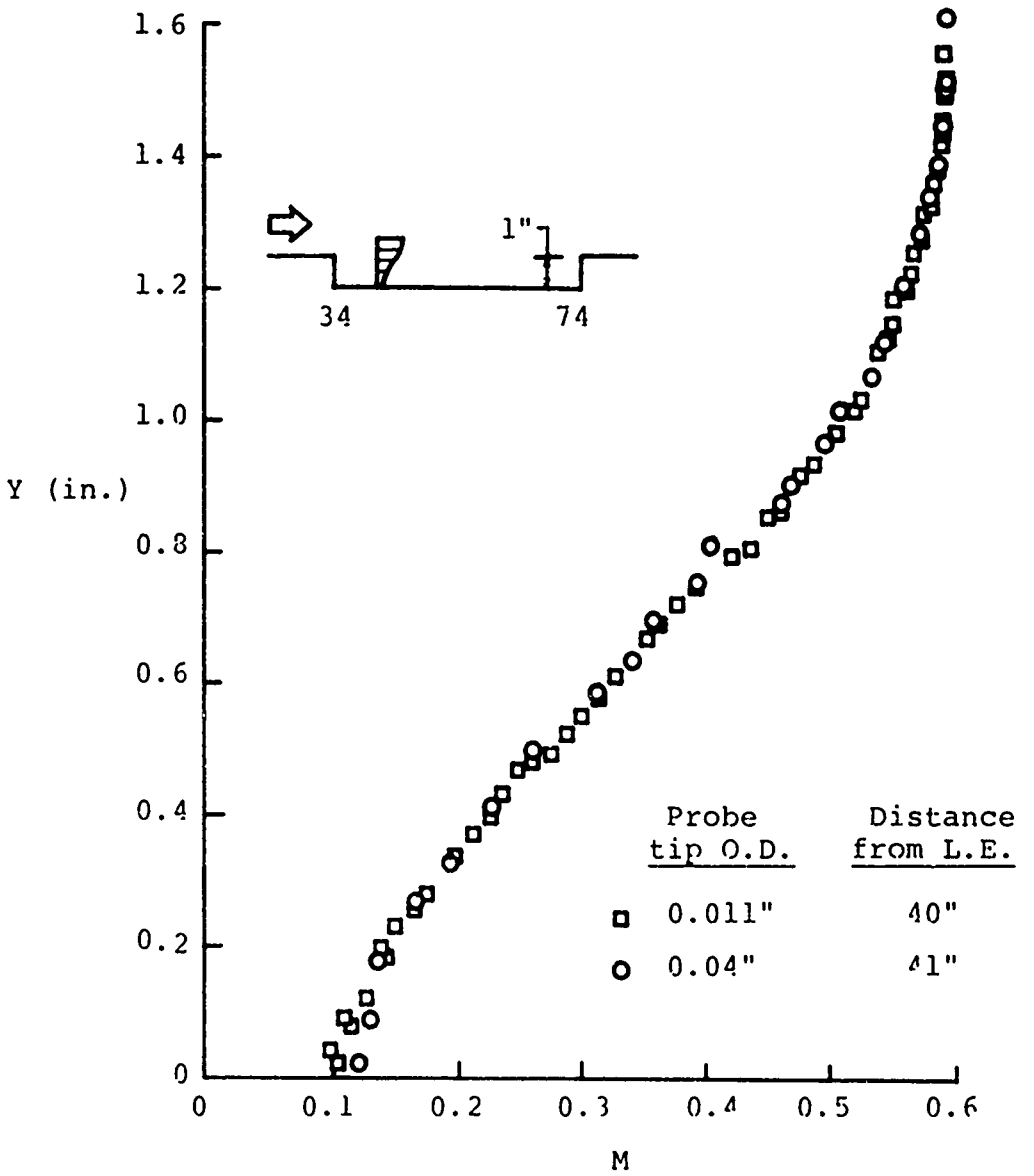

Figure 10. Repeatability of velocity profiles as measured by 0.011- and 0.04-inch pitot-probes.

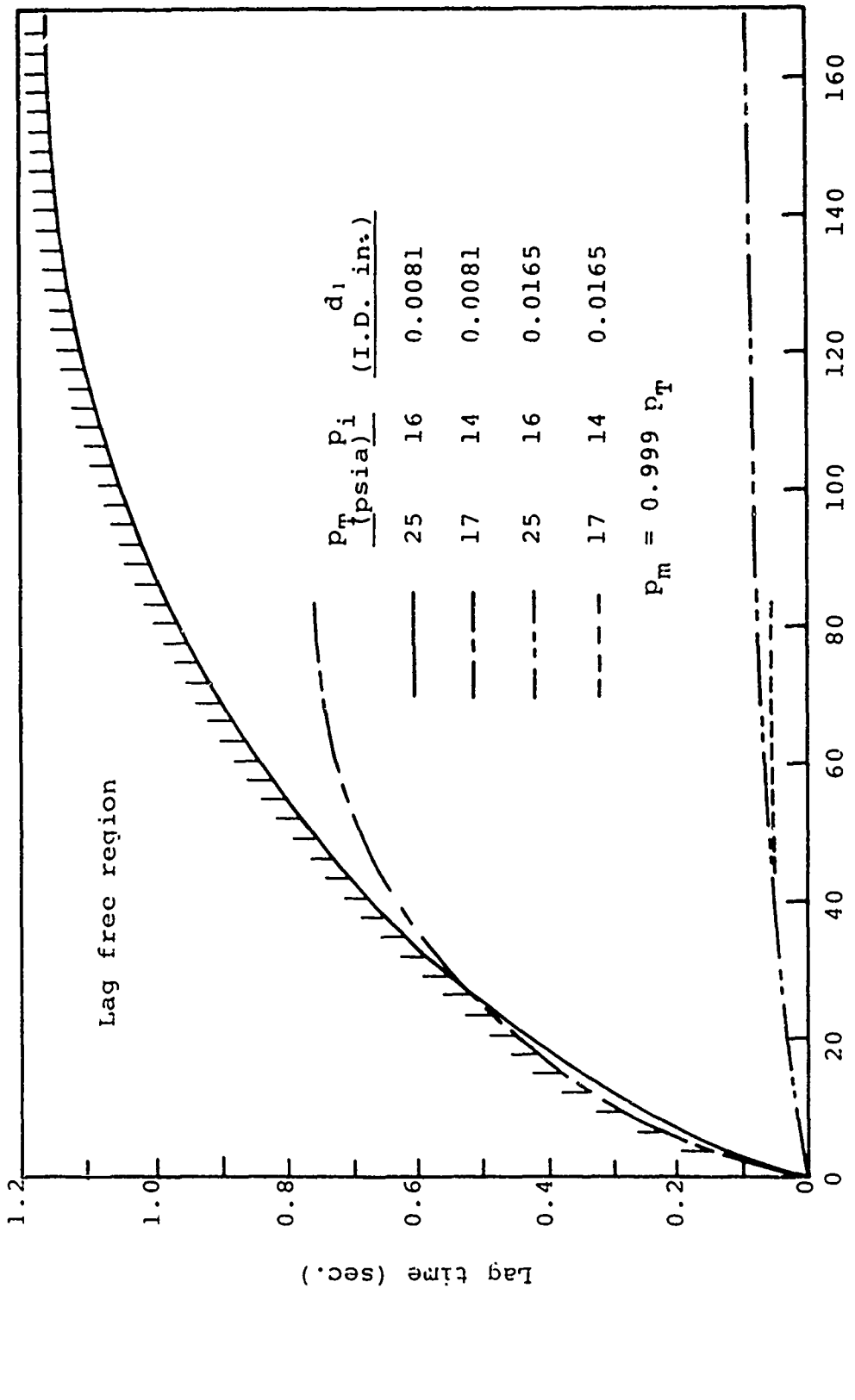

Figure 11. Theoretical values of pitot-probe lag time.

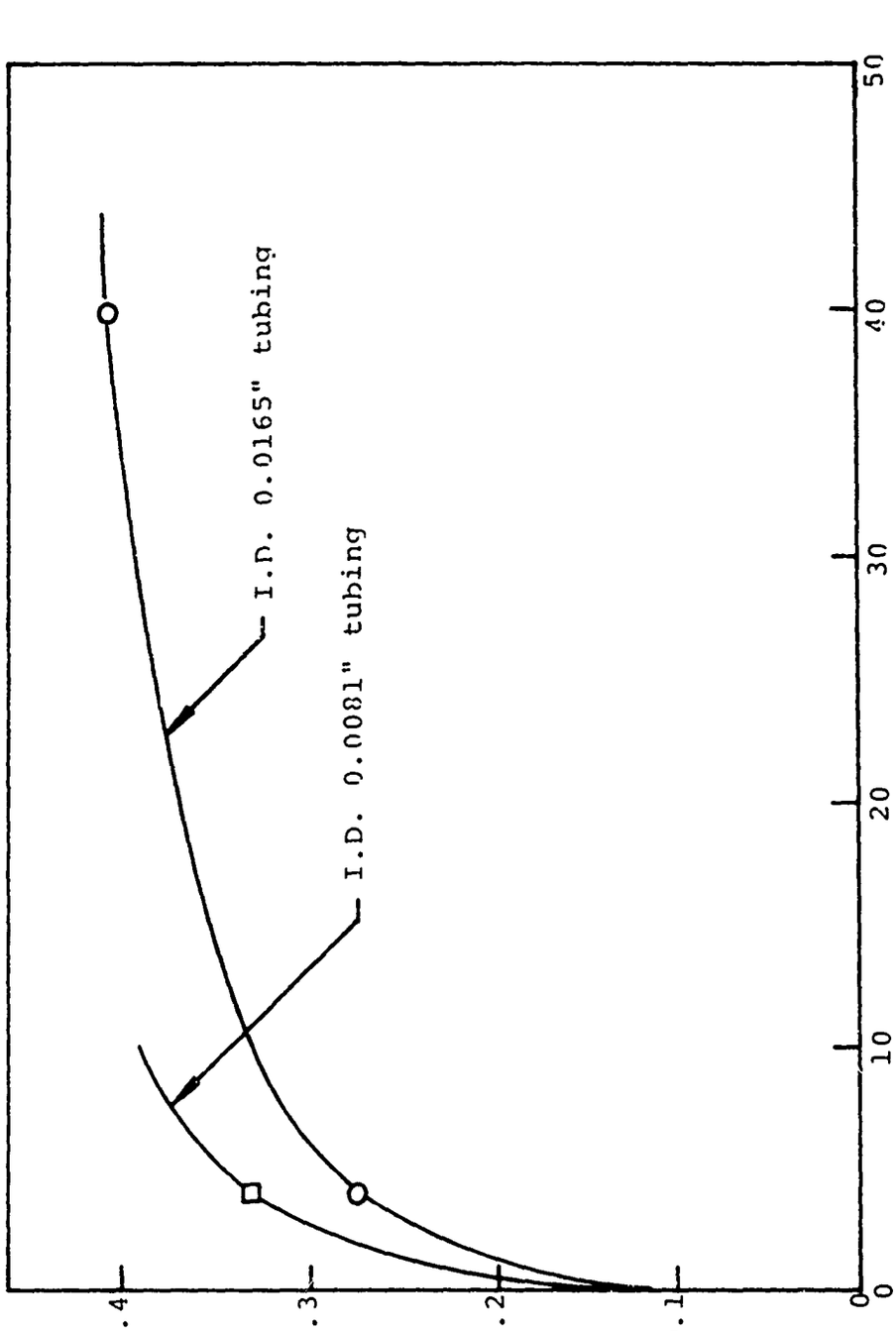

Figure 12. Calibration values of pitot-probe lag time.

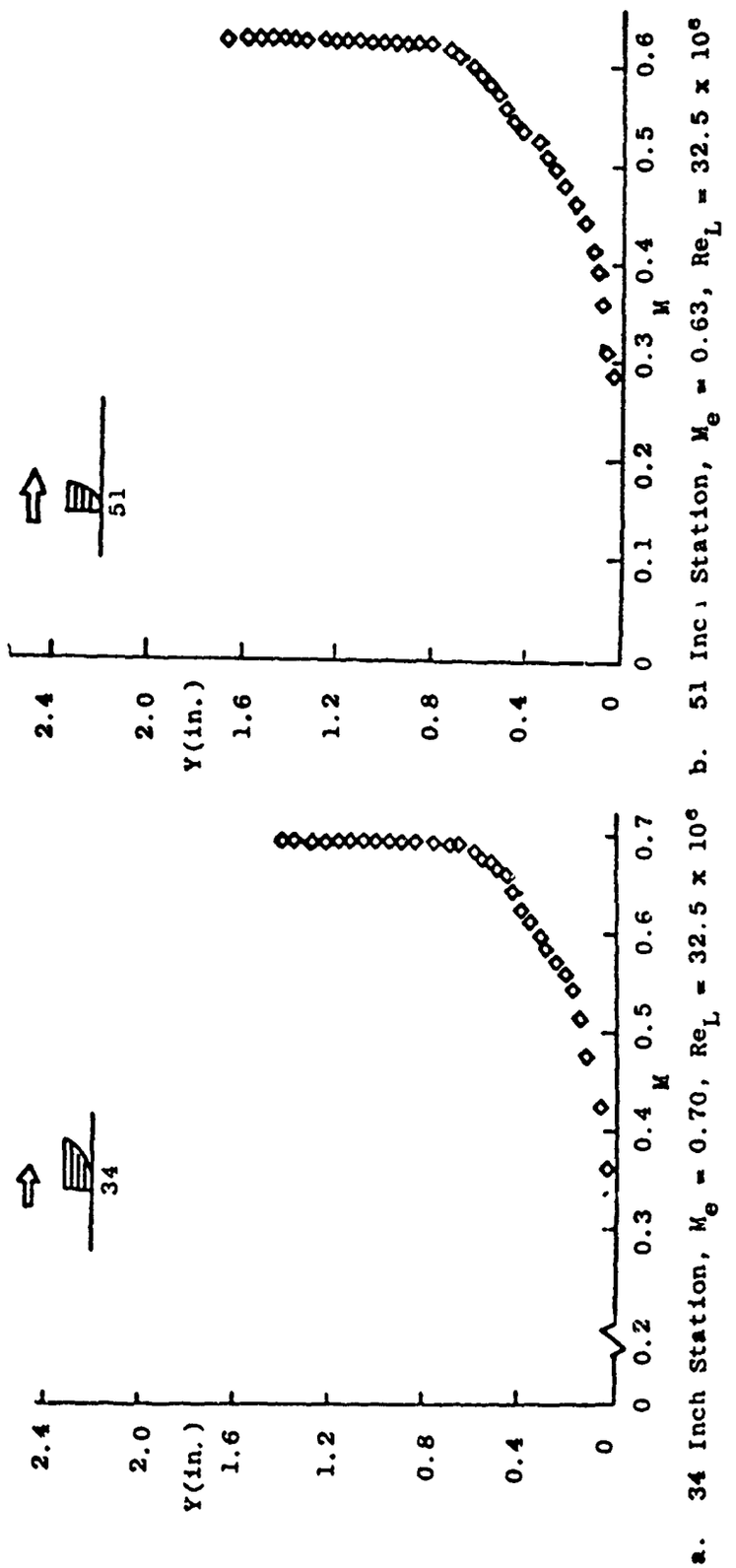

a. 34 Inch Station, M_e = 0.70, Re_L = 32.5 x 10^6 b. 51 Inch Station, M_e = 0.63, Re_L = 32.5 x 10^6

Figure 13. Velocity profiles on flat plate model

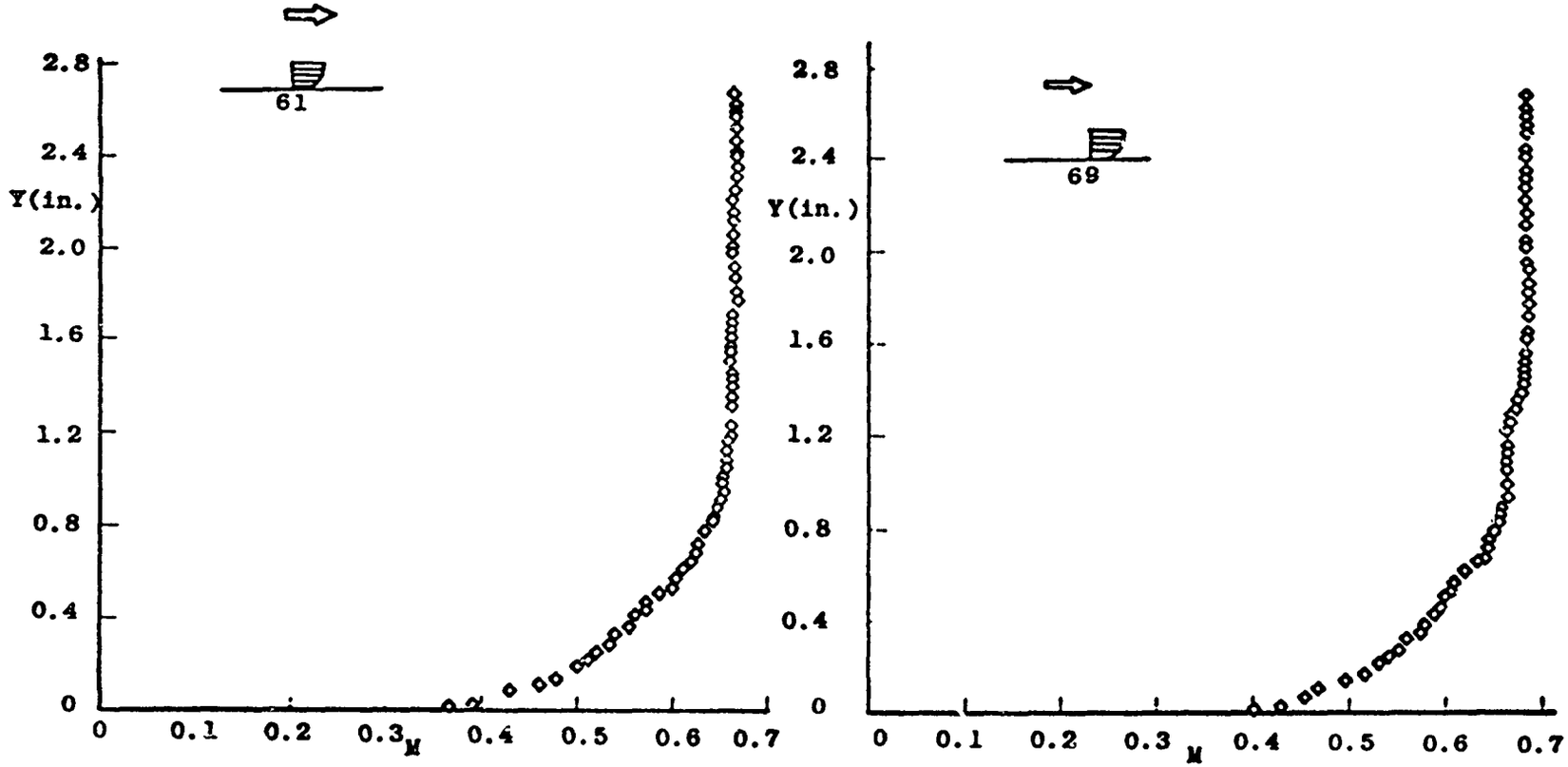

c. 61-inch Station, M_e = 0.66, Re_L = 32.5 x 10^6 d. 69-inch Station, M_e = 0.68, Re_L = 32.5 x 10^6

Figure 13. Concluded

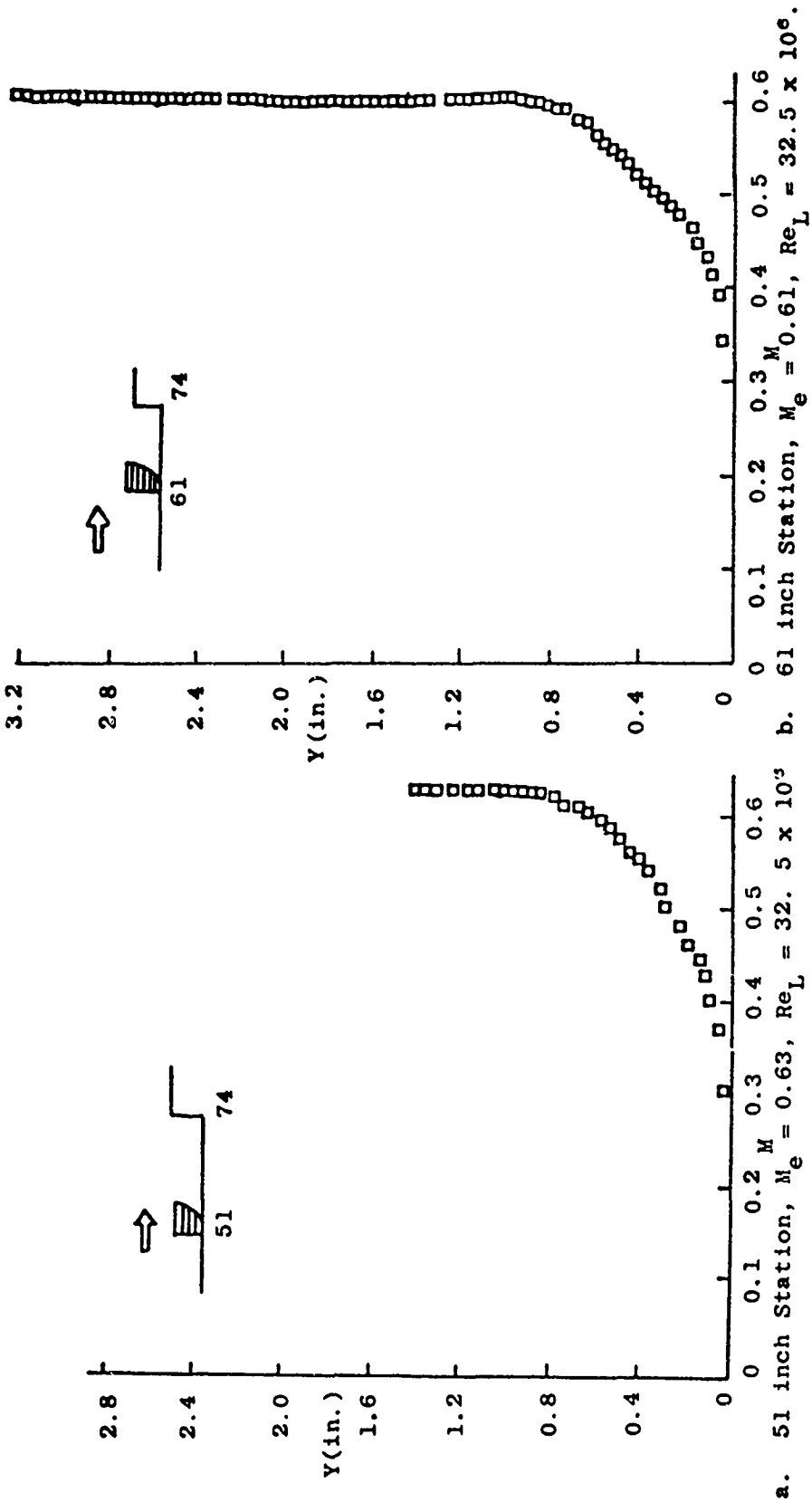

a. 51 inch Station, $M_e = 0.63$, $Re_L = 32.5 \times 10^6$ b. 61 inch Station, $M_e = 0.61$, $Re_L = 32.5 \times 10^6$.

Figure 14. Velocity profiles on forward facing step model

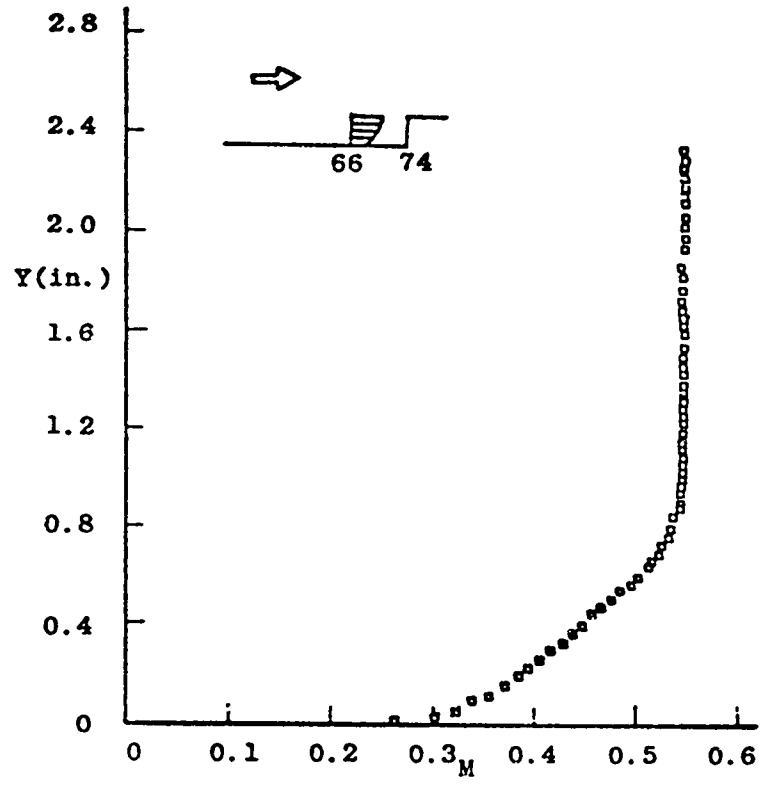

c. 66-inch Station, M_e = 0.55, Re_L = 32.5 x 10^6

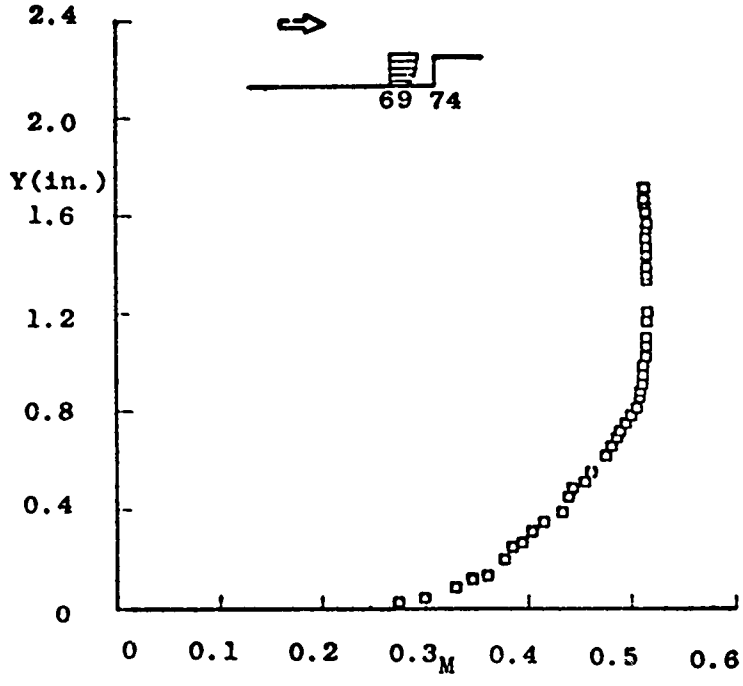

d. 69-inch Station, M_e = 0.52, Re_L = 32.5 x 10^6

Figure 14. Continued

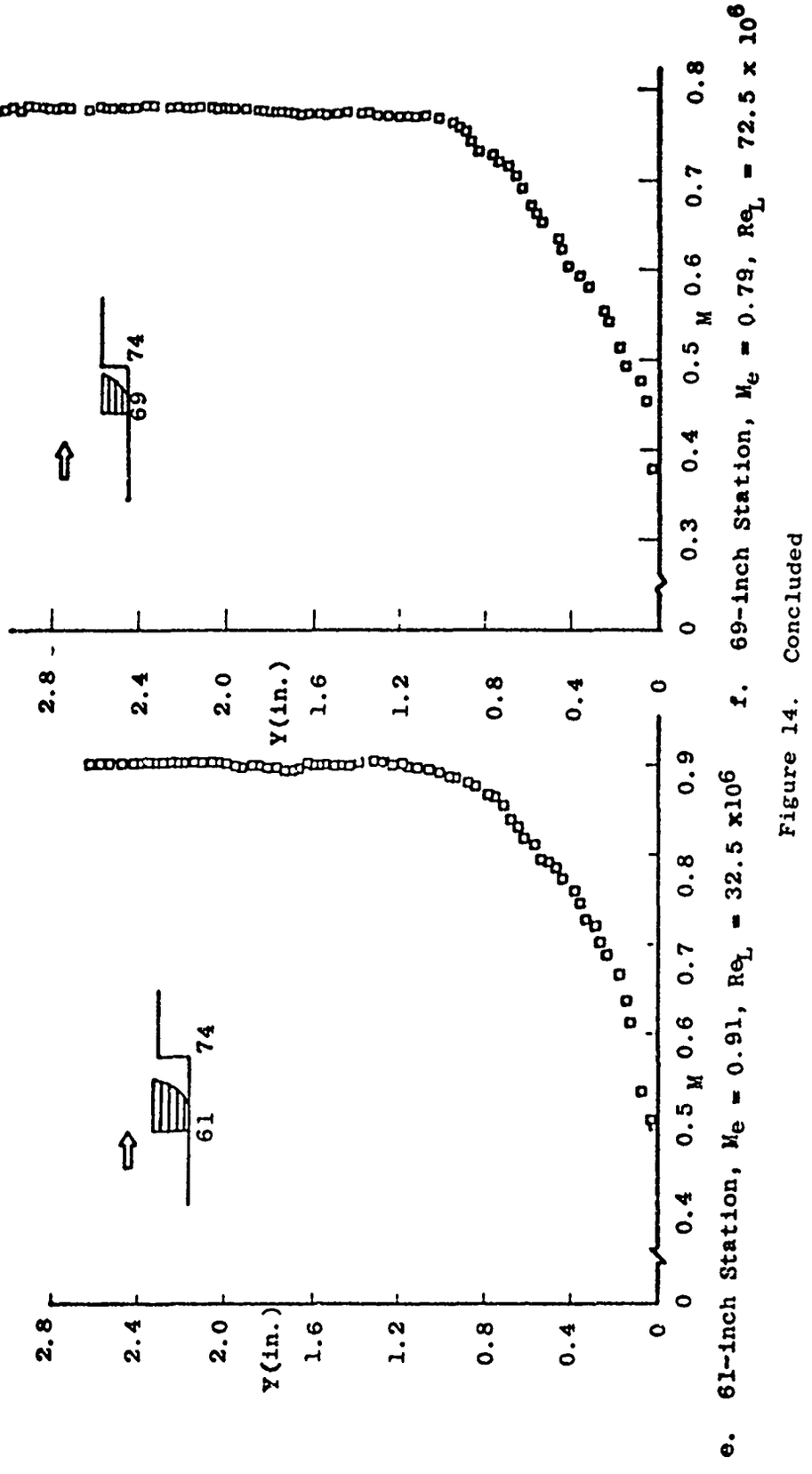

e. 61-inch Station, M_e = 0.91, Re_L = 32.5 x10^6

f. 69-inch Station, M_e = 0.79, Re_L = 72.5 x 10^6

Figure 14. Concluded

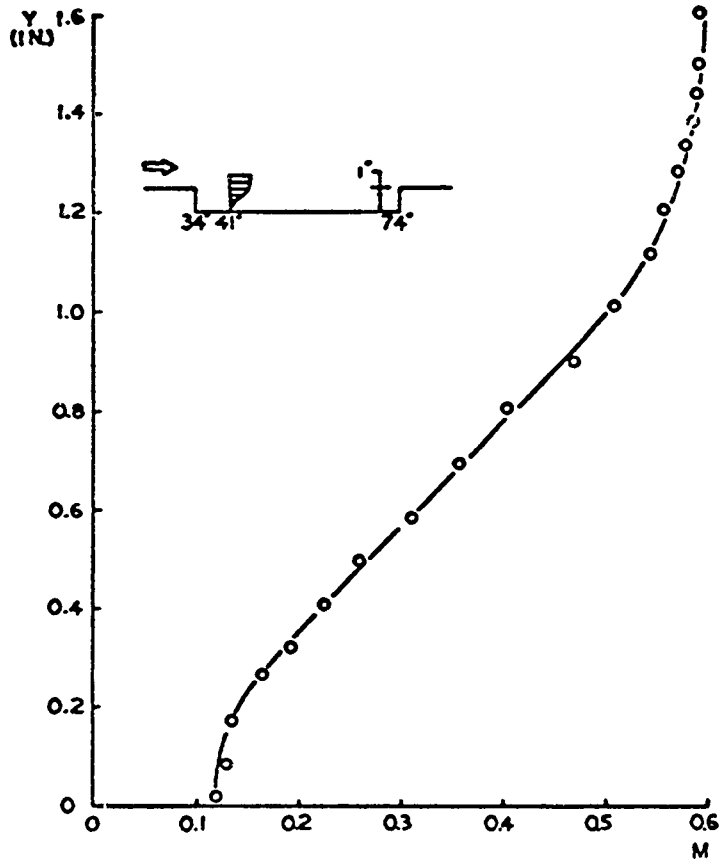

a. 41-inch Station, $M_e = 0.60$, $Re_L = 32.5 \times 10^6$

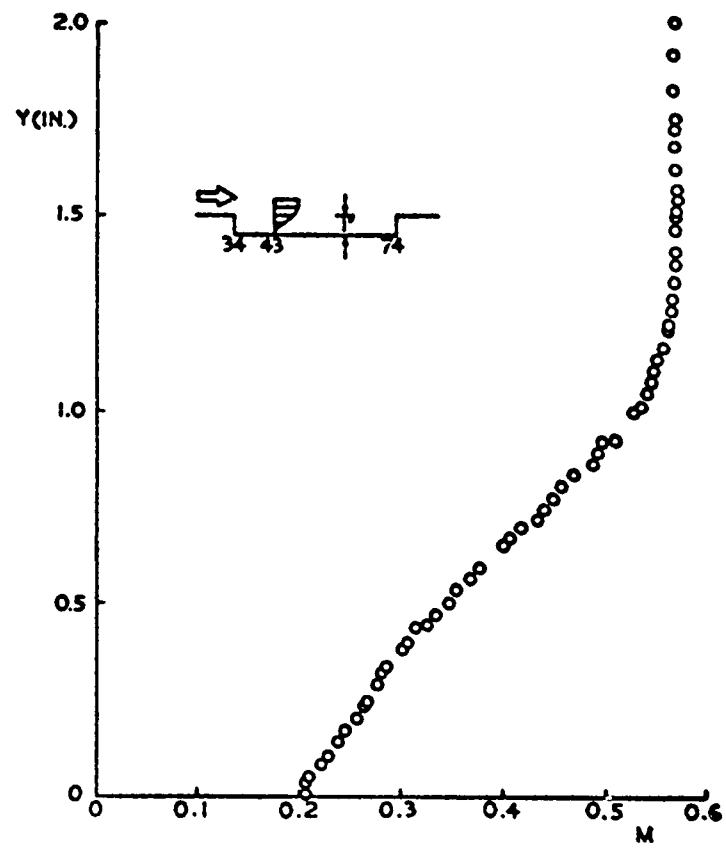

b. 43-inch Station, $M_e = 0.55$, $Re_L = 32.5 \times 10^6$

Figure 15. Velocity profiles on 40 inch long cavity like model

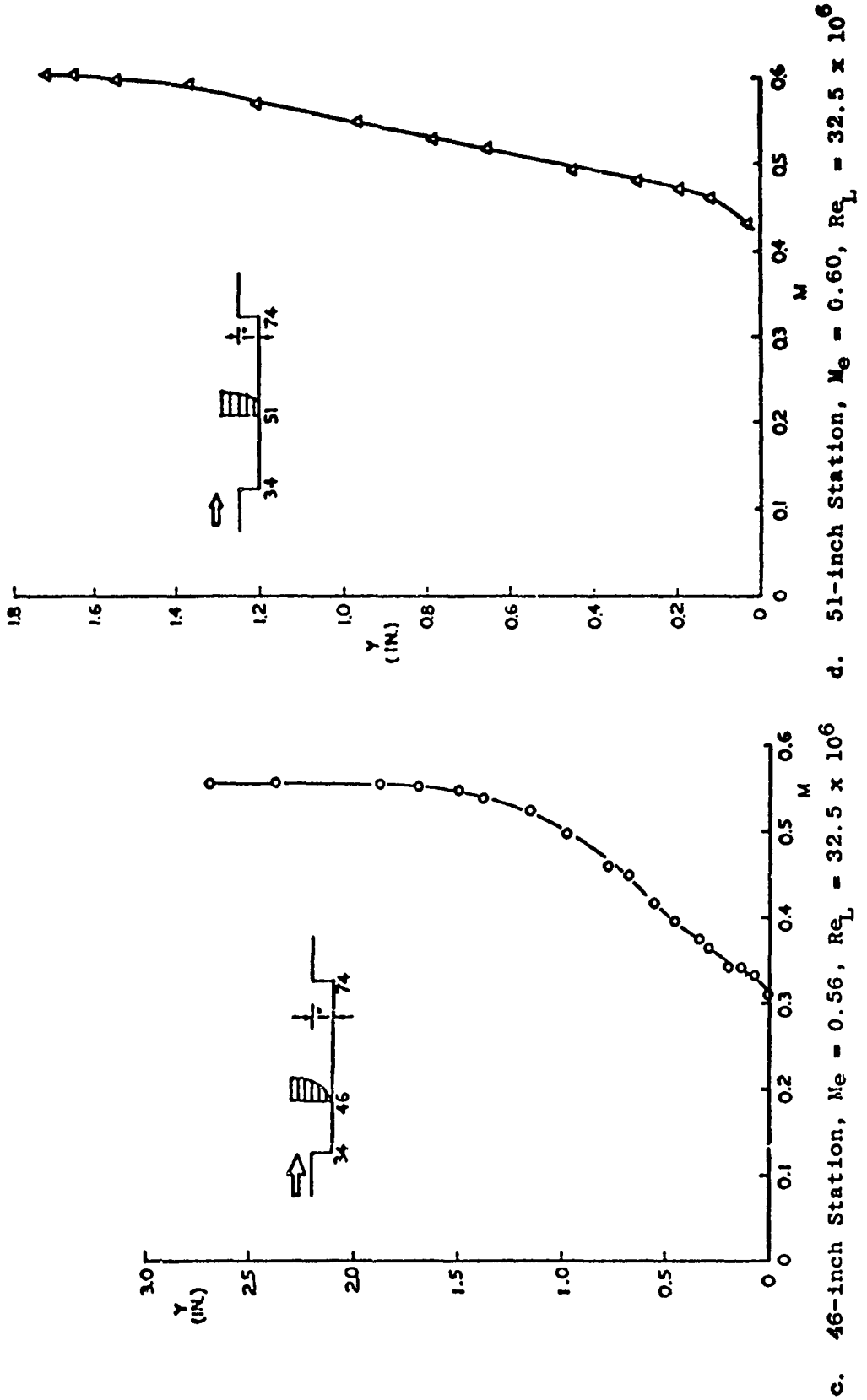

c. 46-inch Station, M_e = 0.56, Re_L = 32.5 x 10^6 d. 51-inch Station, M_e = 0.60, Re_L = 32.5 x 10^6

Figure 15. Continued

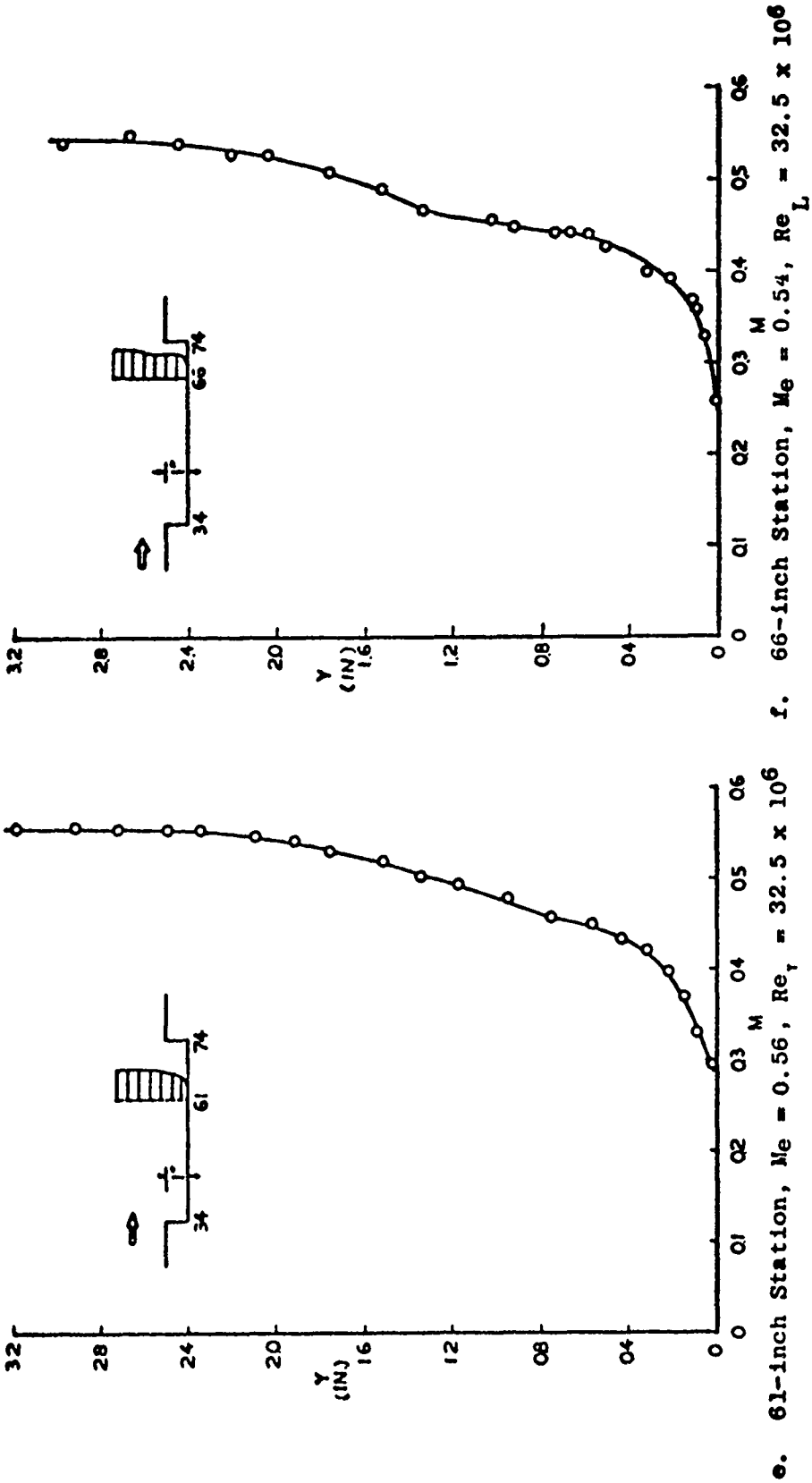

Figure 15. Continued

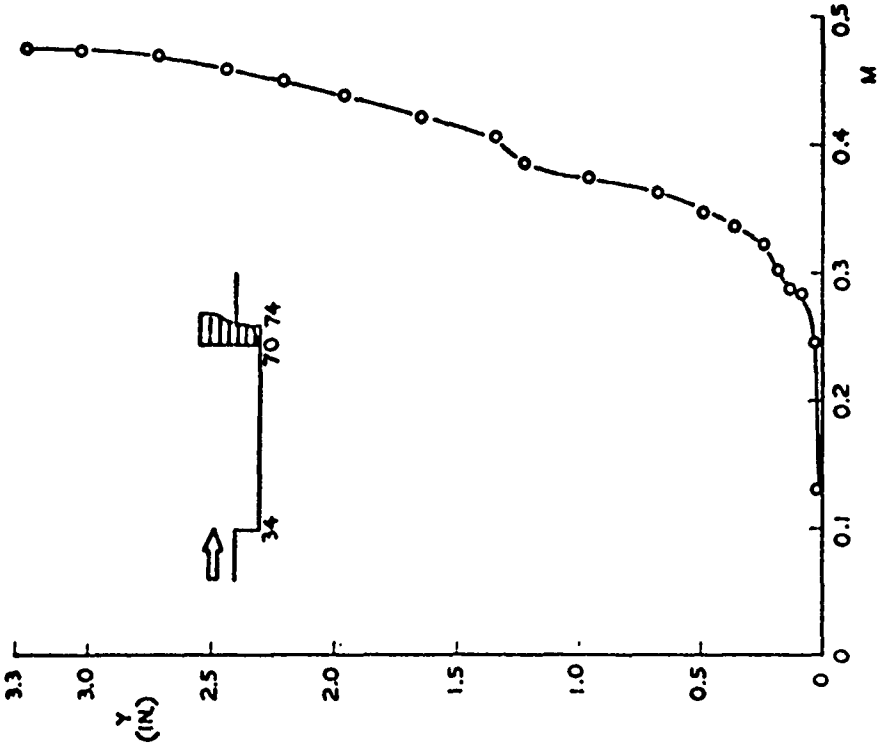

g. 70-inch Station, M_e = 0.48, Re_L = 32.5 x 10^6

Figure 15. Concluded

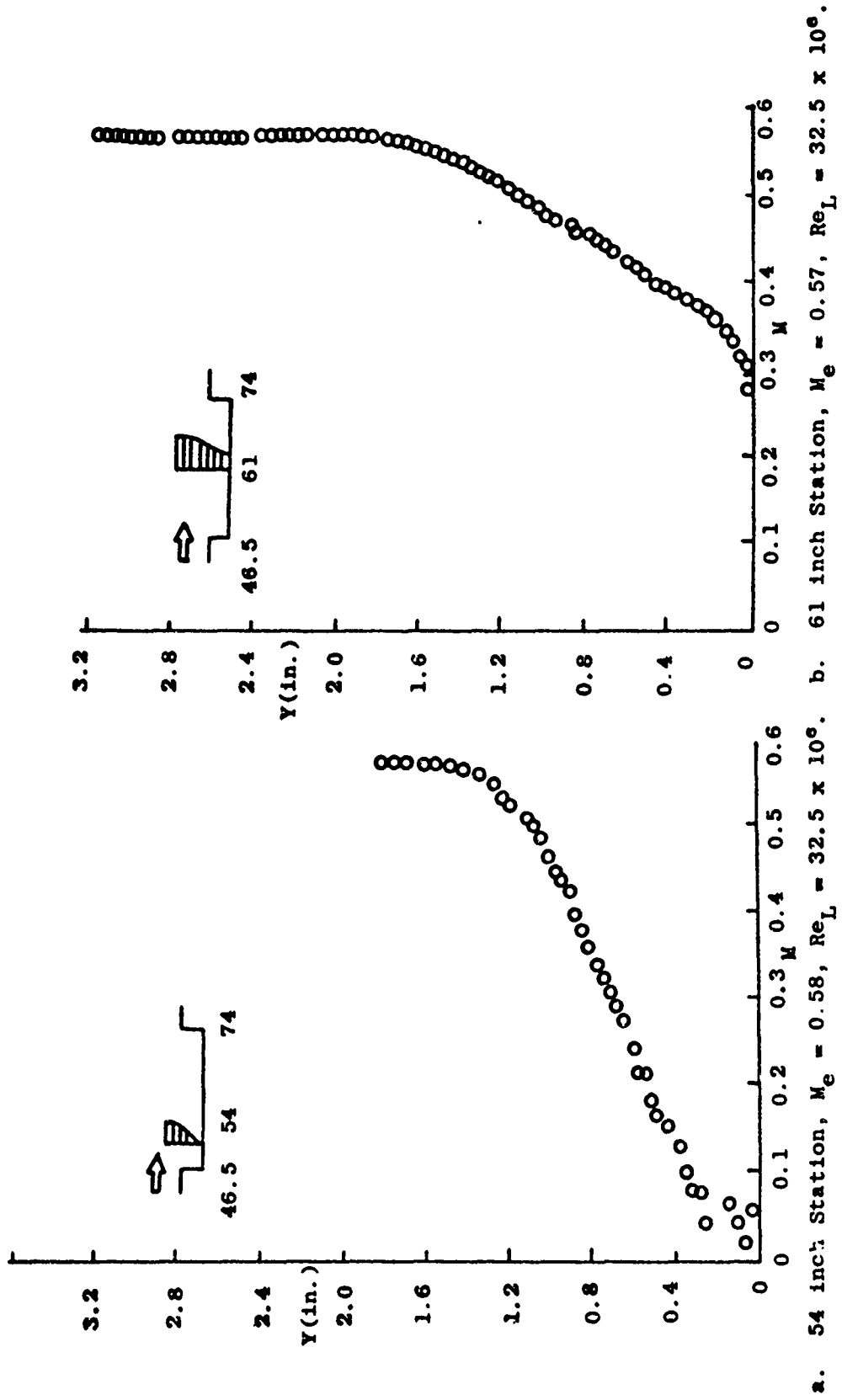

a. 54 inch Station, M_e = 0.58, Re_L = 32.5 x 10^6. b. 61 inch Station, M_e = 0.57, Re_L = 32.5 x 10^6.

Figure 16. Velocity profiles on 27.5 inch long cavity like model

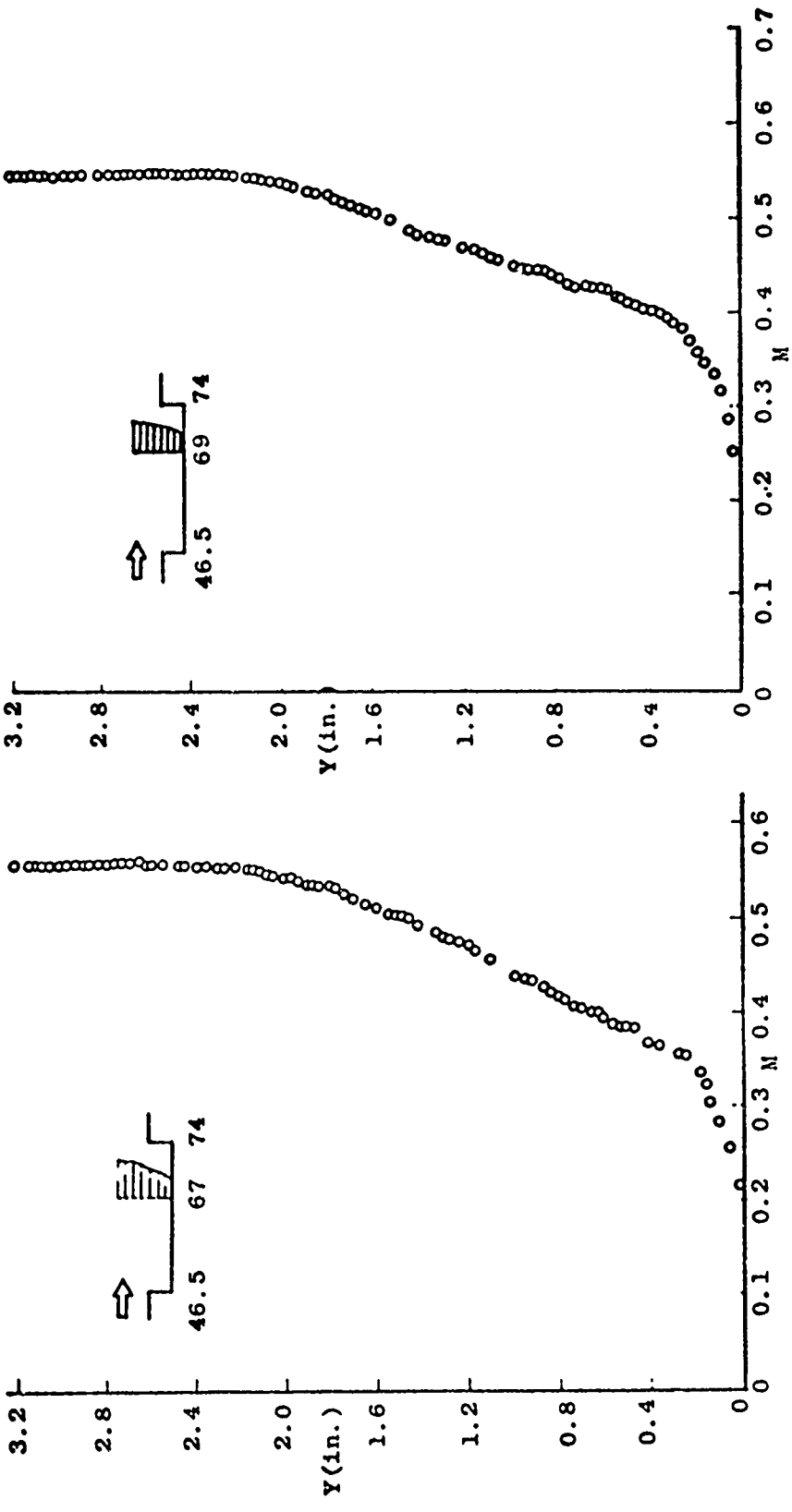

c. 67-inch Station, M_e = 0.56, Re_L = 32.5 x 10^6 d. 69-inch Station, M_e = 0.55, Re_L = 32.5 x 10^6

Figure 16. Concluded

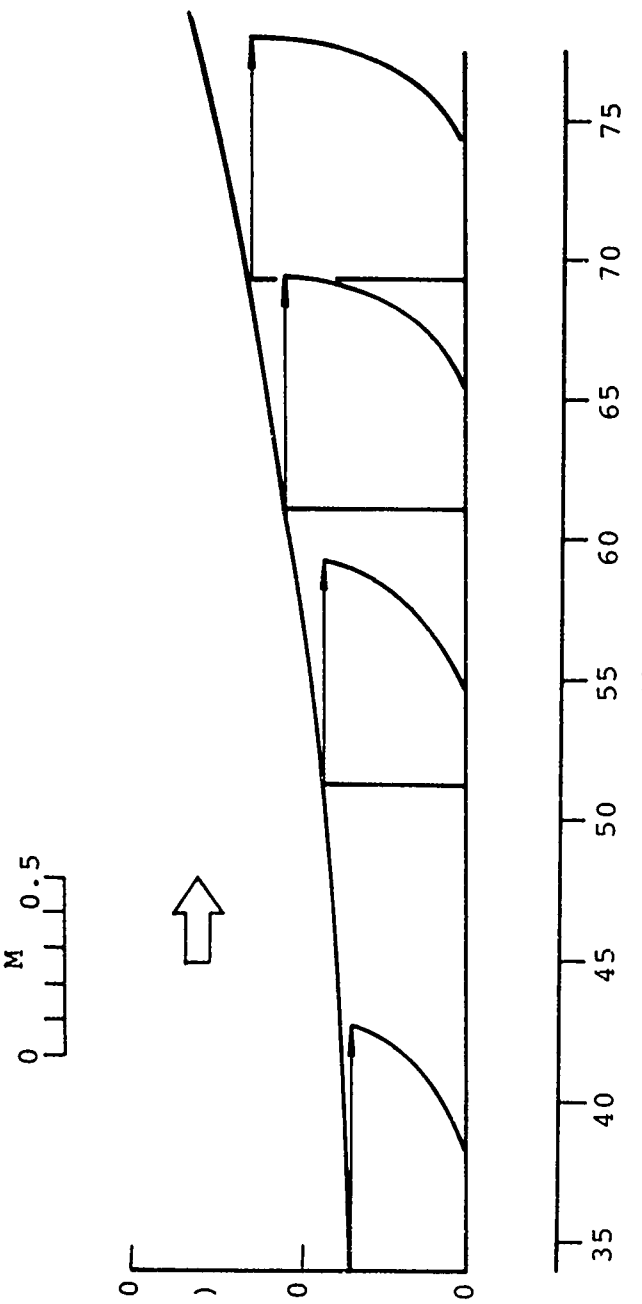

Figure 17. Flow variation along the flat-plate model.

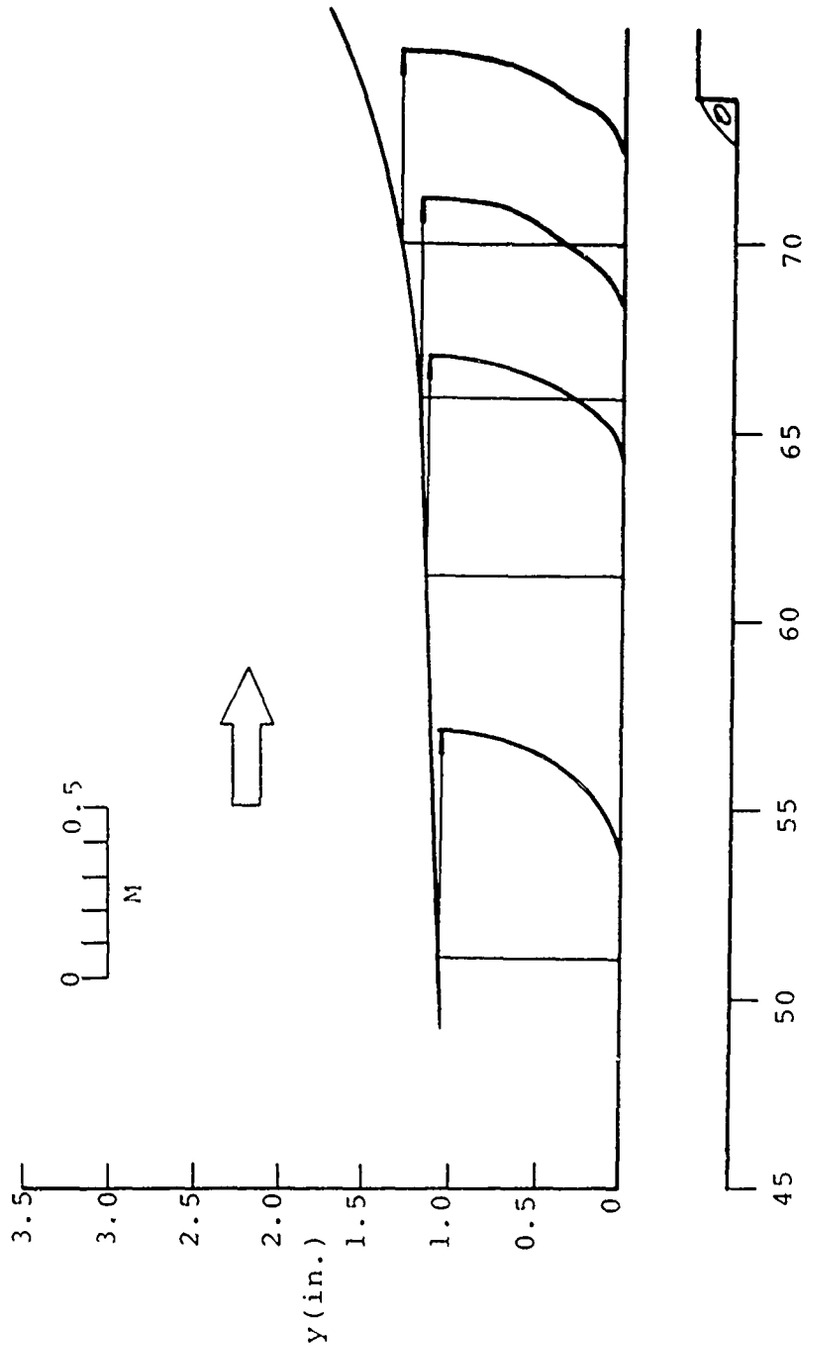

a. $M_\infty = 0.6$, $Re_L = 32.5 \times 10^6$

Figure 18. Flow variation along the forward-facing step model

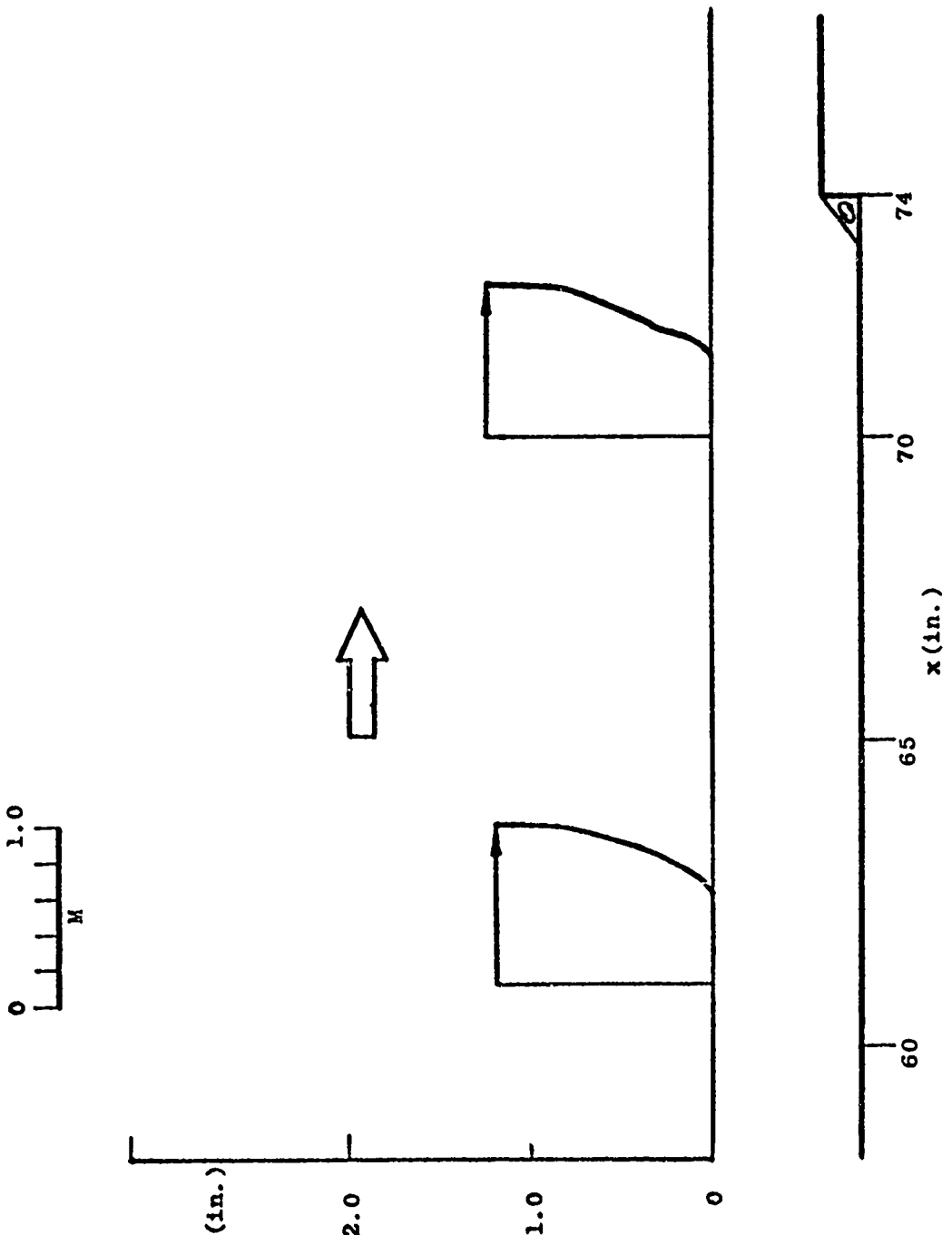

b. $M_e = 0.9$, $Re_L = 72.5 \times 10^6$

Figure 18. Concluded

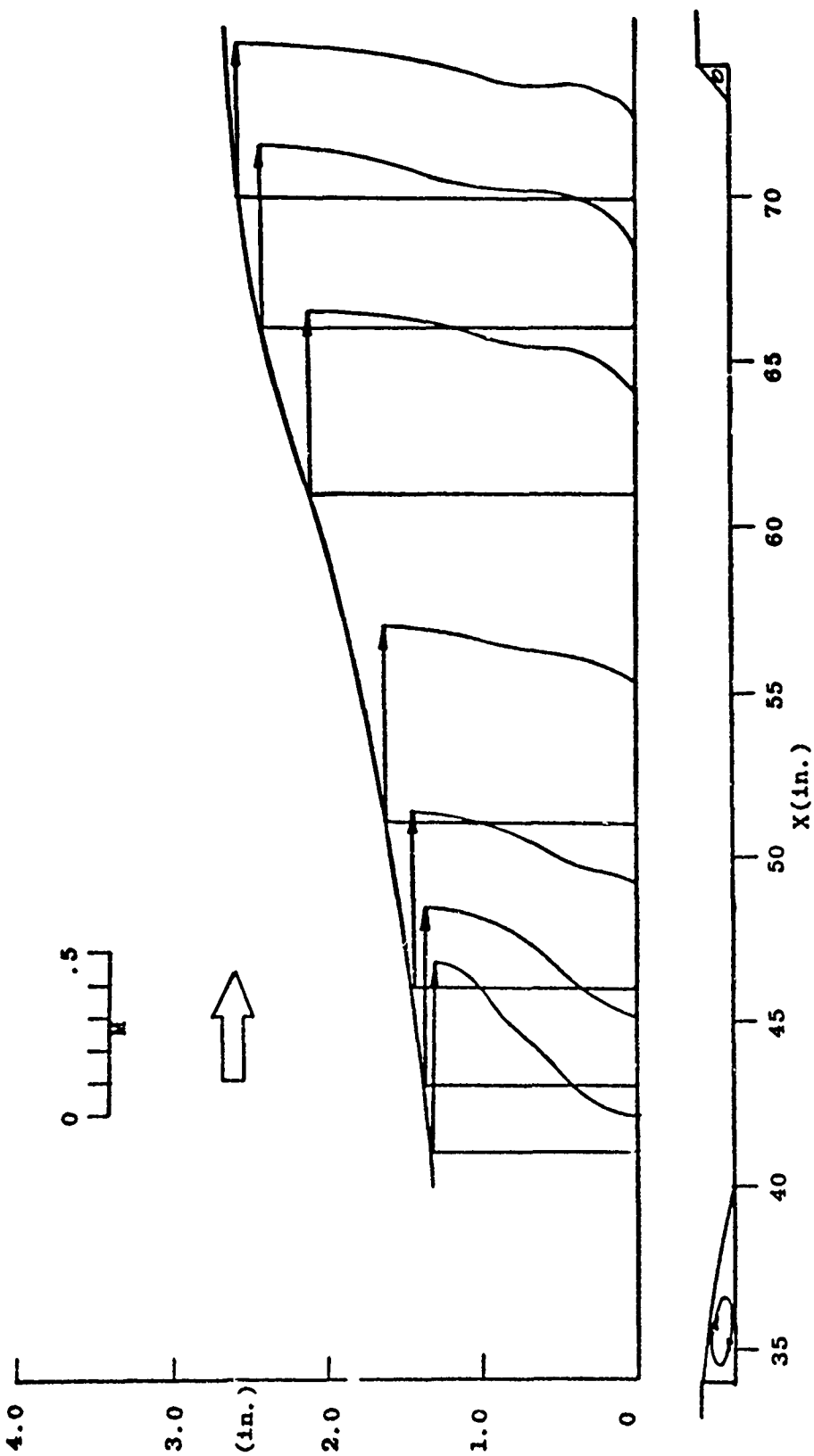

Figure 19. Flow variation along the 40 inch long cavity model

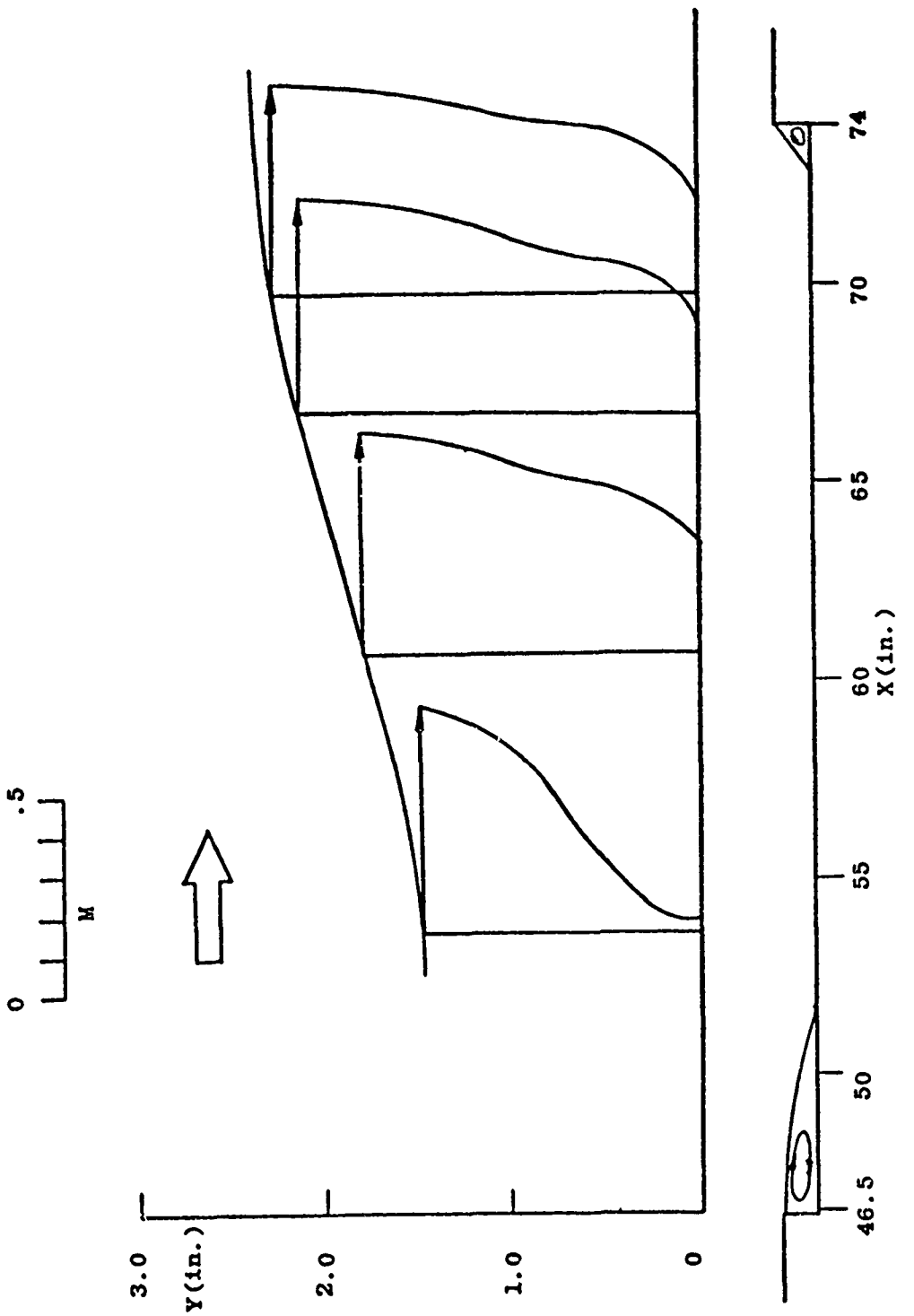

Figure 20. Flow variation along the 27.5 inch long cavity model.
$M_e = 0.6$, $Re_L = 32.5 \times 10^6$

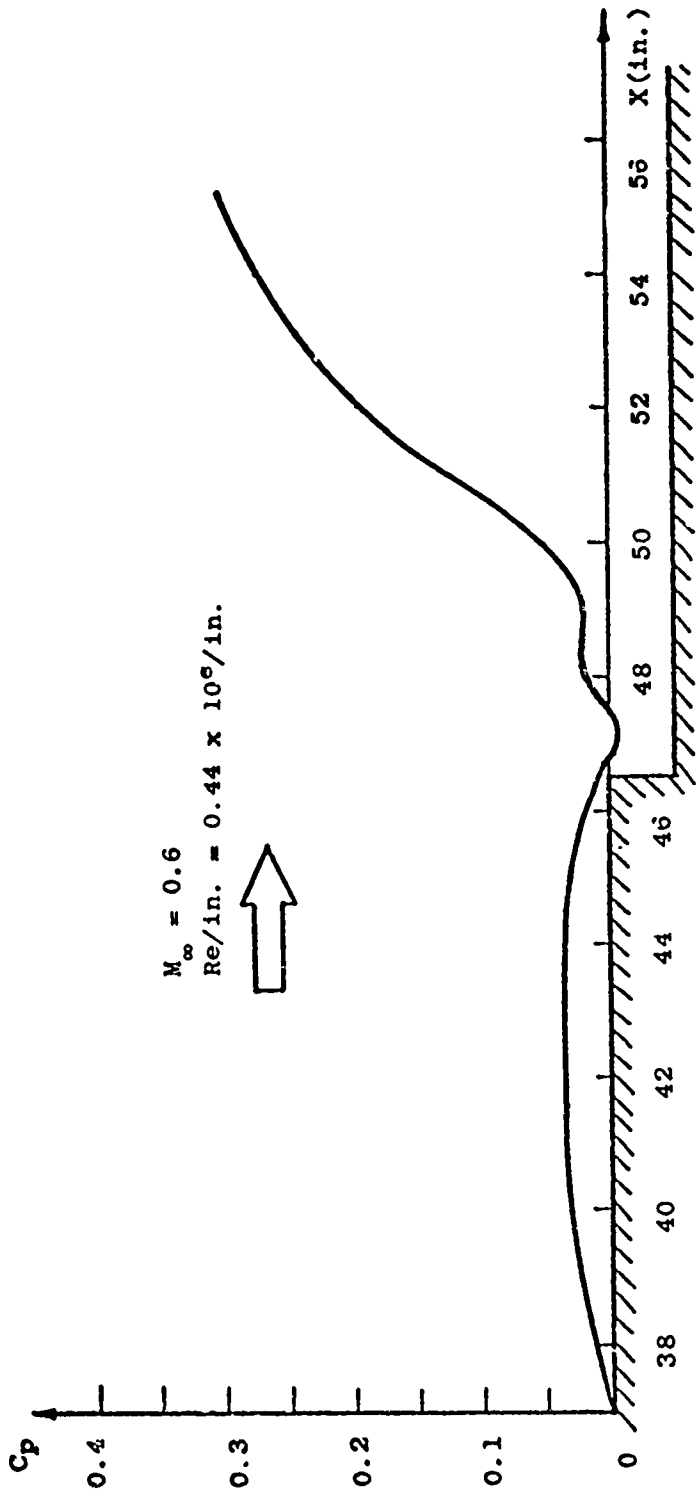

Figure 21a. Static pressure distribution on the model surface near the rearward facing step region.

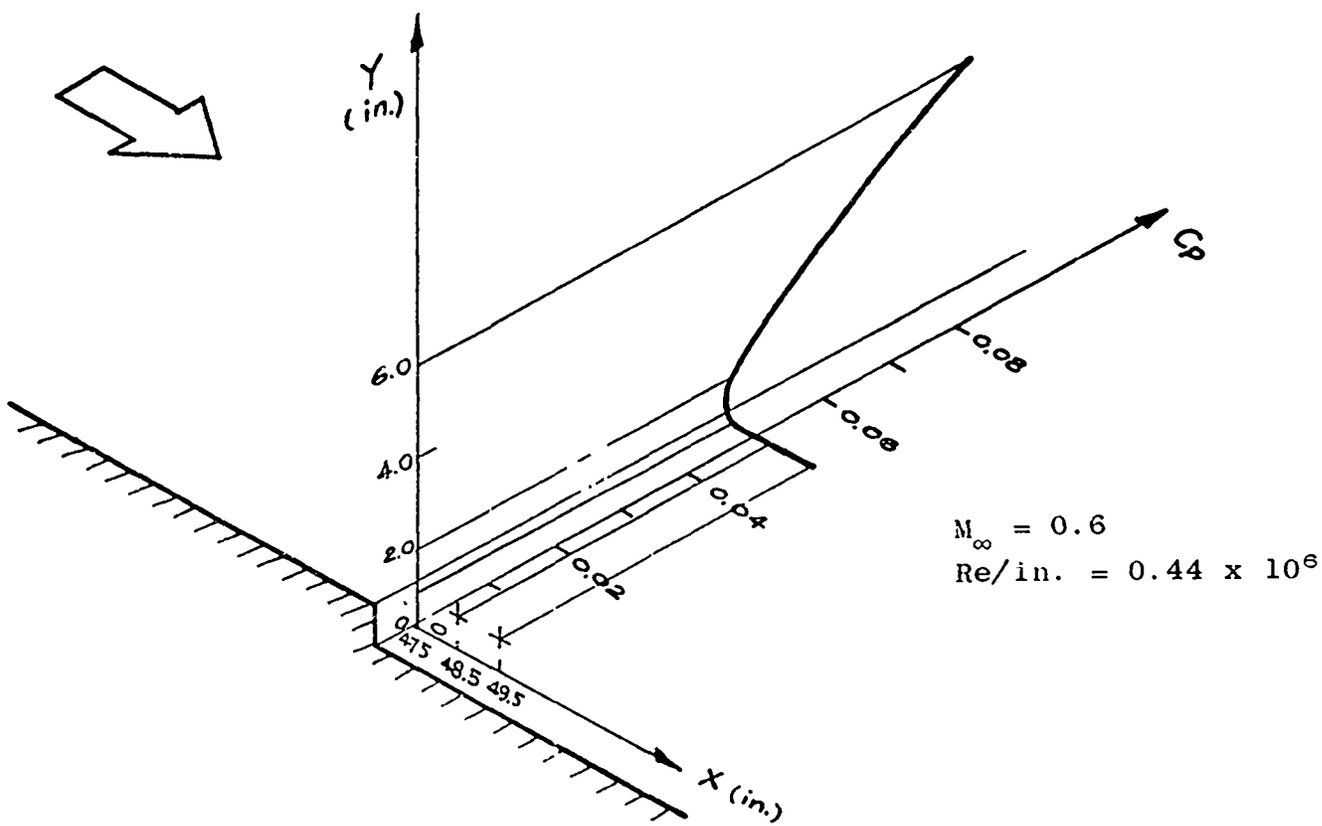

Figure 21b. Static pressure distribution on the side wall near the rearward facing step region.

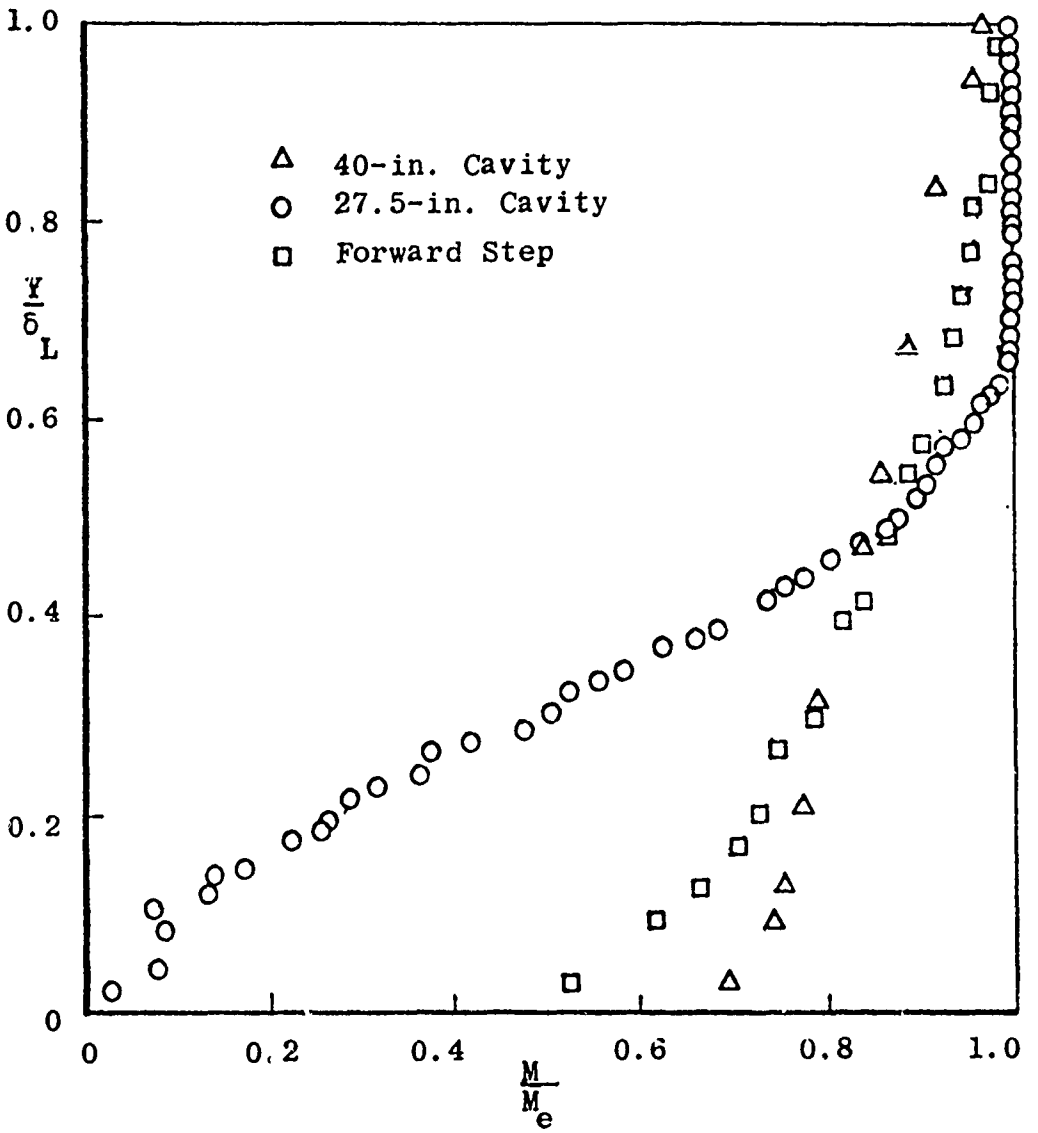

a. 51-inch Station

Figure 22. Effect of model configuration on the velocity profile

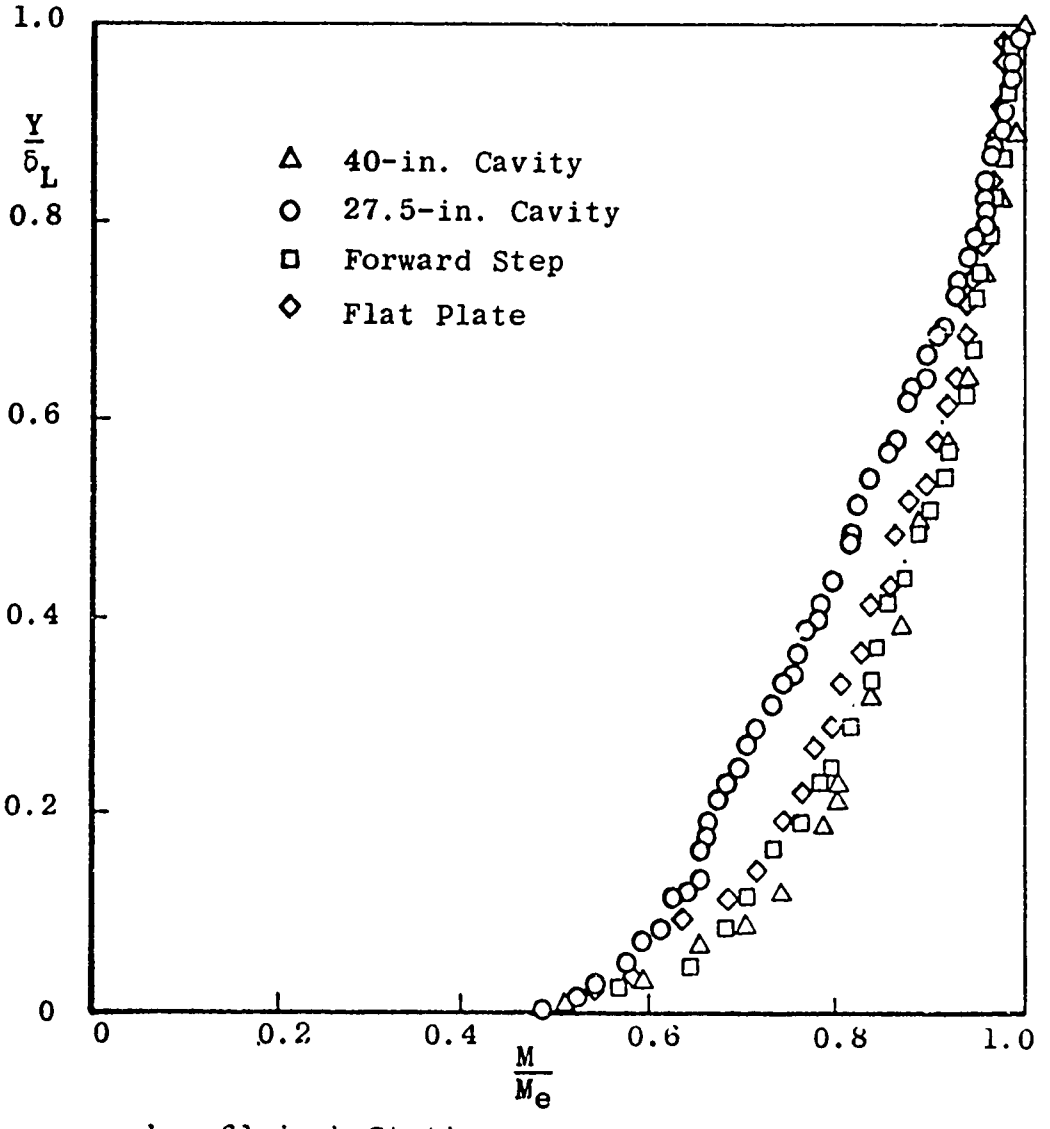

b. 61-inch Station

Figure 22. Continued

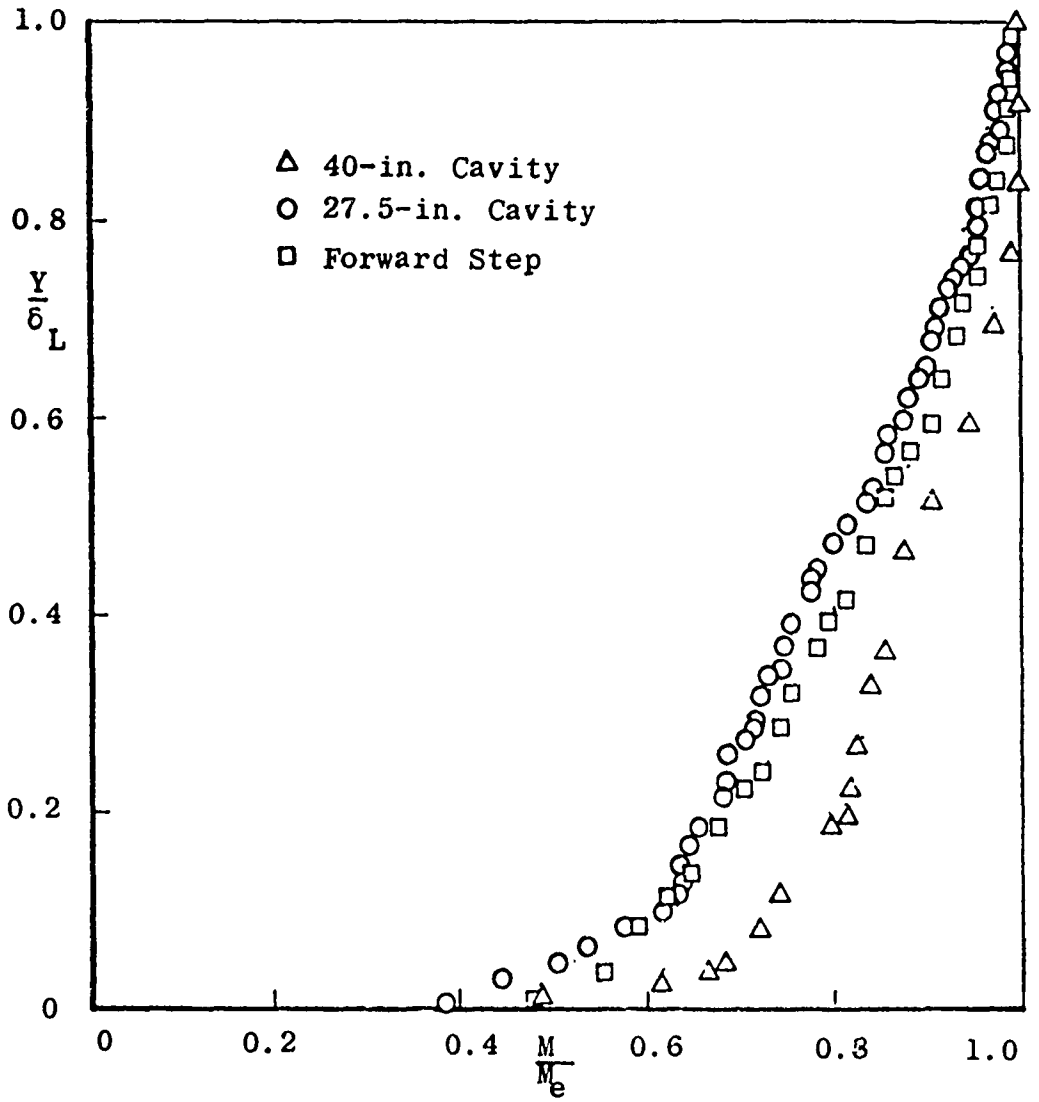

c. 66-inch Station

Figure 22. Continued

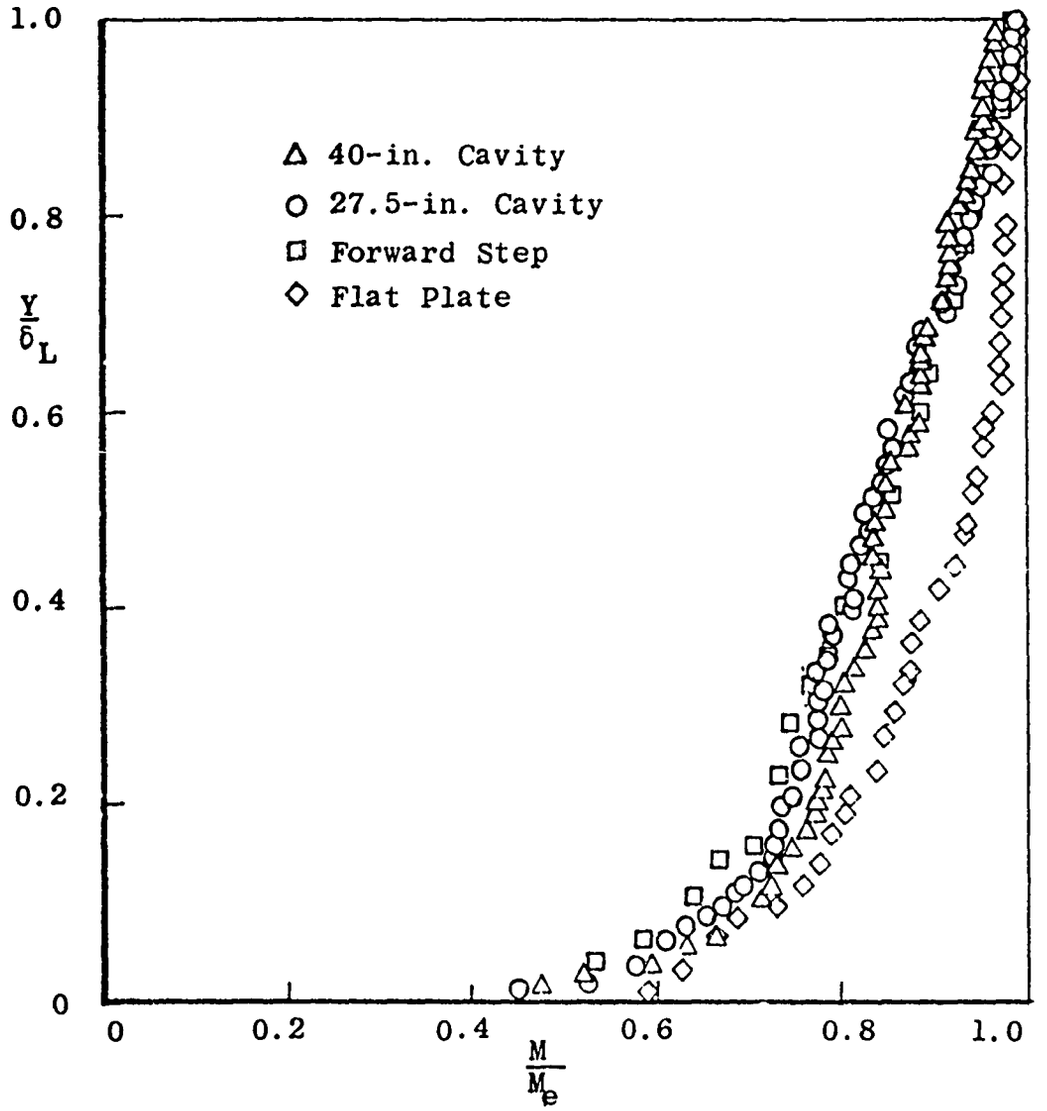

d. 69-inch Station

Figure 22. Continued

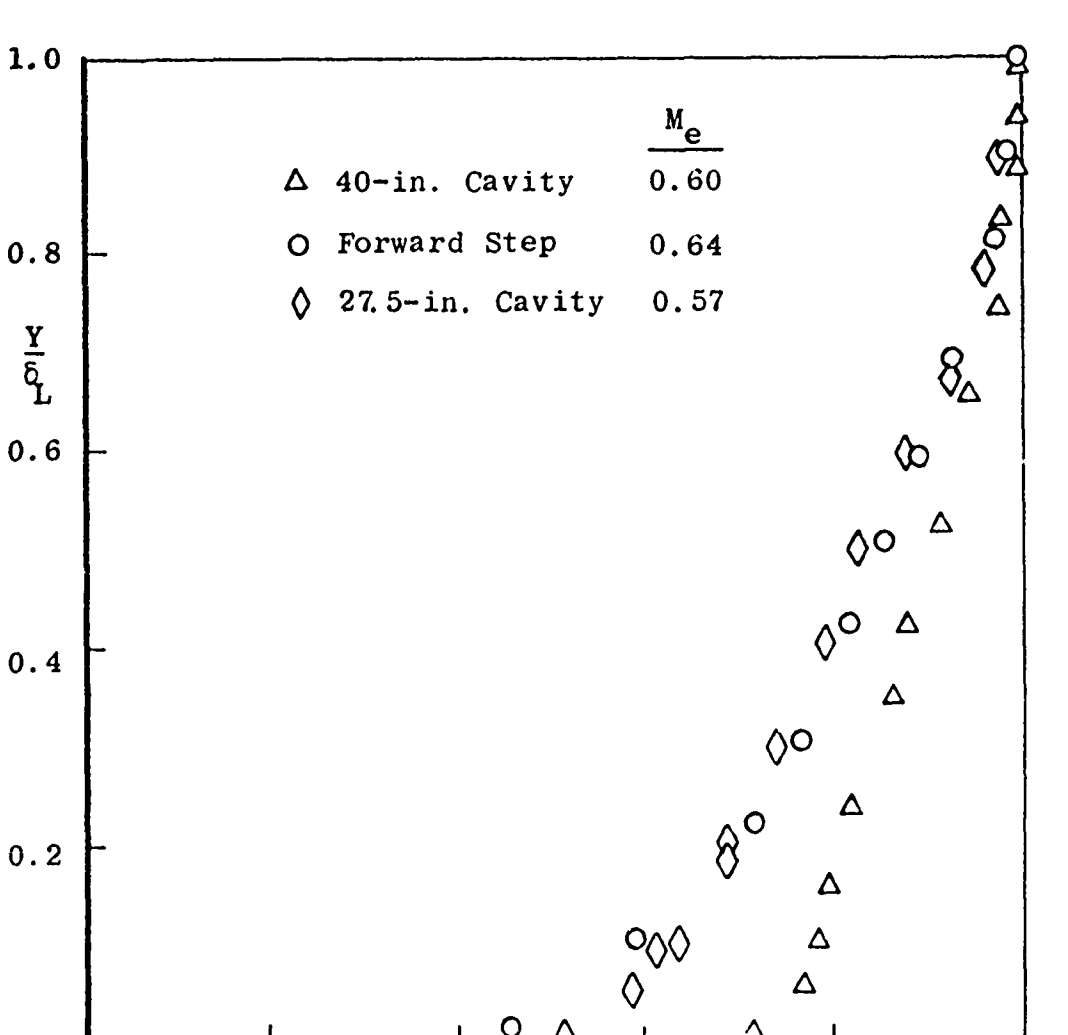

e. At Reference Station

Figure 22. Concluded

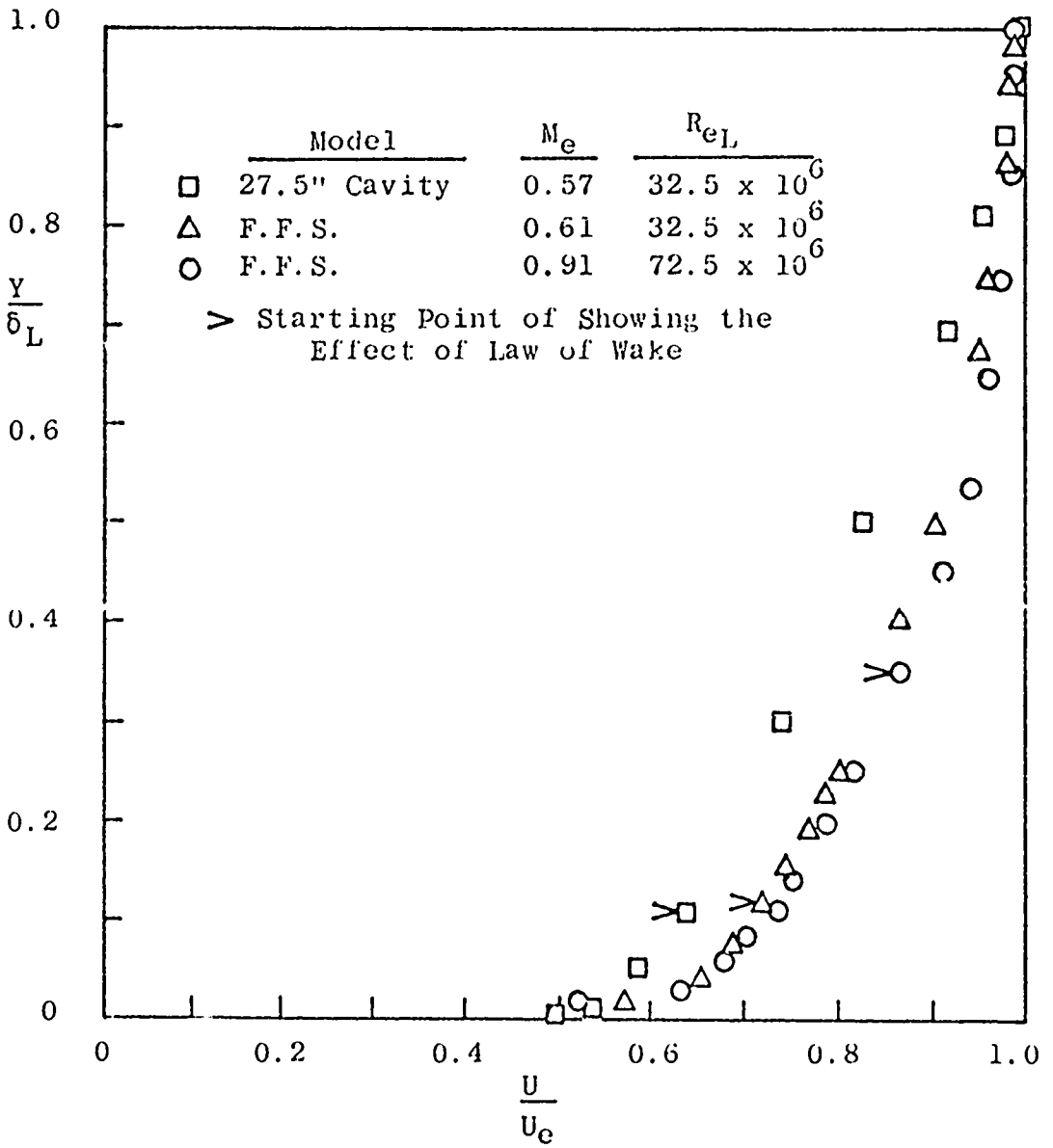

a. Station 61-in. on the Forward-Facing Step and 27.5-in. Cavity Models.

Figure 23. Mach number effect on velocity profile

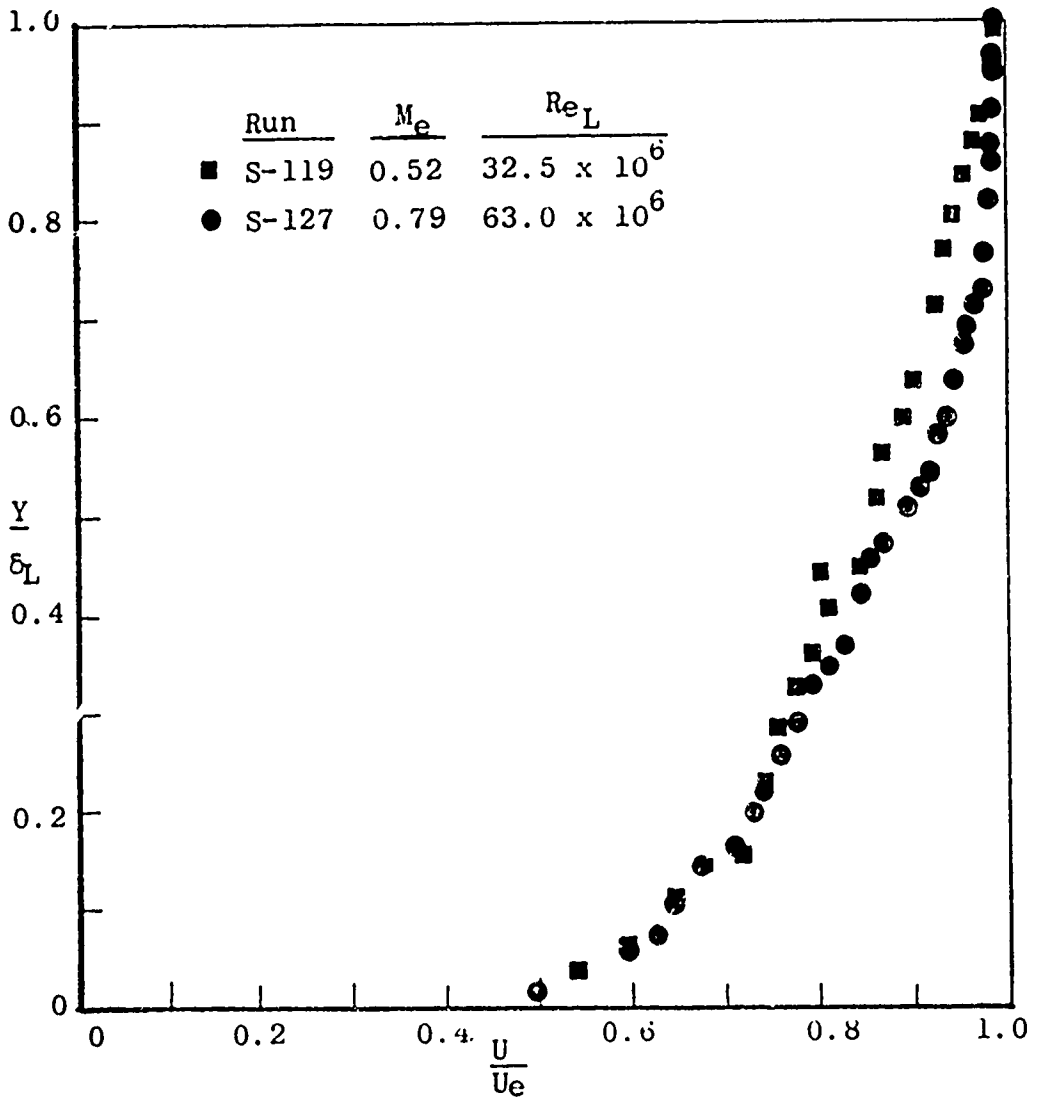

b. Station 69 in. on the Forward-Facing Step Model

Figure 23. Concluded

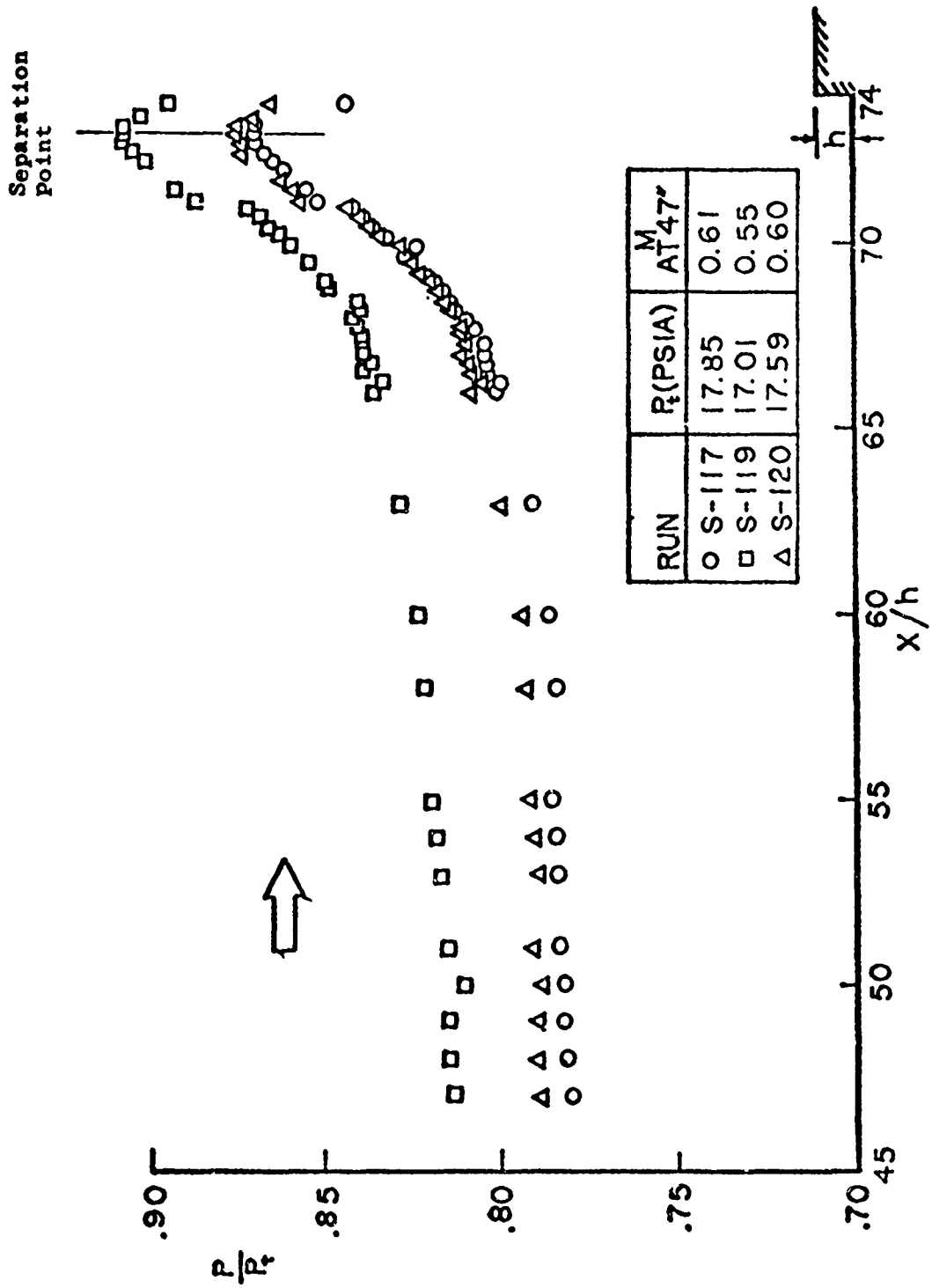

a. $M_1 = 0.6$, $Re_L = 32.5 \times 10^6$

Figure 24. Forward Facing Step Model

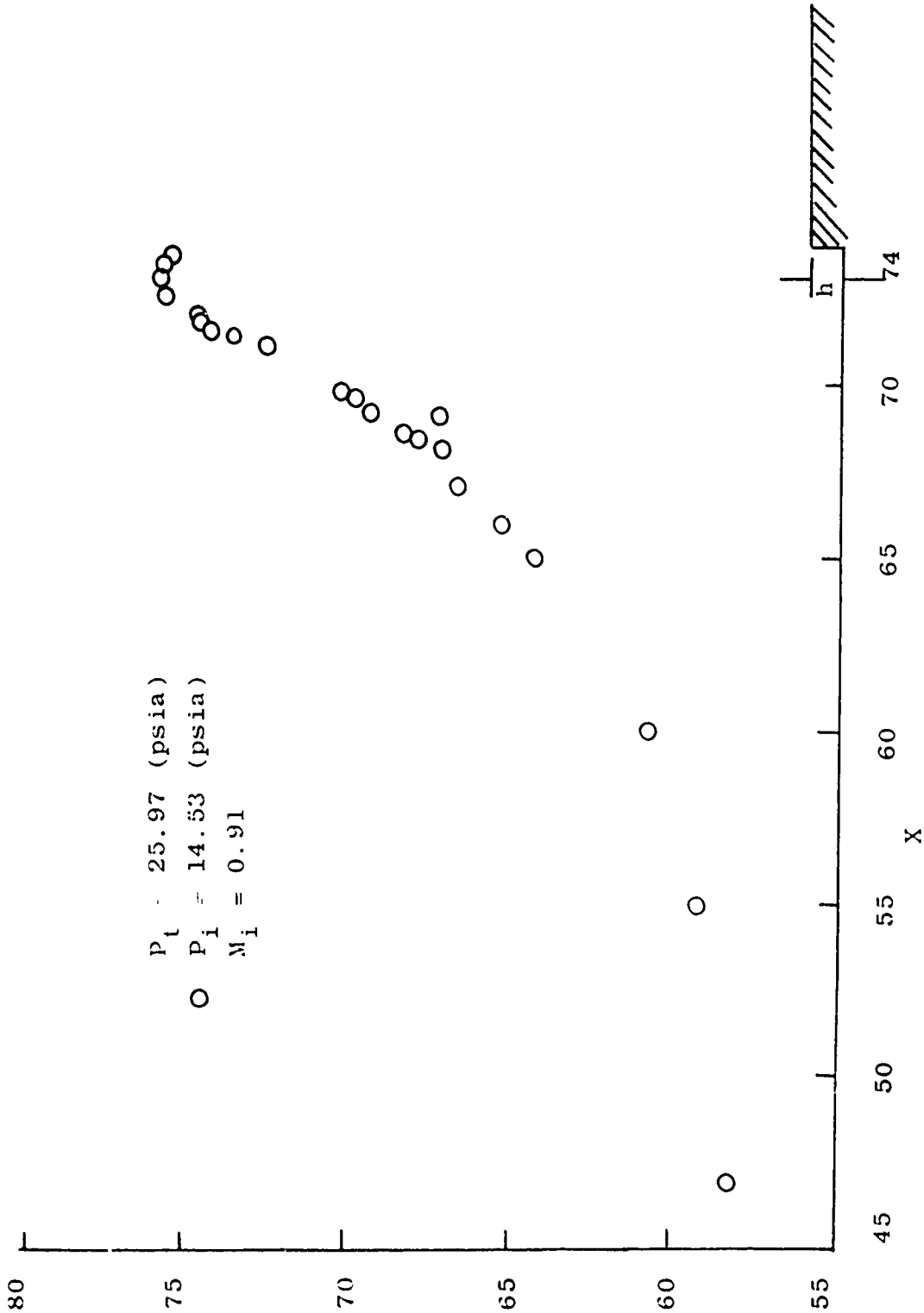

b. M_i = 0.91, Re_L = 72.5 x 10^6

Figure 24. Continued

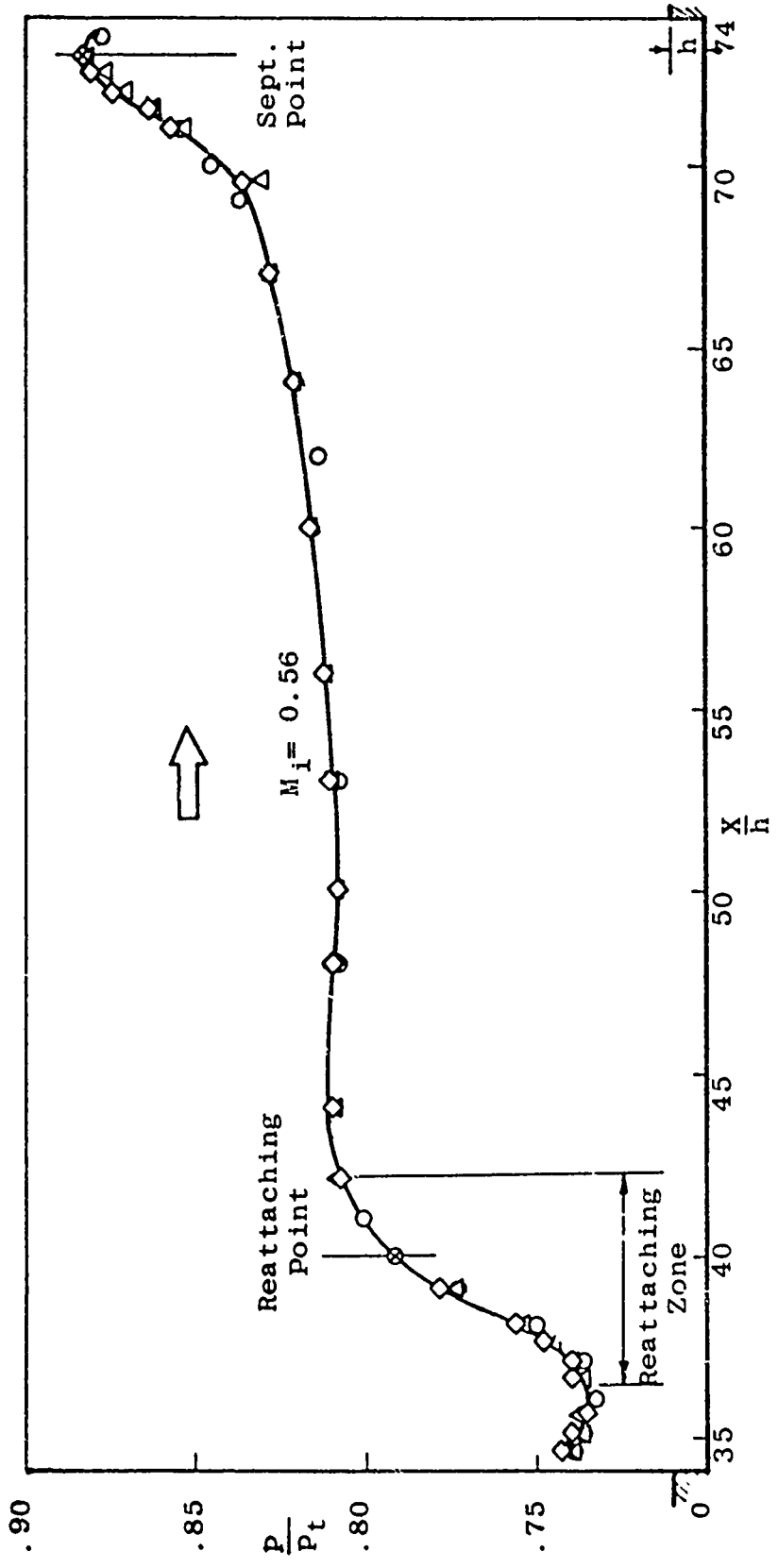

Figure 24c. 40 inch long cavity like model. M_i = 0.56. Re_L = 32.5 x 10^6.

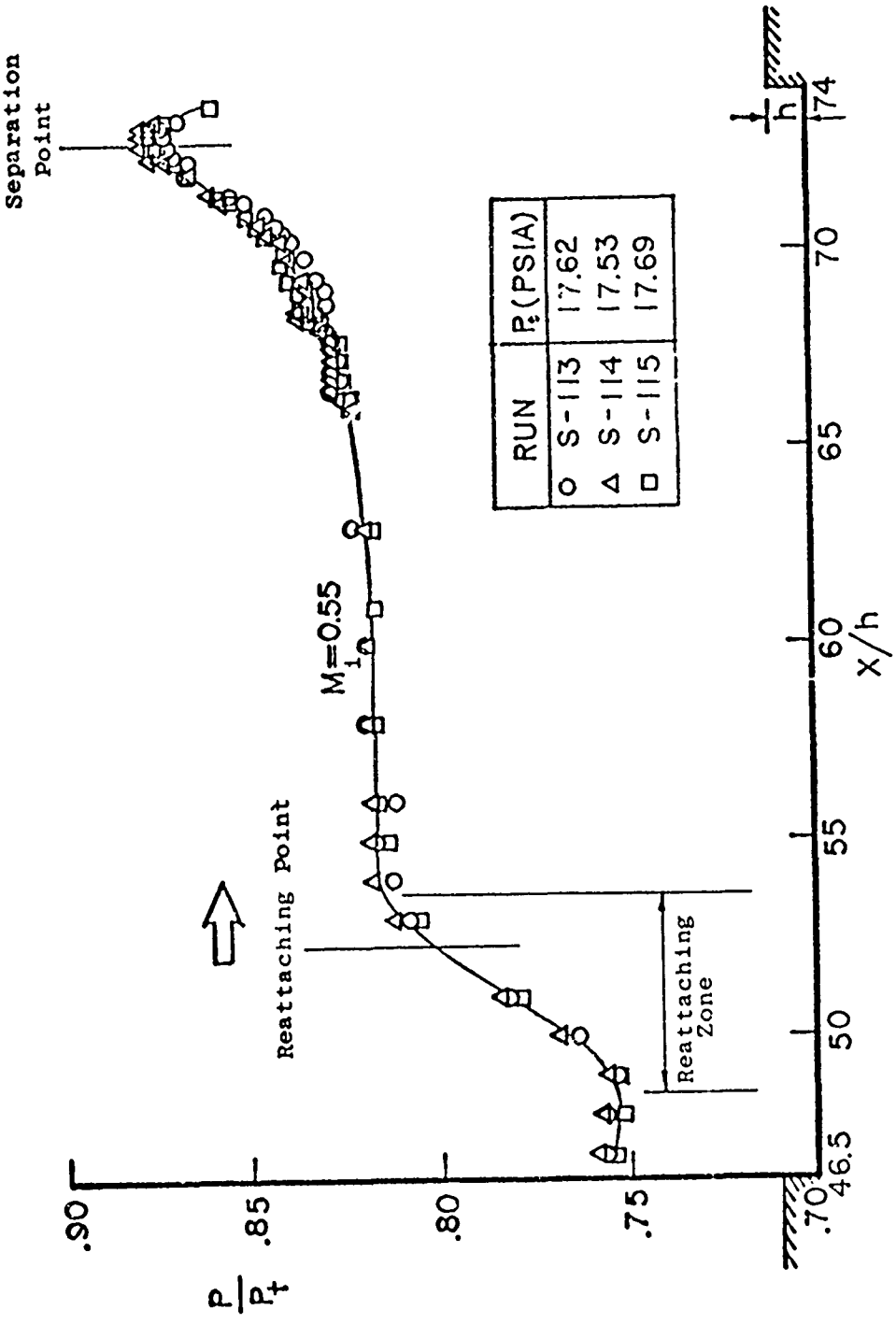

Figure 24d. 27.5 inch long cavity like model, $M_1 = 0.56$, $Re_L = 32.5 \times 10^6$

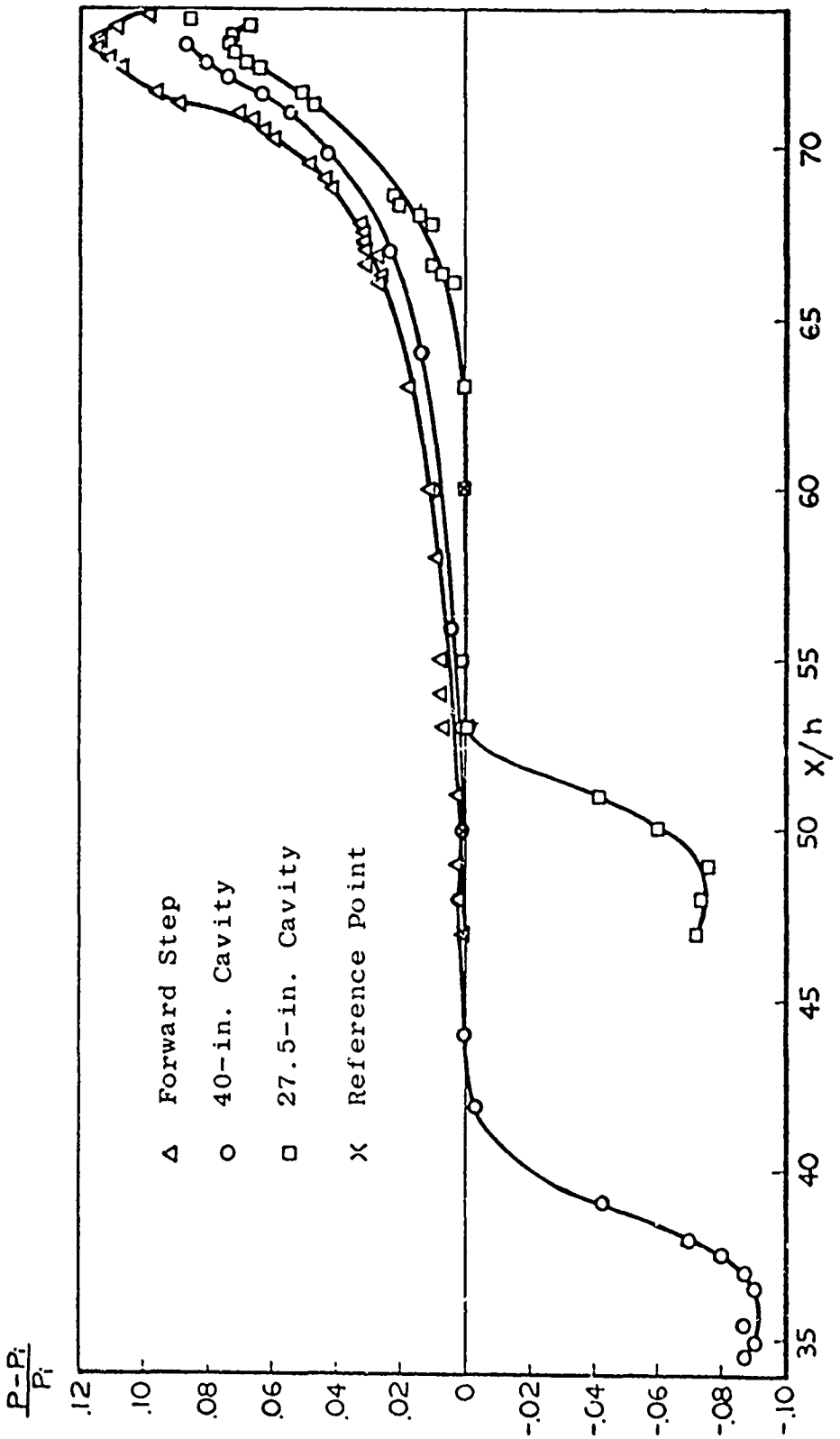

Figure 25. Comparison of wall static pressure distribution on different models

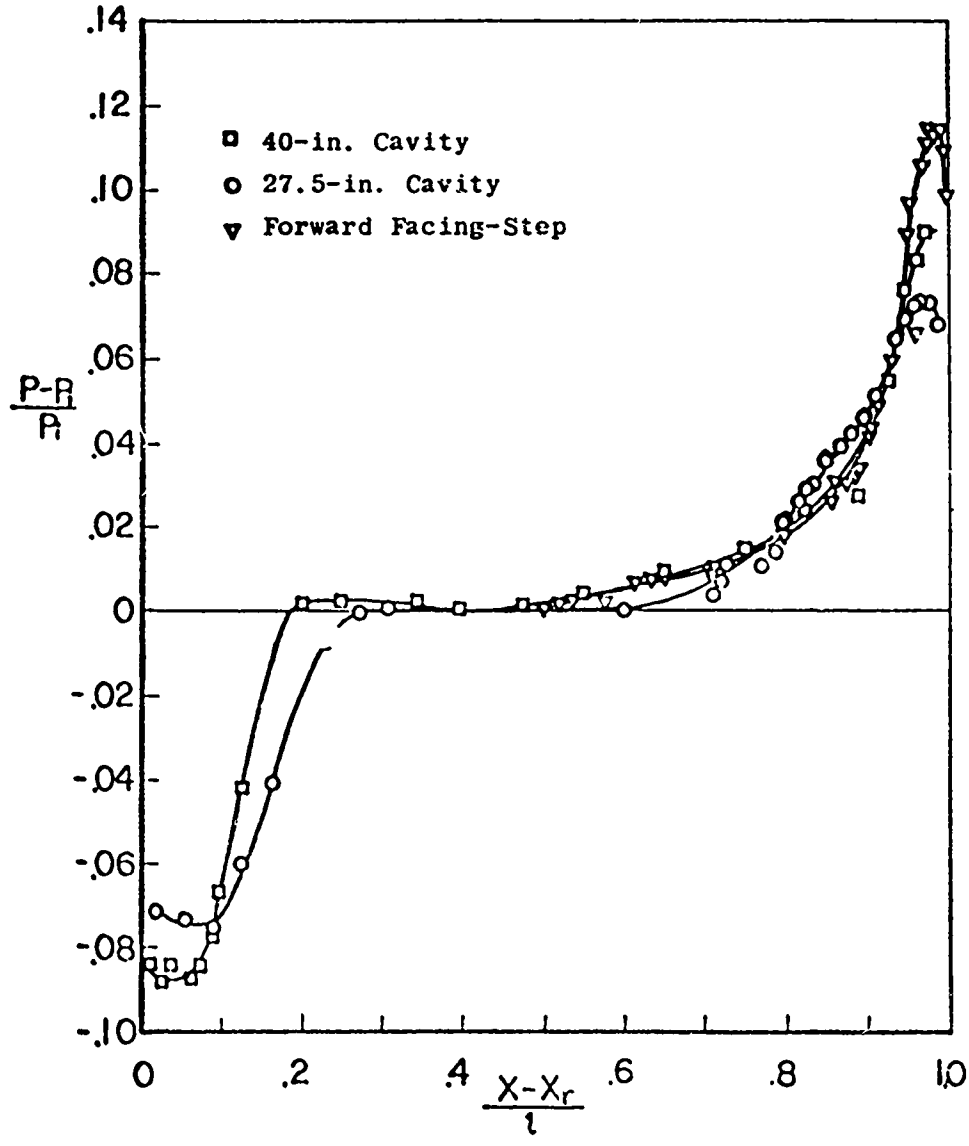

b. $\frac{(P - P_i)}{P_i} \sim \frac{(x - x_r)}{\ell}$, With Normalized Cavity Length

Figure 25. Concluded

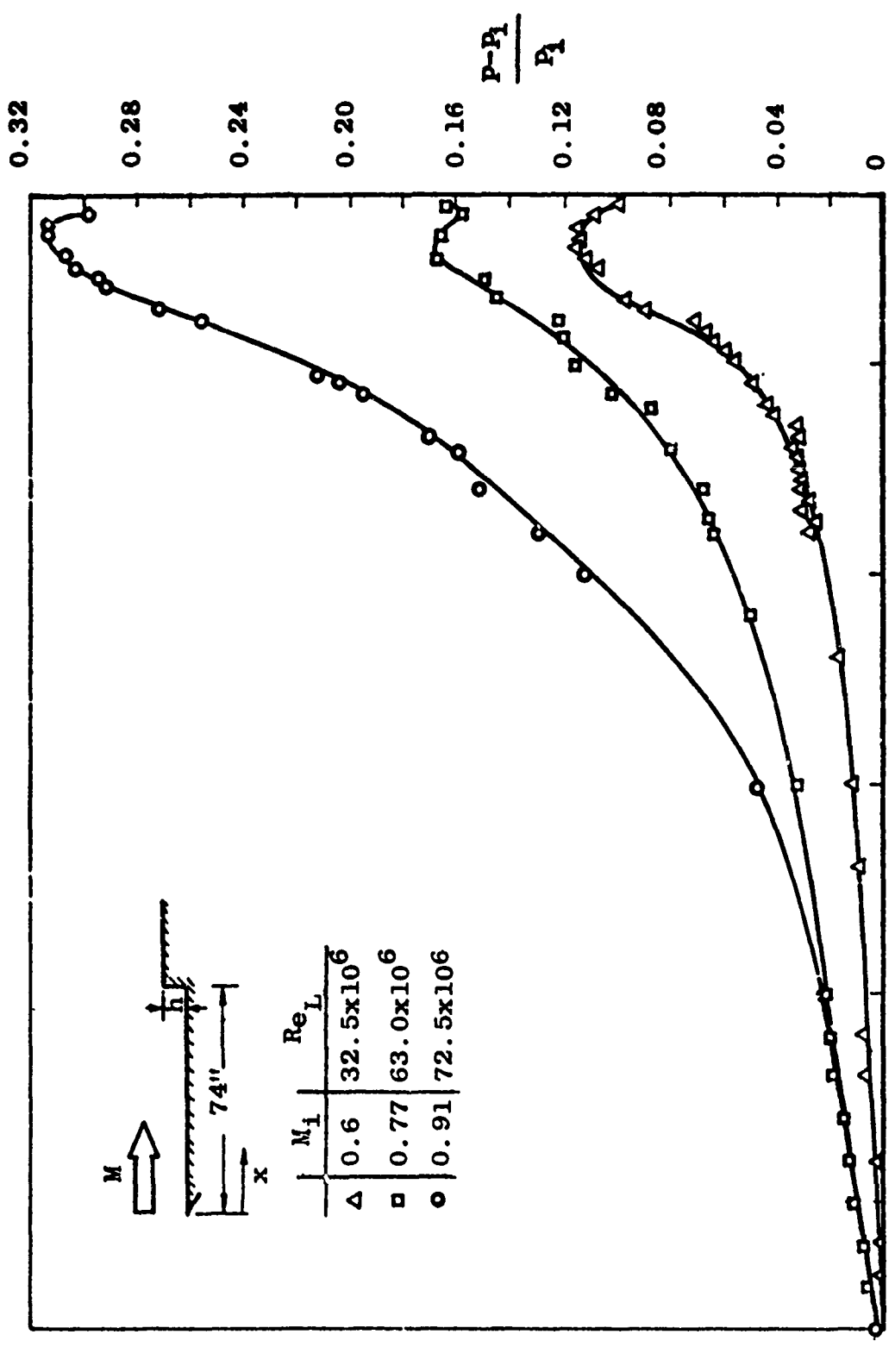

Figure 26. Mach number effect on the wall pressure distribution

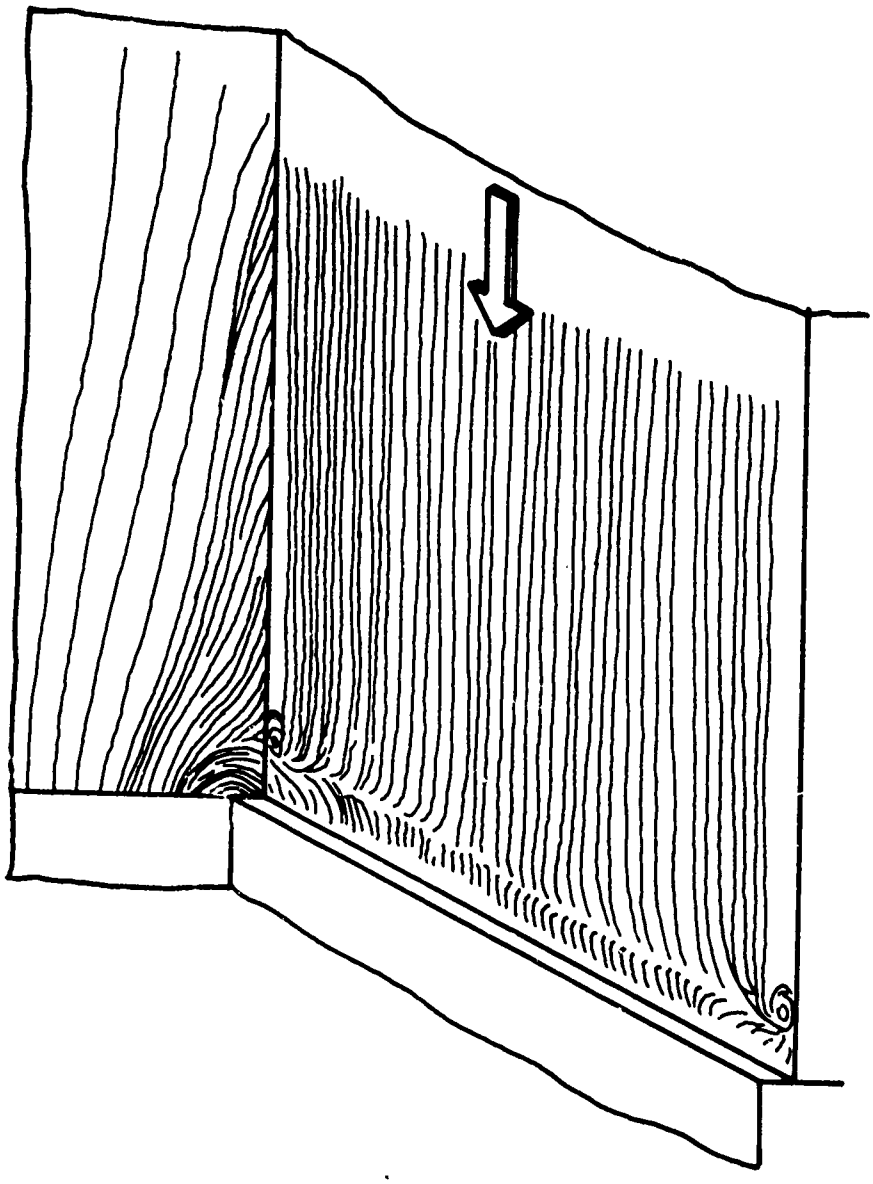

Figure 27 Three-dimensional sketch of oil flow pattern on the forward-facing step model and the side wall.

Figure 28. Surface oil photographs, $M_e = 0.6$, $Re_L = 32.5 \times 10^6$

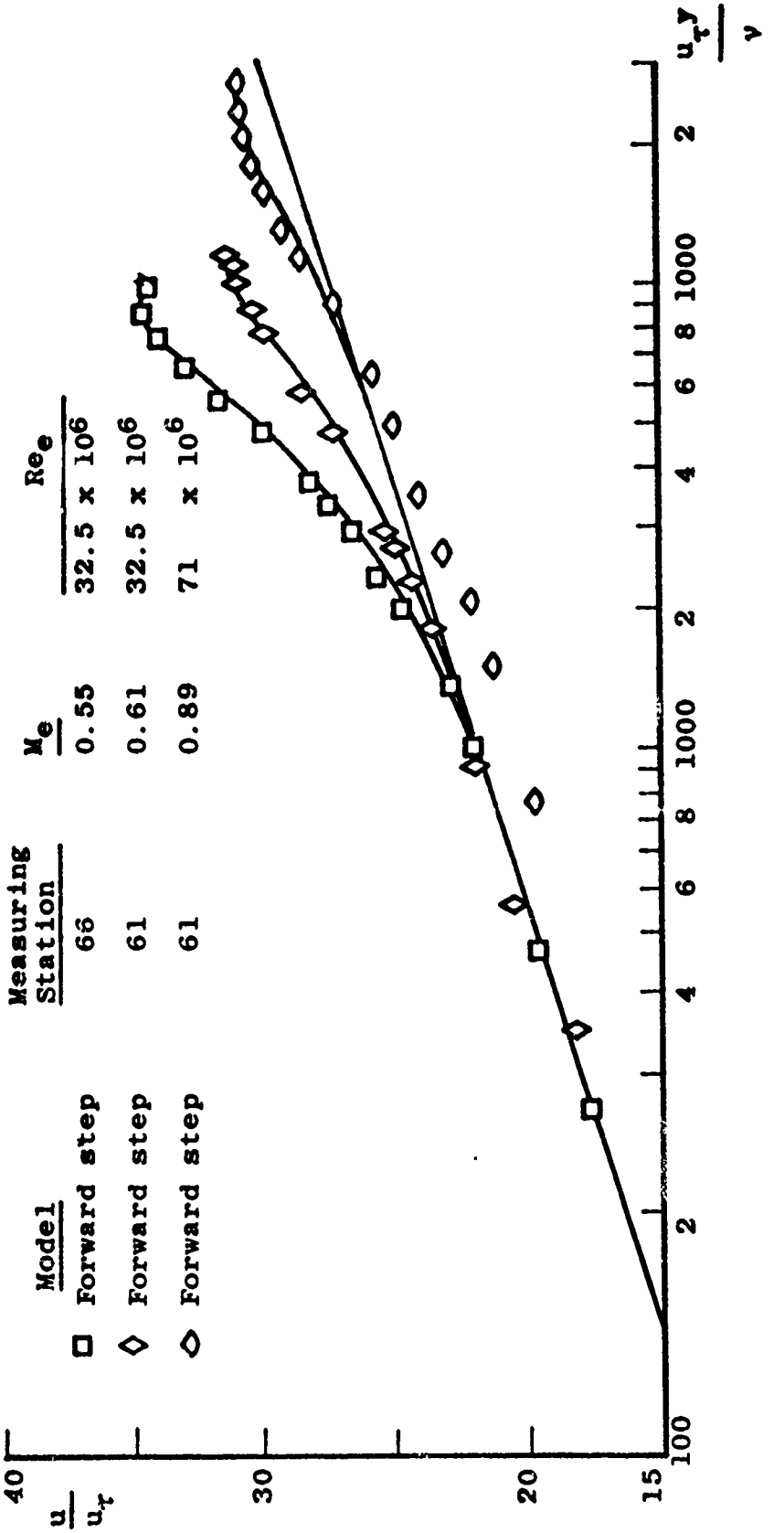

Figure 29. Velocity profile by law of wall and law of wake

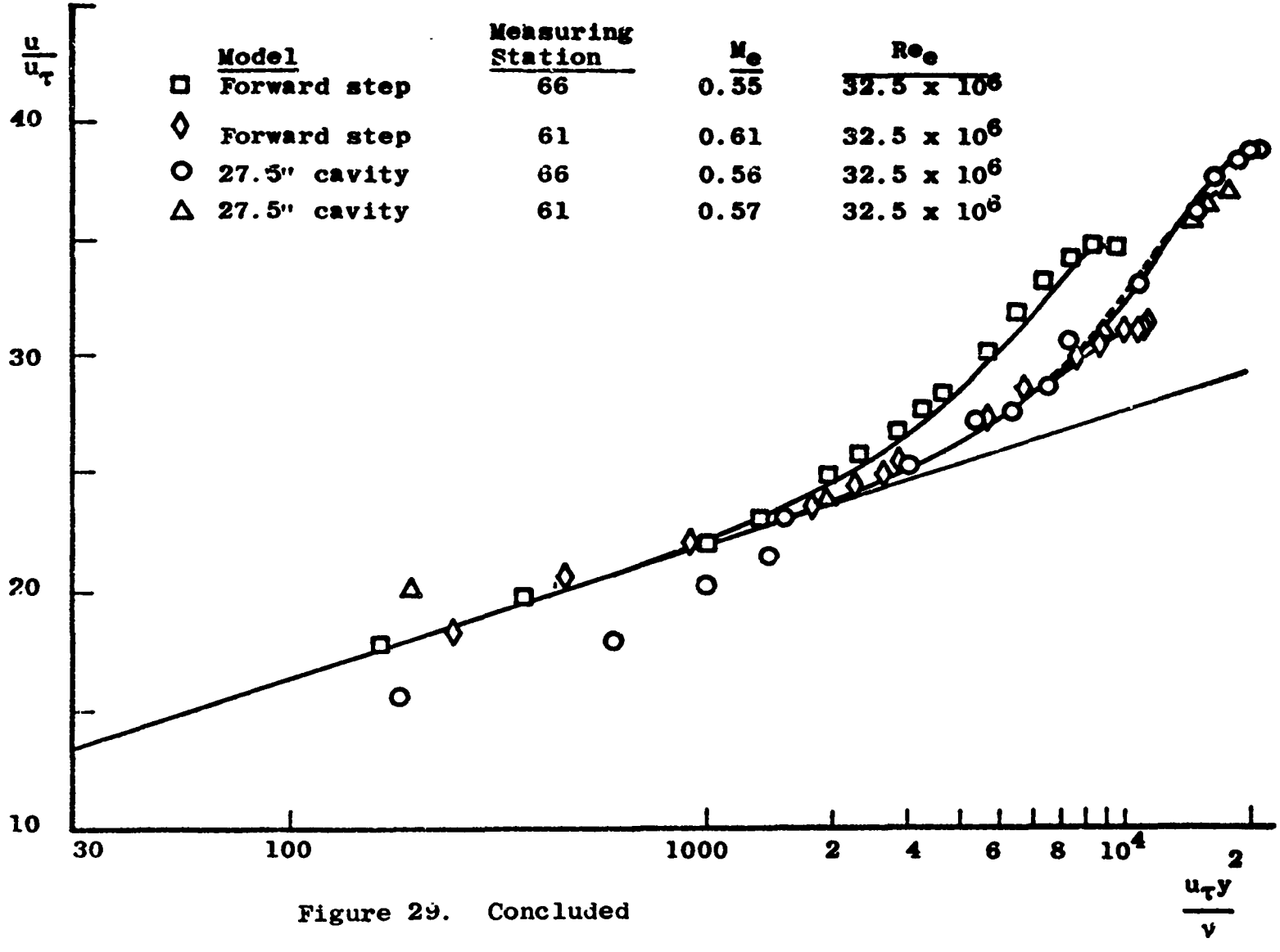

Figure 29. Concluded

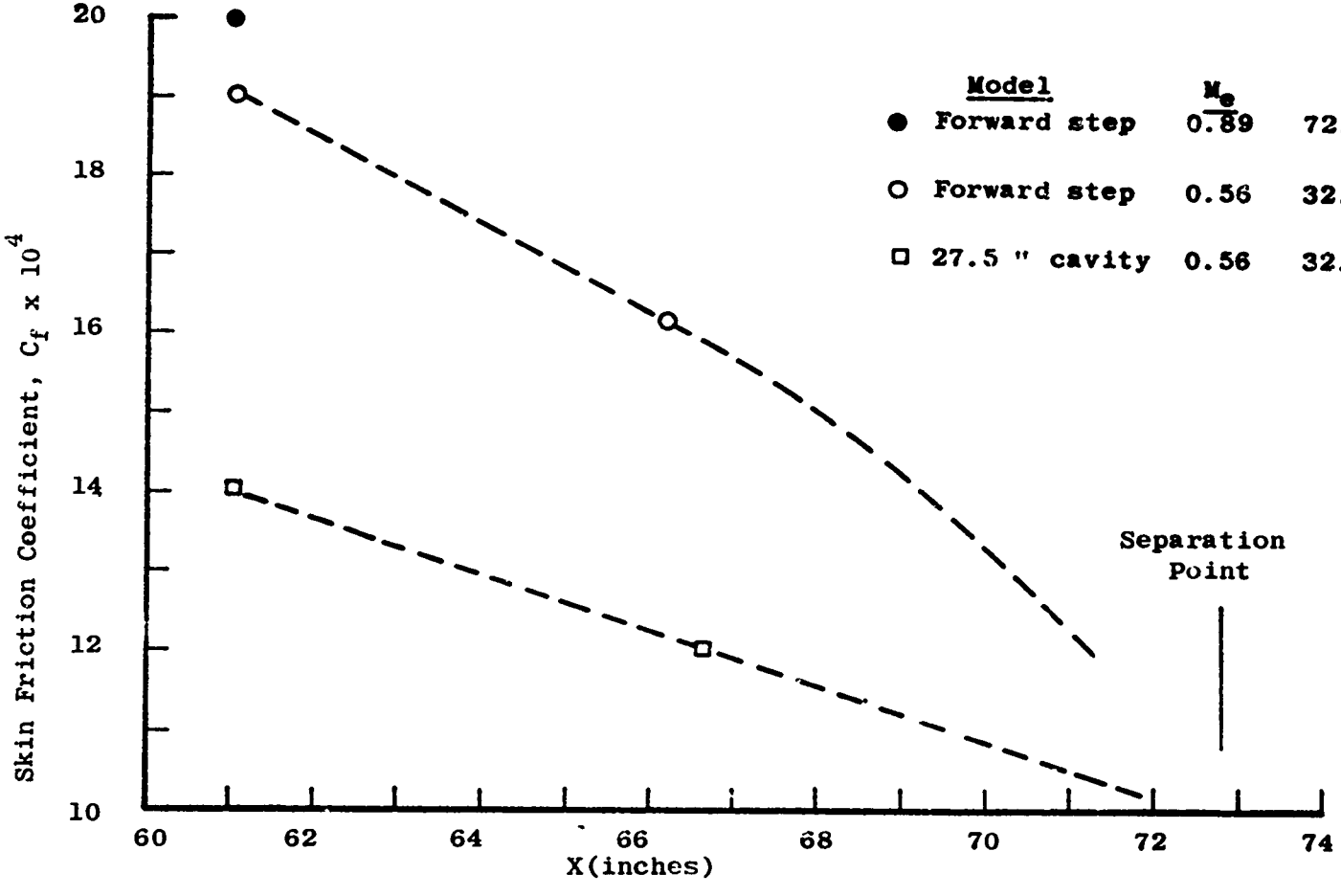

Figure 30. Mach number, model configuration and station effects on skin friction

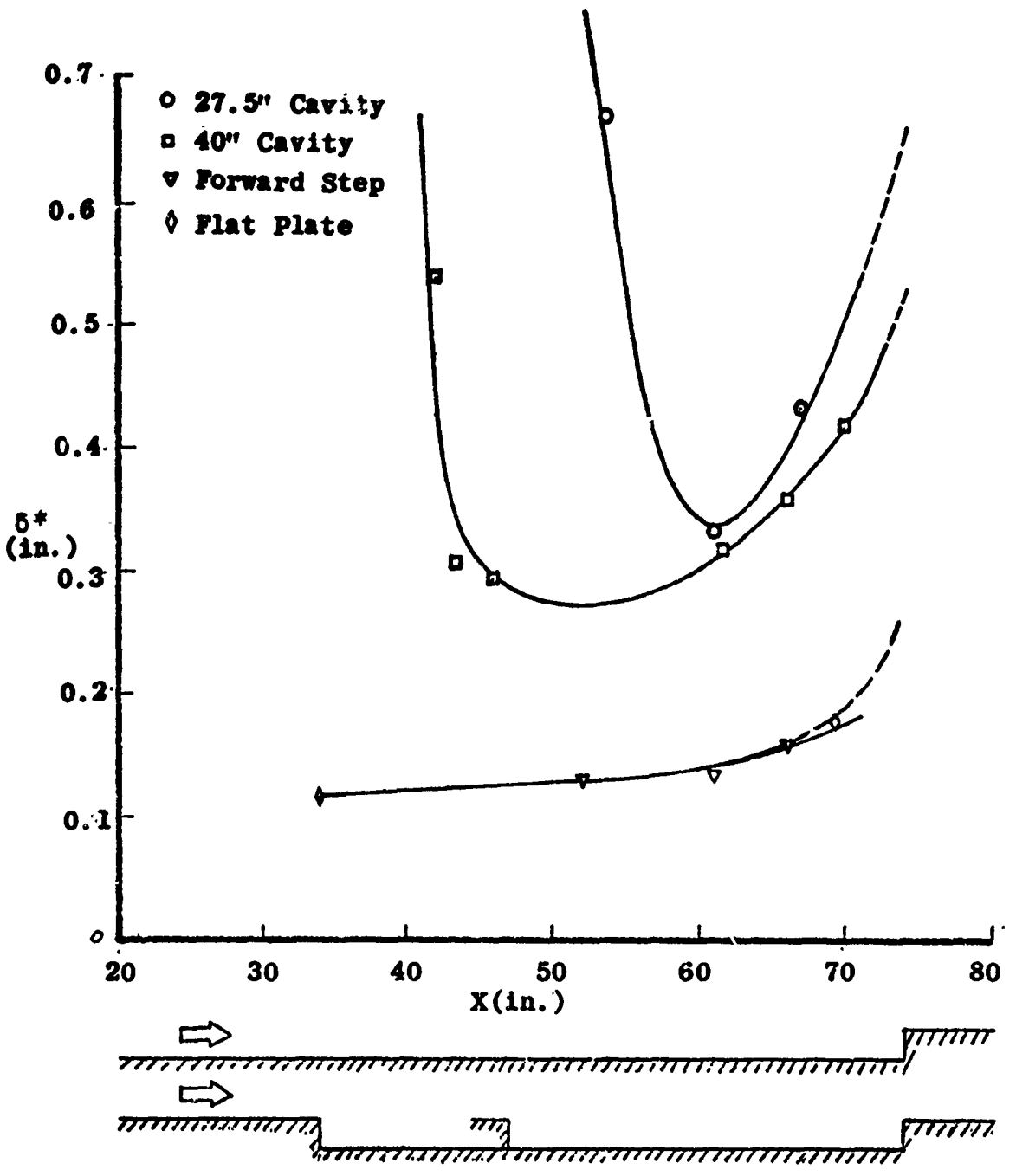

Figure 31. Development of shear layer displacement thickness along the models

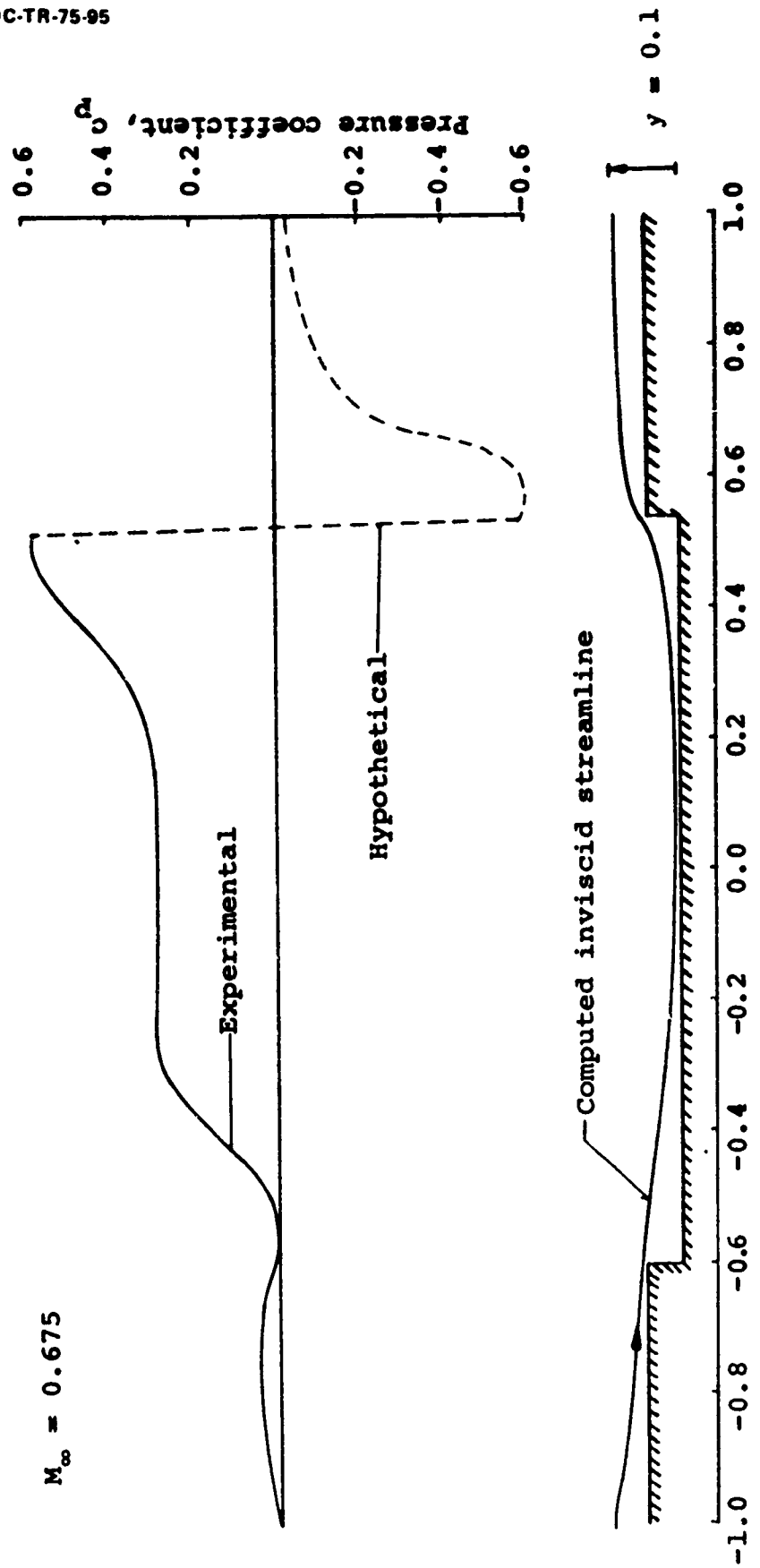

Figure 32. Computer inviscid streamline corresponding to an extended experimental pressure coefficient distribution

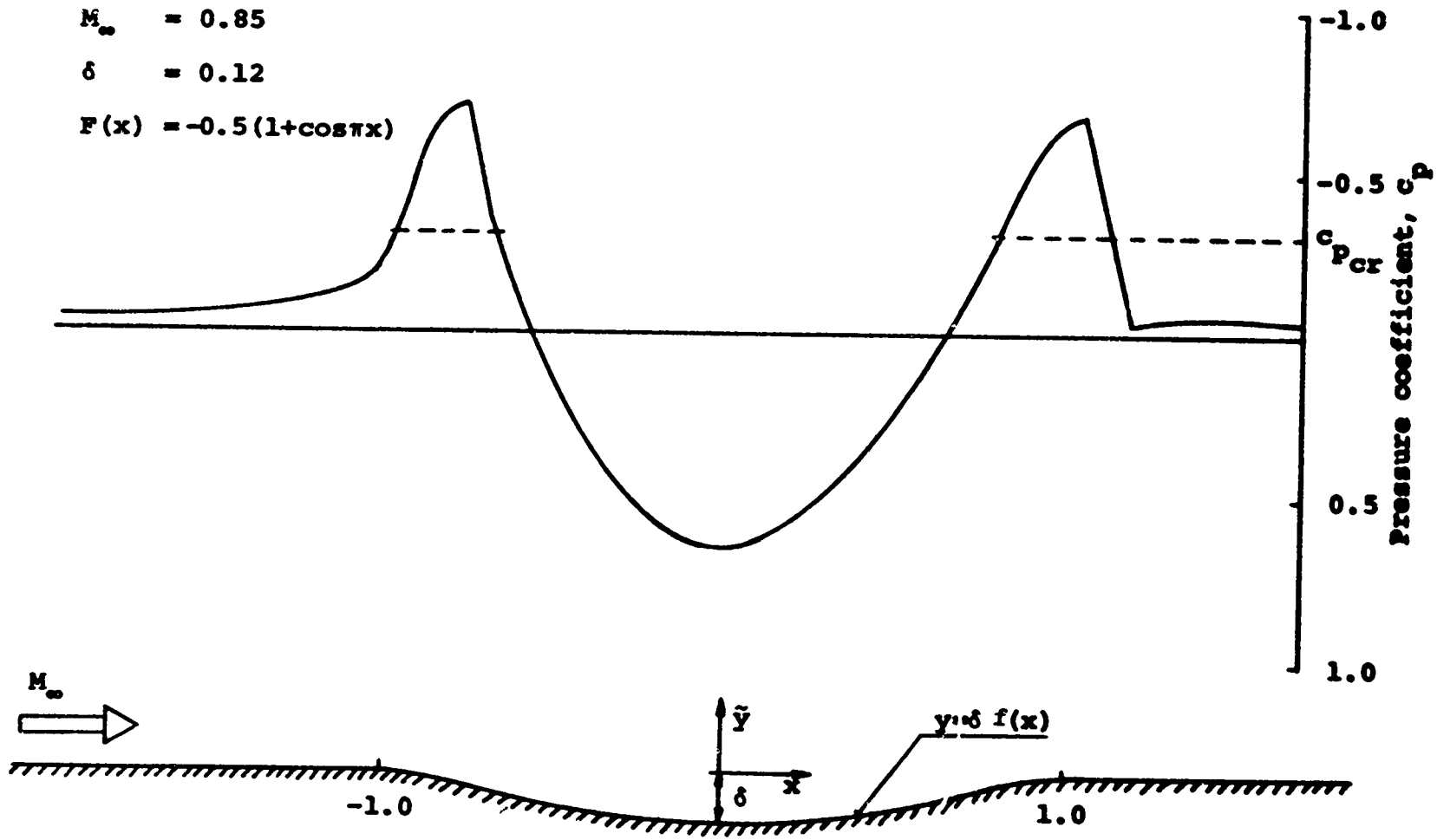

Figure 33. Computed pressure coefficient distribution for a flow over an assumed cavity.

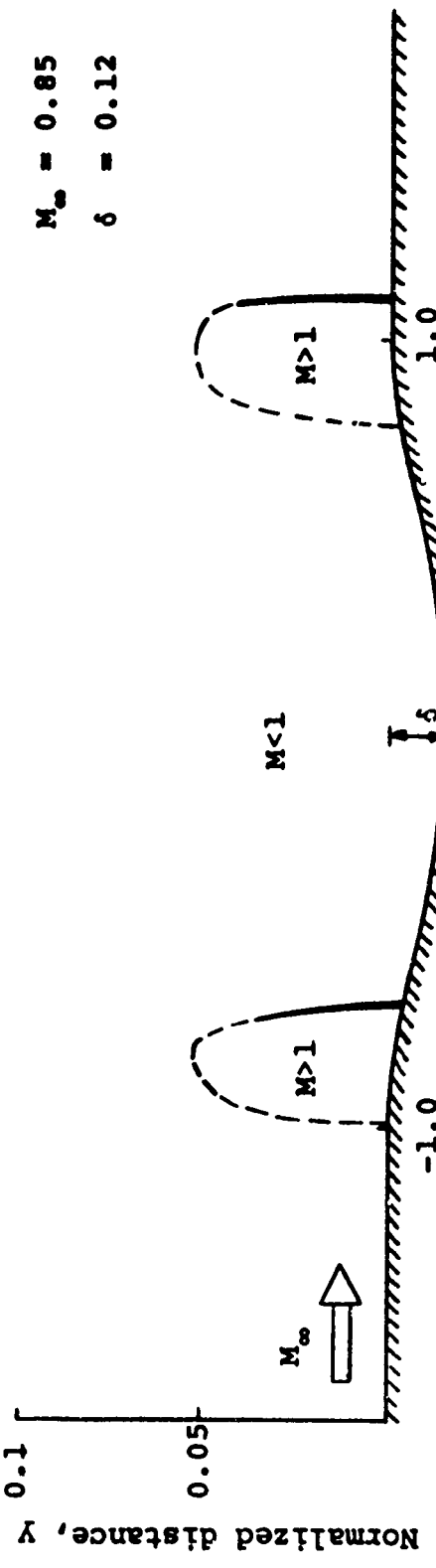

Figure 34. Extension of supersonic pockets for a cavity flow.

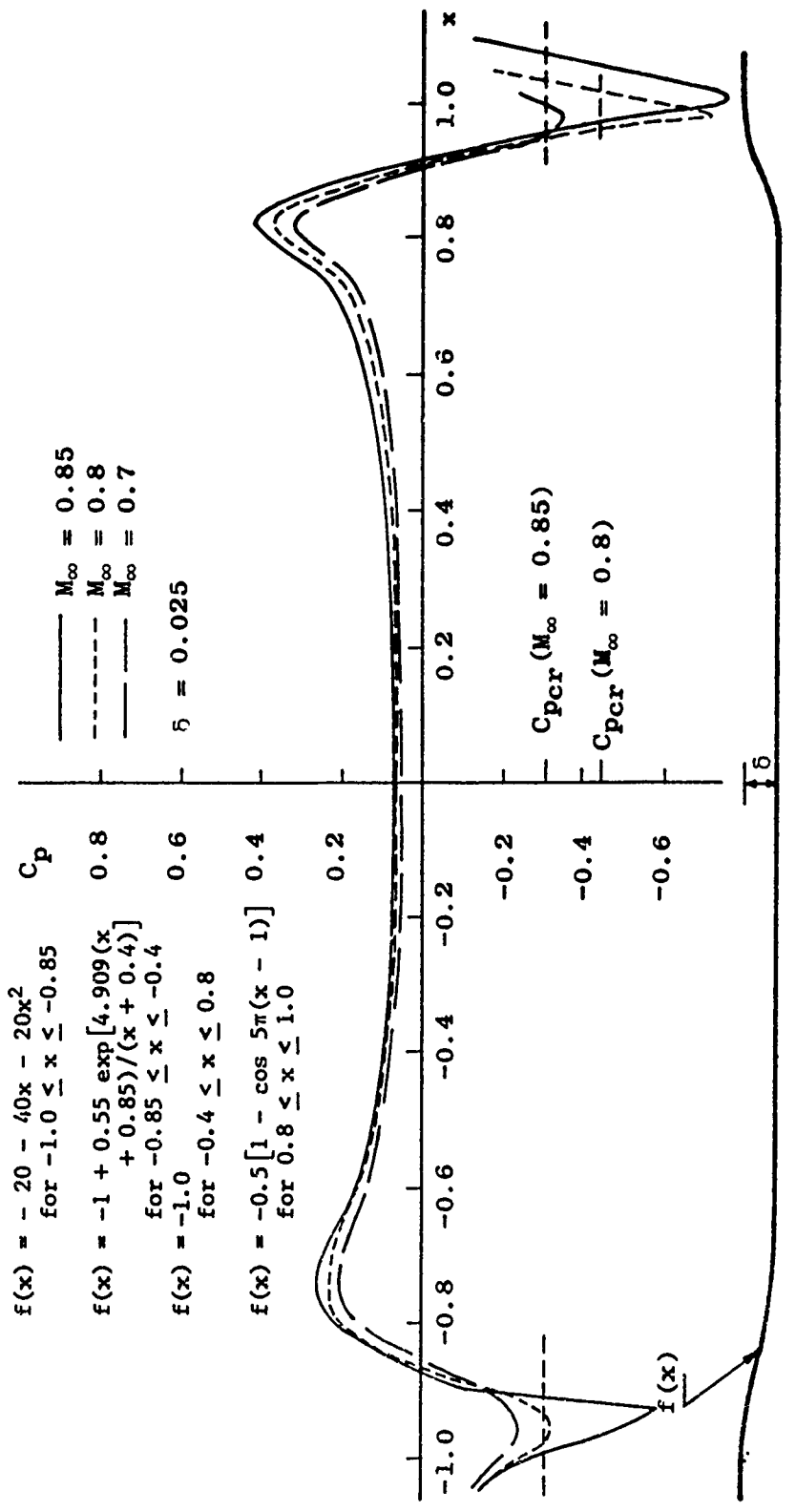

Figure 35. Effect of Mach numbers on pressure distribution for a cavity configuration

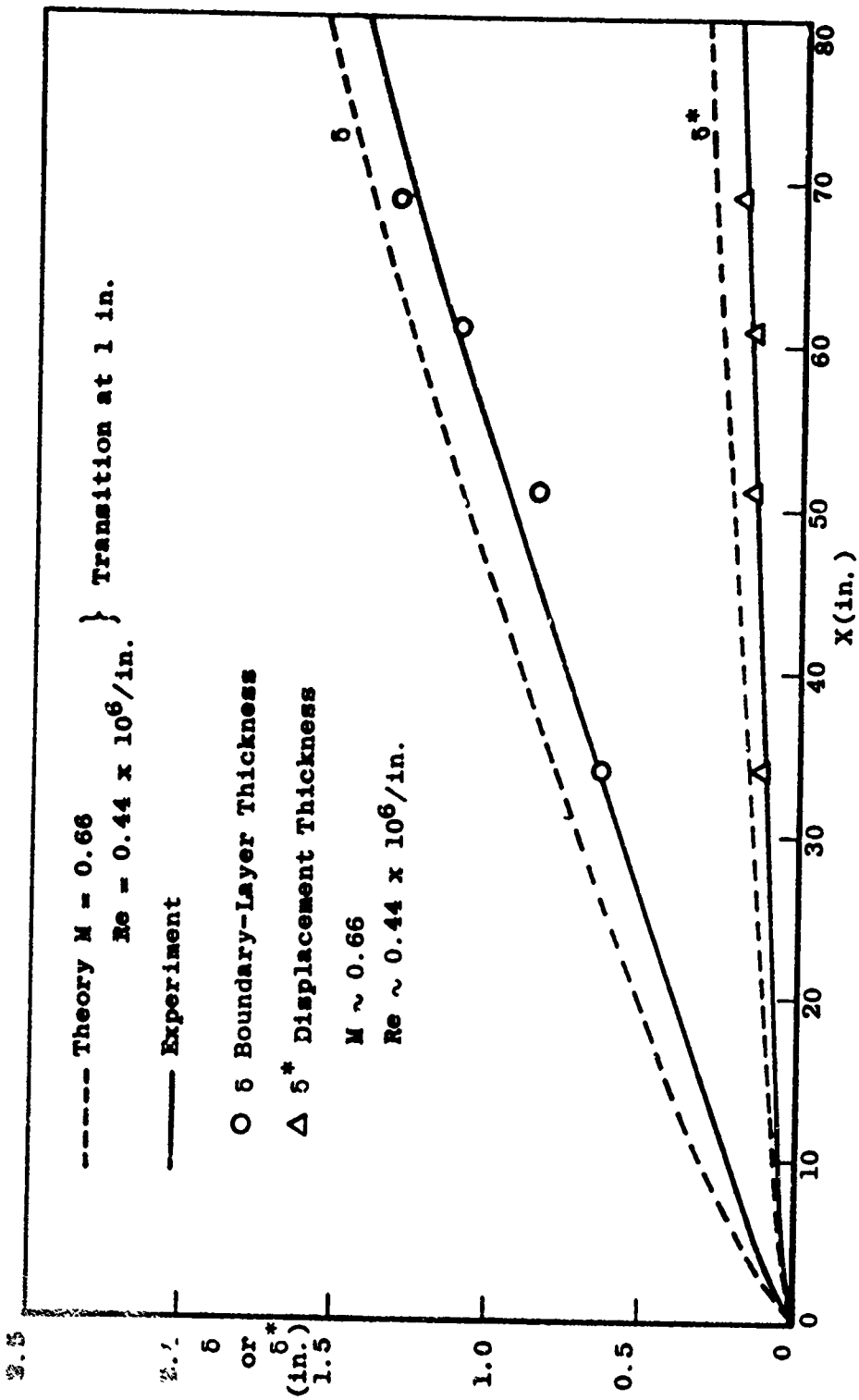

Figure 36. Comparisons of experimental data and theoretical computations for boundary layer thickness and displacement thickness

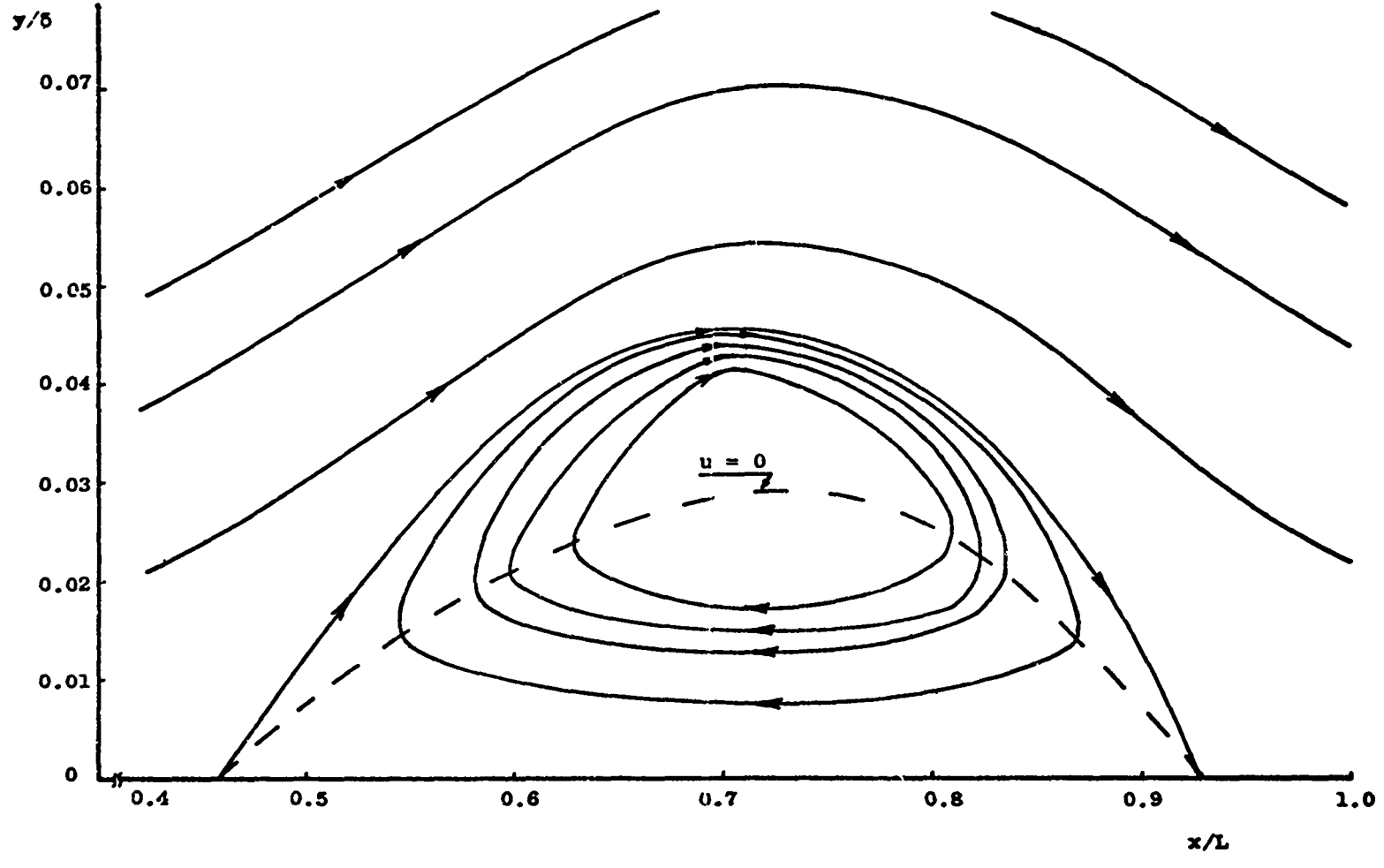

Figure 37. Streamline pattern for a flow with separation linearized equation model

APPENDIX A
WIND TUNNEL FLOW QUALITY

The mass flow rate in the wind tunnel is a function of the Mach number, the maximum value being about 190 lb/sec. The operational envelope of the tunnel is given in Fig. A-1. The control pressure is a function of the mass flow rate, and the relation between these two variables is shown in Fig. A-2. The nominal running time of the tunnel is in the range of 10 to 60 seconds (see Fig. A-3).

After design and fabrication, the wind tunnel calibration was carried out. The main nozzle design was found to be very satisfactory. The Mach number distribution in the vertical direction (i.e., perpendicular to the flow) just downstream of the nozzle exit plane is very uniform. However, initially the flow downstream of the model leading edge was distorted by about ±8% (Fig. A-4). The reason for this distortion is the difficulty in properly shaping the leading edge for a subsonic flow. Considerable time was spent in fixing this leading edge problem. After proper adjustments of the leading edge and the boundary layer suction device, a considerable improvement was achieved. The improved vertical Mach number distributions downstream of the leading edge at two locations are shown in Fig. A-5. The distortion is about ±0.1% close to the leading edge location and ±0.2% at a far downstream location, for this particular run.

The Mach number distribution along the flow direction for typical subsonic and supersonic flows are shown in Figs. A-6 and A-7. For the subsonic flow case, the flow uniformity is quite good when considered over a distance of 75 inches. For the supersonic flow, a further improvement is needed. In this phase of the study, emphasis has been placed upon the subsonic flow, and the improvement to the supersonic flow quality will be carried out in the future.

The flow is very uniform when the model configuration was adjusted to have a forty inch long cavity. The total pressure distribution corresponding to the free stream region has practically no distortion at all (see Fig. A-8). The oil flow traces confirmed that the flow is very much two-dimensional on the flat plate portion downstream of the leading

edge. The side wall induced three-dimensional effect appeared to be very minute for the rearward facing step configuration and was confined to within a 10~20% wide region at the side for the forward facing step configuration. Therefore, along the central 60~80% of the tunnel floor, the flow two-dimensionality is very satisfactory. Some typical oil flow traces will be shown in section 3.

For the present experiments, it is desirable to have adiabatic wall conditions during the testing period. For this purpose, some surface temperature variations were recorded during the run. A typical result is shown in Fig. A-9. The wall temperature decrement during the testing period is 3.2°C and 1.0°C respectively for two different locations on the model. The ratio of T_w/T_0 can be compared with the theoretical estimate based upon a recovery factor of 0.91 (chosen somewhat arbitrarily). The Mach number at the start of the test period shown on Fig. A-9 is approximately 0.5. Under these conditions the adiabatic wall temperature ratio $T_{wa}/T_0 = 0.996$ which compares with a measured wall temperature ratio of 1.04 at the start of the test period and 1.06 at the end. These data indicate that the tunnel wall is somewhat hotter than the adiabatic wall temperature and that there is heat transfer into the test gas. The significance of these heat transfer rates will be the subject of a separate study.

A.1 WIND TUNNEL TESTING CONDITIONS

In order to understand the flow variation along the model, the surface pressure distribution (P) along the model surface and the total pressure (P_t) profiles across the boundary layer are measured. The detailed information for these measurements are listed in Table A-1.

By adjusting the total pressure from 17 to 50 psia, the Reynolds number based on the model length was varied from 30×10^6 to 130×10^6. The undisturbed boundary layer thickness was then about one inch in the vicinity of 70 inches downstream of the leading edge. This unusually thick boundary layer along the model surface offers an excellent opportunity for accurate measurements in the viscous layer. The present study includes Mach numbers of 0.6, 0.8 and 0.9 based on manometer data.

The additional test parameters include (1) the reference external flow Mach number (M_i), measured at the station where the static pressure begins to rise ahead of the forward facing step, (2) the reference Reynolds number ($Re_L = LV/\upsilon$), where L equals 70 inches and V is the external flow velocity at the 70 inch station, (3) the reference boundary layer thickness (δ_L), measured on the flat plate at the 70 inch station, (4) the blockage ratio (h/H), where h is the step height and H is the height of the test section and (5) the ratio of the step height to the reference boundary layer thickness (h/δ_L). These are summarized in the accompanying table (Table A-1).

For the tests at a Mach number of 0.91, a 1/4" thick plate with perpendicular holes giving a porosity of 23% is used as the ceiling of the test section. This ceiling plate separated the plenum chamber and the test section, as discussed in section 3.1.

According to the calibration result, the lag time for the 0.011 inch pitot tip is 0.32 sec. for $\Delta p = 5$ psig and the vertical traversing speed of the pitot probe is 0.35 in./sec. which is approximately 1/110,000 of the flow speed at a location of 0.05 inch above the model surface. Therefore, the traversing effect of the pitot probe on the total pressure measurement is negligible. Since the pitot probe tip opening is circular and its diameter is much less than 4% of the boundary layer thickness, the data acquired is fairly reliable at least in the buffer and the turbulent zones and the displacement effect is also negligible (Refs. 20 and 21).

Surface oil flow visualization techniques have been used to extract details of the separation and the reattaching regions. It has also been applied to the side walls in order to obtain a qualitative idea of the three-dimensional structure of the flow. A mixture of titanium dioxide and kerosene oil is used for this purpose.

In order to avoid an excessive oil accumulation near the separation line and to keep the oil from forming U-shaped waves, some different proportions of titanium dioxide to kerosene oil are tested and used for the different skin friction regions (Ref. 22). On the side wall, the viscosity

of the applied mixture is high enough so that the patterns are not believed to be affected by the gravitational force. Several selective runs are made at Mach numbers of 0.6 to 0.9 and Reynolds numbers of 32.5 x 10^6 to 72.5 x 10^6 over various model configurations (Table A-1).

A.2 THE UTSI AIR SUPPLY SYSTEM

The UTSI Air Supply System can be described as three basic components, the compressor and dryer section, the air storage bottles and the flow control section.

The compressor and dryer section utilizes a two stage tandem, double acting electrically driven water cooled reciprocating compressor (Fig. A-10A) to compress 90 standard cubic feet per minute (SCFM) of atmospheric air. An automatic unloading system maintains the outlet pressure between 250 and 275 psig. The outlet air passes through an after cooler (Fig. A-10B) (counter-flow water heat exchanger) which cools the air to approximately ambient temperature (maximum 90°F in summer, minimum 40°F in winter), and a centrifugal separator (Fig. A-10C) to the two receivers (Fig A-10E) (total volume approximately 33 cu. ft.).

Air from the receivers passes through a two stage regenerative type dryer (Fig. A-10F) where moisture is removed resulting in a dewpoint of -90°F at standard conditions. At this point a small quantity is tapped off and reduced to 100 psig for the operating and control purposes. The dry air is piped to the high pressure compressor (Fig. A-10H).

The basic high pressure compressor is a three stage, diesel powered, hydraulically driven, double piston and dry piston compressor. Maximum output pressure is 6000 psig and minimum inlet pressure is 100 psig. At 250 psig inlet pressure, its capacity is about 45 SCFM. Maximum operating pressure is limited to 325 psig by the storage bottles.

Five additional compressors capable of pumping 15 SCFM each from ambient to 3500 psig have been installed. These are four stage combination rotary reciprocating compressors with built-in drying systems. However, they have been notoriously undependable.

The air storage system consists of three bottles of 250 cu. ft. capacity each with associated valves and piping. The bottles are pumped to a maximum 3250 psig. Total air stored is approximately 166,000 SCF (12,400 lbm). However, for larger flow rate runs (greater than 100 lbm/sec) only about one half of this is available as the sudden colling caused by quickly emptying the bottles would result in a temperature which would endanger their structural integrity.

When preparations for a tunnel run are completed, air from any or all of the three storage bottles is opened to the control system. Valving is set to supply operating air either to the combustion tunnel or the transonic tunnel.

A four inch pneumatically operated control valve is used to regulate air flow to the tunnel. A pressure signal at the valve outlet is used by a pneumatic computer to position the control valve. Using this system stable air flows of approximately 10 to 200 lbm/sec can be obtained. For lower flows, a one inch regulator system is available.

TABLE A-1 TEST CONDITIONS

Model Configuration	Equivalent External Flow Mach (M_e)	Reynolds No. ($\frac{LV}{\nu}$)	Boundary Layer Thickness (δ_L)	$\frac{h}{\delta_L}$	$\frac{h}{H}$	Stations** of P_t Measurement	Regions** of P Measure-	Oil Flow
Flat Plate	0.6	32.5×10^6	1.5	0.67	0.08	34, 51, 61, 69	0.4 ~ 73.75	
Forward-Facing Step (1 in. high)	0.6	32.5×10^6	1.5	0.67	0.08	61, 66, 69	48 ~ 73.75	x
	0.8	63×10^6	1.3	0.77	0.08	69	48 ~ 73.75	x
	0.9	72.5×10^6	0.87	1.15	0.08	61, 66, 69	48 ~ 73.75	x
Long Cavity (1 in. high 40 in. long)	0.6	32.5×10^6	1.5	0.67	0.08	41, 43, 46, 51 61, 66, 69	34 ~ 73.75	x
Short Cavity (1 in. high, 27.5 in. long)	0.6	32.5×10^6	1.5	0.67	0.08	53, 61, 66, 69	48 ~ 73.75	x

* Equivalent external flow Mach number M_e is the Mach number corresponding to the station e as indicated. For a cavity-like flow case, it is slightly different from M_∞.

** All distances in inches measured from the leading edge of the flat-plate configuration.

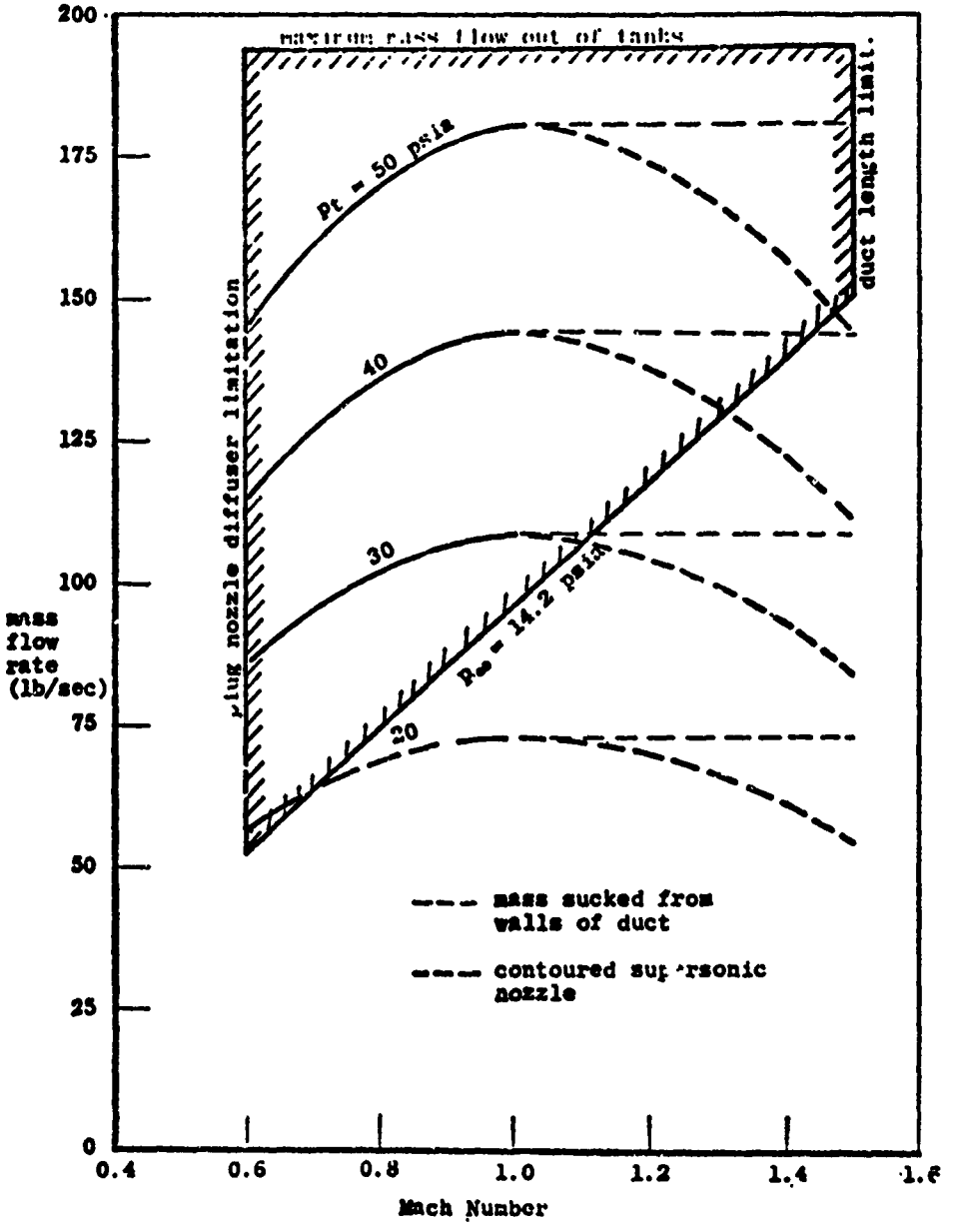

Figure A-1. Mass flow rate as a function of Mach number in 12 by 12 inch duct (T_o = 20°F).

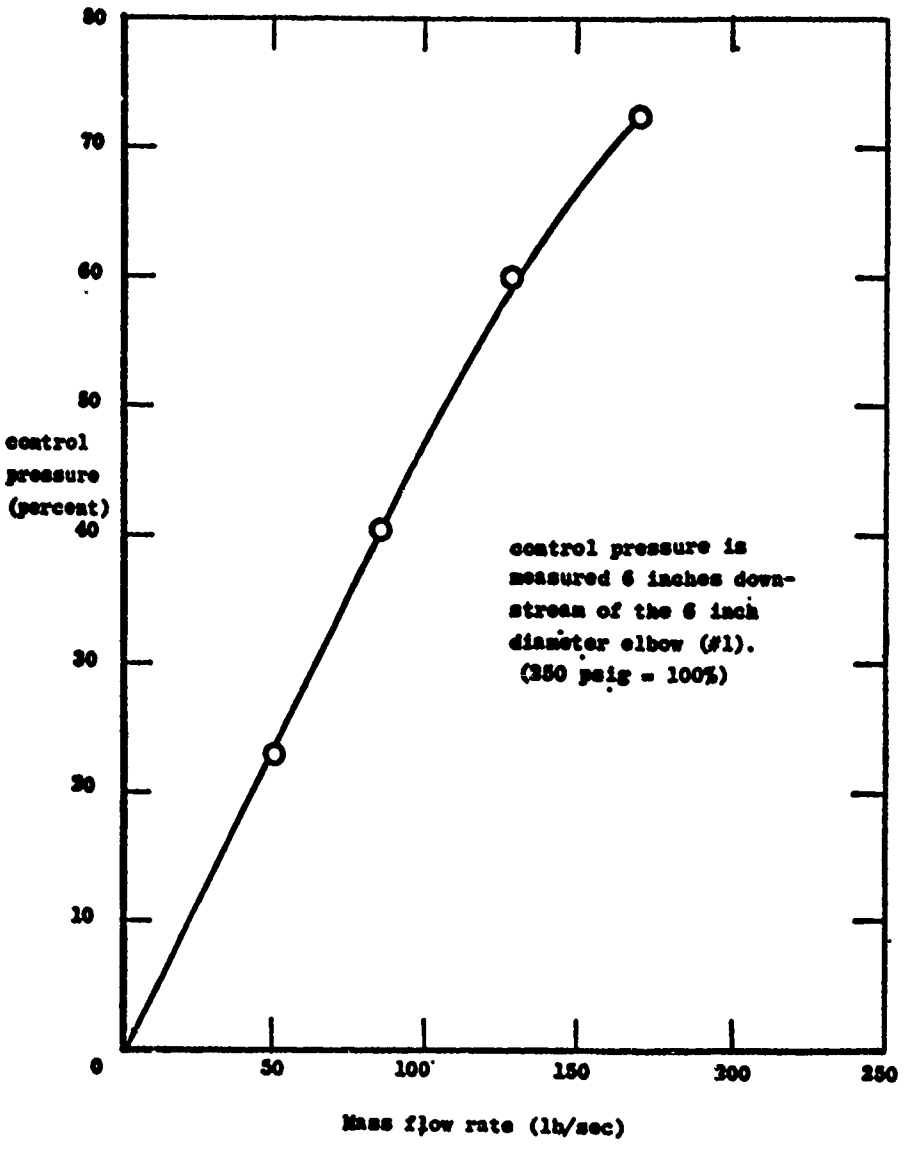

Figure A-2. Control pressure as a function of mass flow rate.

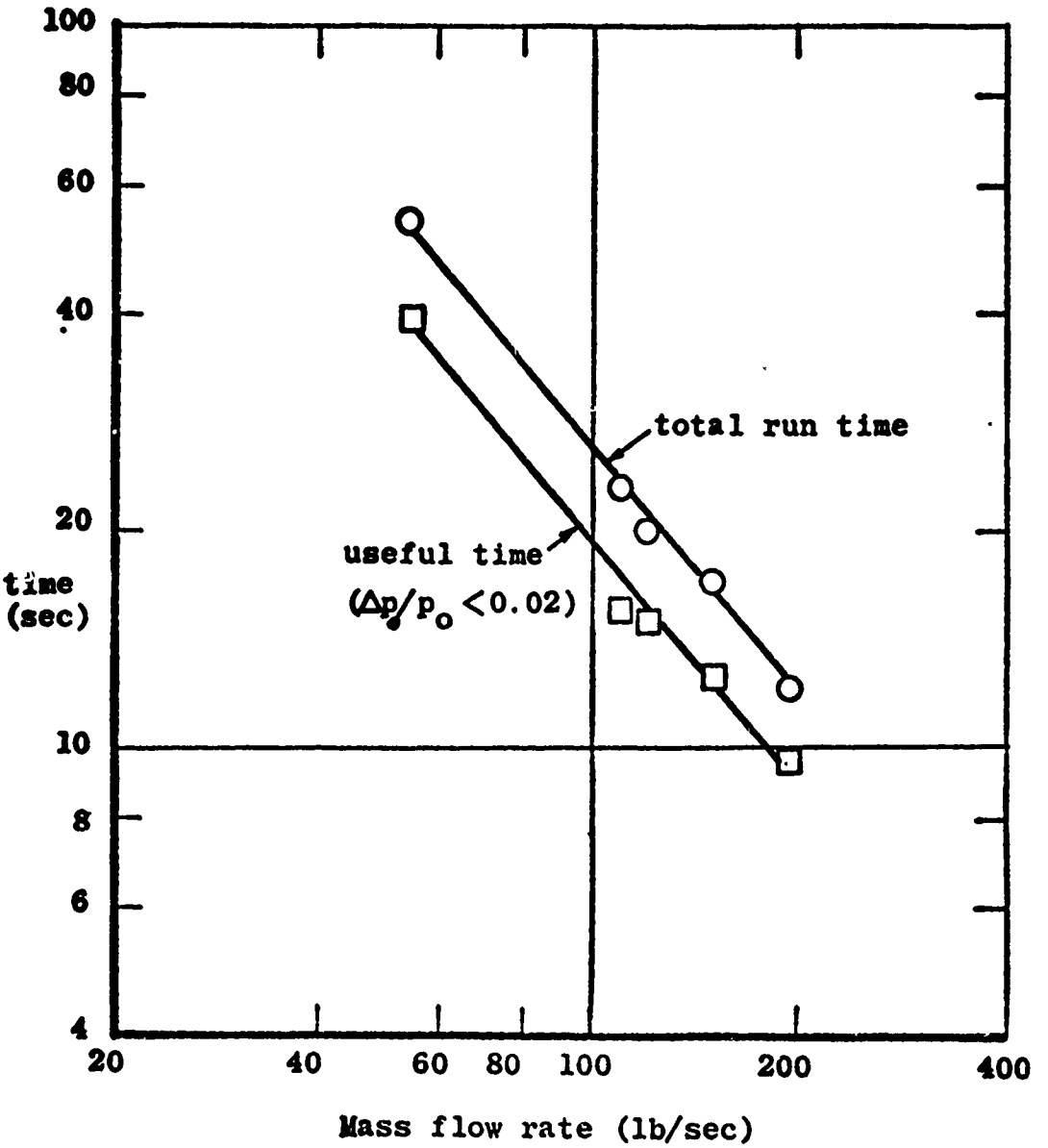

Figure A-3. Test time available as a function of mass flow rate.

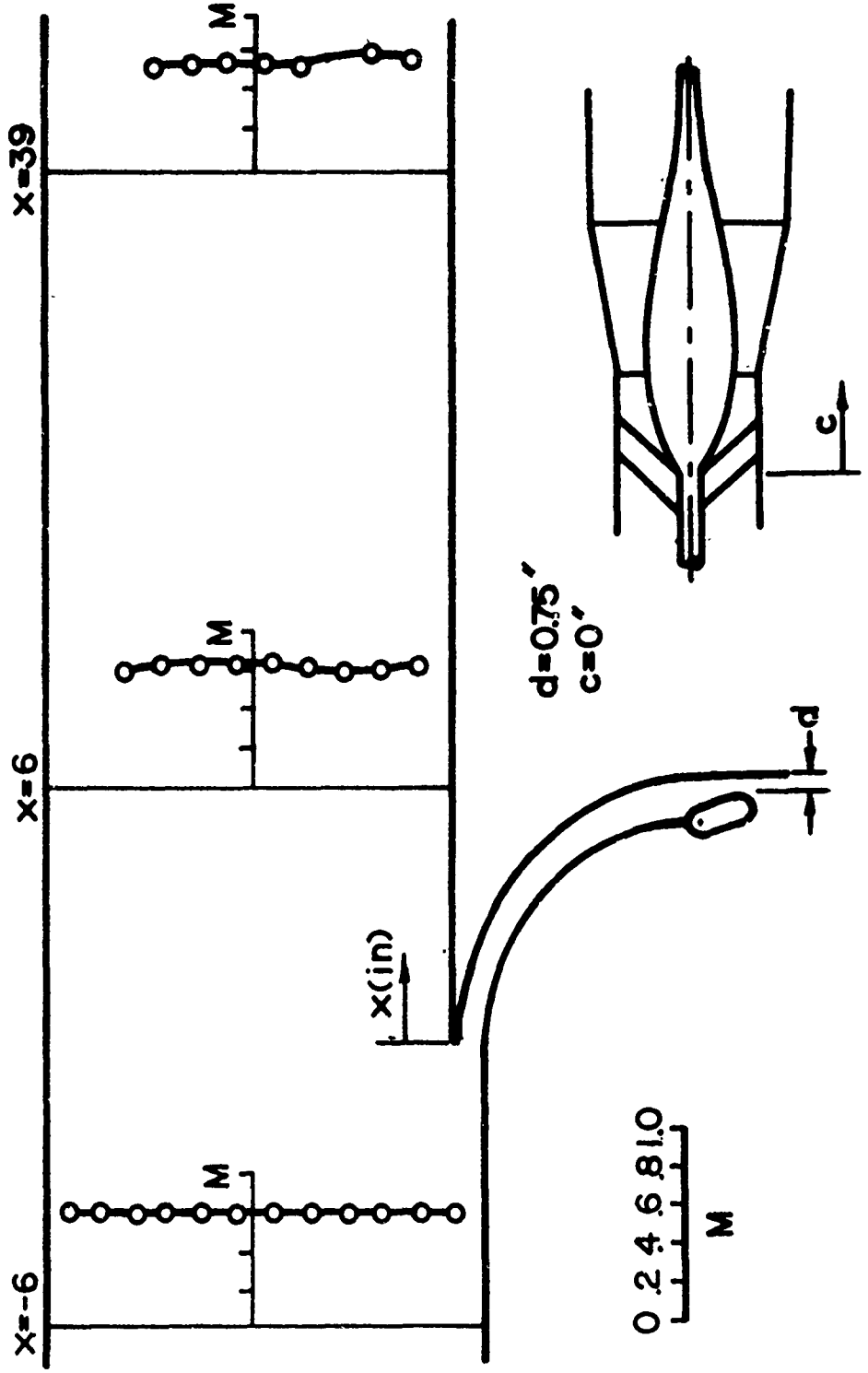

Figure A-4. Vertical Mach number distribution across the test-section.

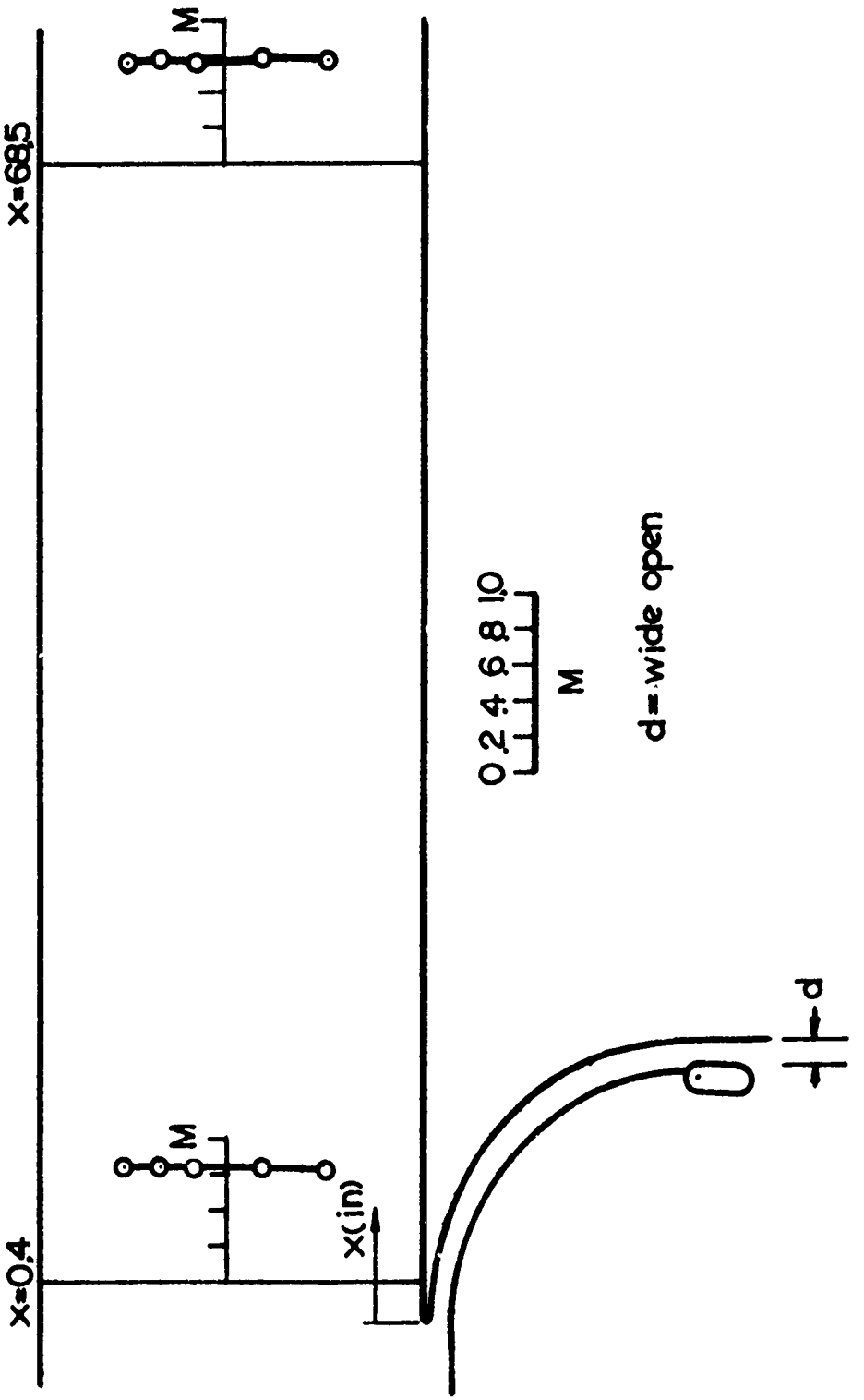

Figure A-5. Vertical Mach number distribution across the test-section for a long range.

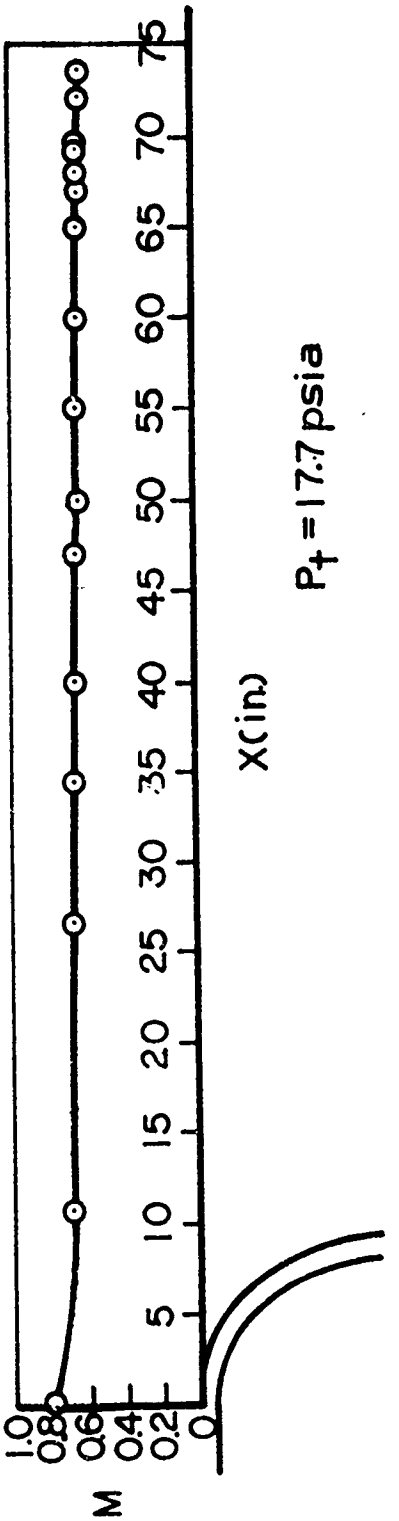

Figure A-6. Axial Mach number distribution for M < 1.

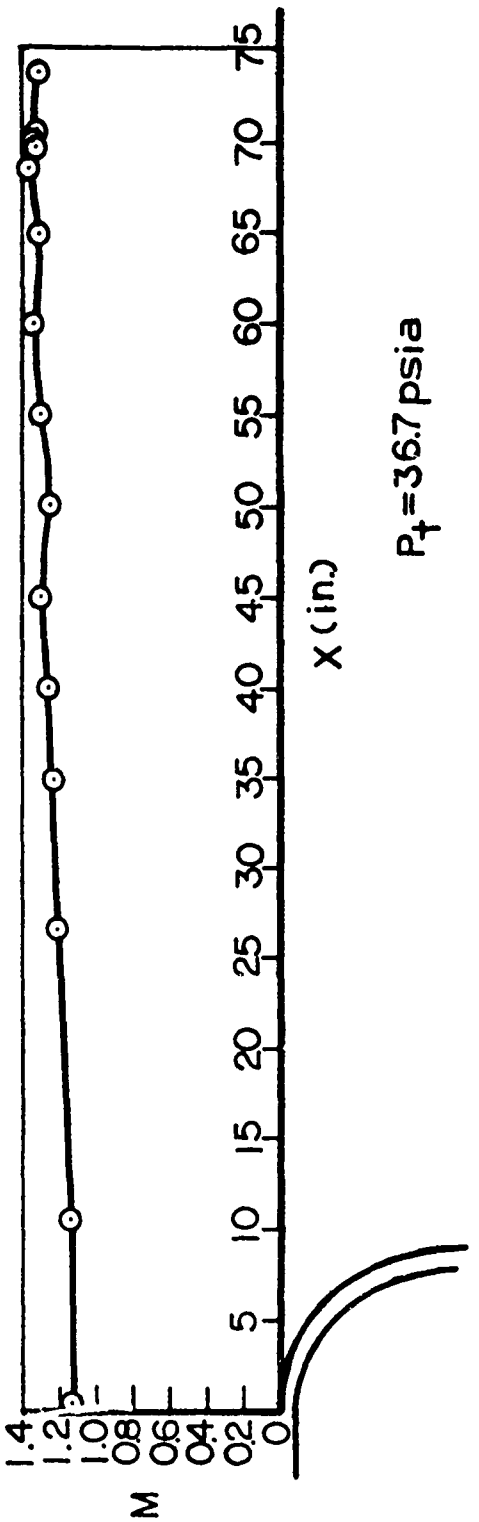

Figure A-7. Axial Mach number distribution for M > 1.

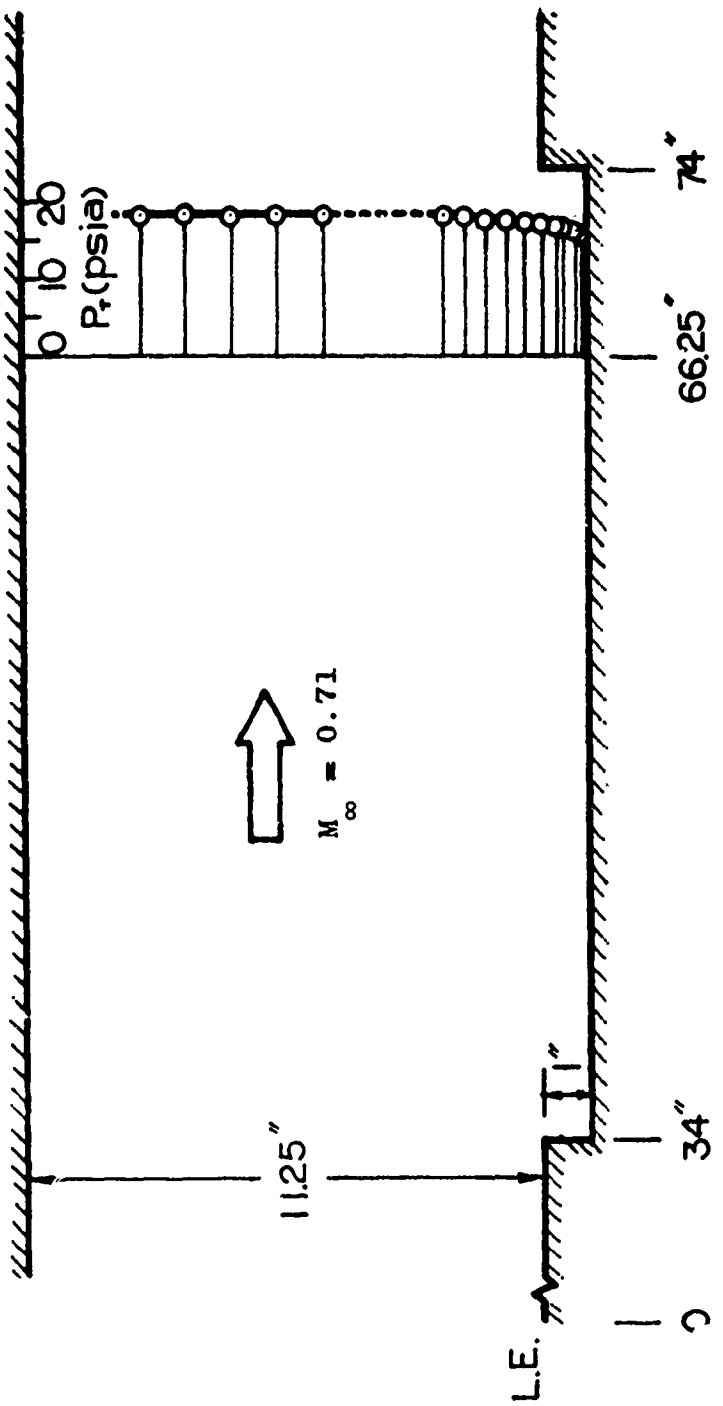

Figure A-8. Total pressure distribution across the test-section for the long cavity case.

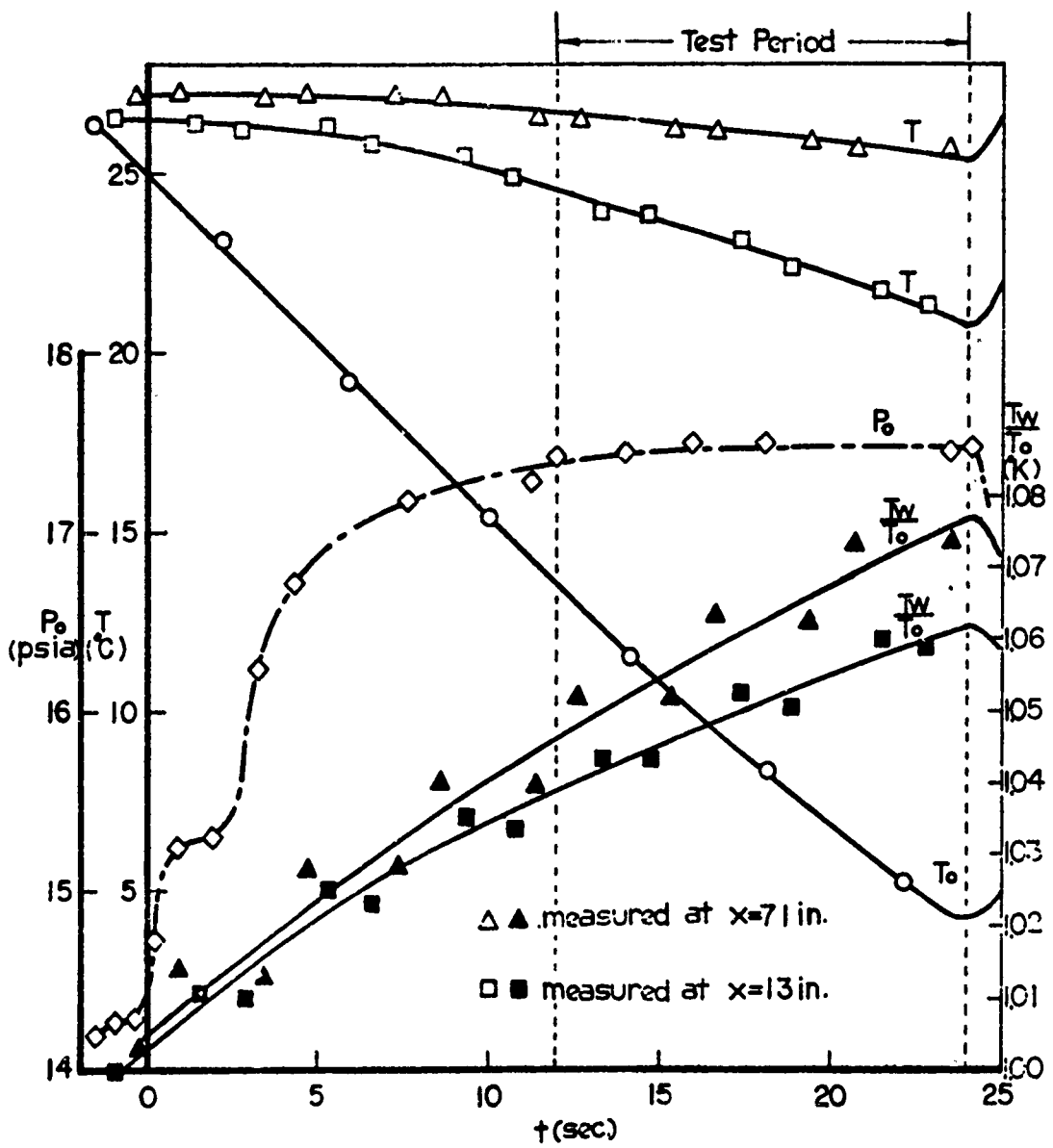

Figure A-9. Surface Temperature Distribution.

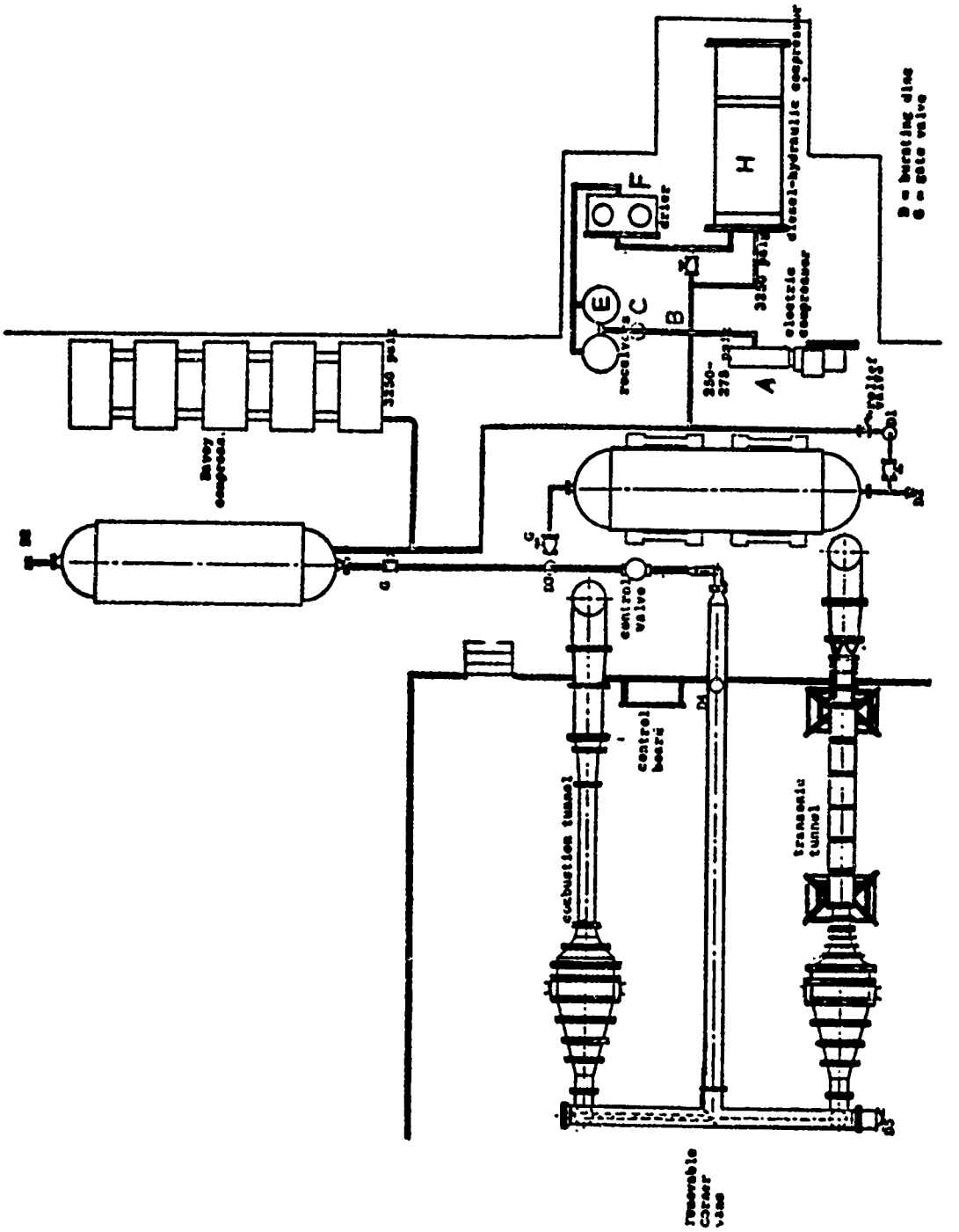

Figure A-10 Air supply and wind tunnel layout

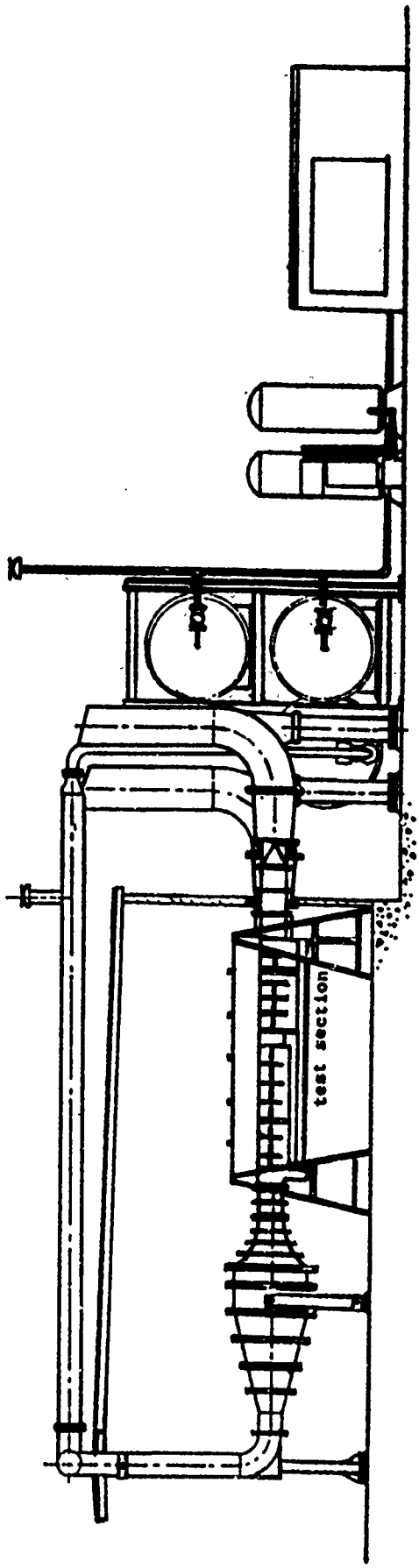

Figure A-10. Concluded

NOMENCLATURE

A	Cross sectional area
A	Constant (Section 5 - see equation 5.9)
B	Constant in law of wake for turbulent boundary layers--equation 4.1
C	Constant defined on page 14
c	Constant-equation 4.4
C_f	Skin friction coefficient
C_p	Pressure coefficient
d	Tube inside diameter
$d/d\xi$	Derivative with respect to independent variable ξ.
F(x)	Arbitrary function in equation 5.16
f(x)	Cavity profile function
g(x)	Function defined by equation 5.6
H	Height of test section
h	Model step height
K	Transonic flow similarity parameter--equation 5.1
K	Constant in the law of the wall for turbulent boundary layers
K_m	Function defined by equation 3.2
L	Distance from the model leading edge to the root of the forward facing step
ℓ	Length
ℓn	Natural logarithm
M	Mach number
P	Pressure
r(x)	Function defined by Equation 5.11
T	Temperature
t	Dummy variable in integration
U	Velocity

u, v	Velocity components along coordinate directions x, y
u_τ	Friction velocity in turbulent boundary layer
V	External flow velocity
V	Tube volume on page 14
Re	Reynolds number
X	Distance from model leading edge
x, y	Rectangular coordinates
$\bar{y}$	Stretched variable defined in equation 5.1
y	Dummy variable in integration
Γ	Velocity profile defined in equation 5.17
δ	Boundary layer thickness
δ	Depth of cavity in Section 5
θ	Boundary layer momentum thickness
λ	Inverse Reynolds number
ν	Fluid kinematic viscosity
ξ	Dummy variable in integration
$\bar{\pi}$	Constant in equation 4.1
ρ	Fluid density
τ	Tube lag time
τ	Boundary layer turbulence term in equation 5.15
η	Velocity profile
ω	Turbulent boundary layer wake function

SUBSCRIPTS:

0	At entrance
1, 2	First and second tube respectively
∞	Free stream condition
e	Local external flow condition

i	Initial condition or condition at the location where the pressure begins to rise ahead of the forward facing step
L	Condition at forward facing step
m	In measuring device
r	Distance from the root of the rearward facing step
t	True or total
w	Condition on wall